STRENGTHENING SLENDER STEEL COMPRESSION MEMBERS USING A FIBRE-REINFORCED POLYMER BUCKLING RESTRAINED BRACING SYSTEM

by

Daina Lee MacEachern

Submitted in partial fulfilment of the requirements
for the degree of Master of Applied Science

at

Dalhousie University
Halifax, Nova Scotia
March 2019

DEDICATION

I want to dedicate this thesis to my parents.

To my dad, who when I was worried about whether I would “pass university”, suggested I worry about getting through first grade first. Thanks for passing down the worrying gene, but also the analytical and detailed thinking that comes with it.

To my mom, who no matter how many times I called her, always reminded me to stop trying to cross bridges before I got to them… Not to mention, who proof-read my school papers long past the point at which she understood what I was talking about.

Thank you both for teaching me that quitting is never an option. There are not many things I could have done without your support, and this most definitely isn’t one of them.

TABLE OF CONTENTS

LIST OF TABLES

LIST OF FIGURES

ABSTRACT

In this thesis, the structural properties and behaviour of slender steel members strengthened against buckling by fibre-reinforced polymer (FRP) shells filled with self-consolidating grout, in the form of buckling restrained bracing (BRB), were investigated. The goal of the FRP-BRB system is to increase the load carrying capacity of the slender member to reach the yielding load of the steel core through the addition of lateral support. A total of 27 strengthened specimens and 9 plain steel cores were prepared and tested. The strengthened specimens were prepared with three different length FRP shells, namely, 300 mm, 600 mm and 900 mm as well as three outer diameters, namely, 41 mm, 53 mm, and 65 mm. Hot rolled steel bars, 25.4 mm by 6.35 mm, with lengths corresponding to 30 mm longer than the FRP shell length were prepared with 45 mm long tapered tabs. The self-consolidating grout for filling the shells was prepared to have a compressive strength of 20 to 35 MPa. A lubricant was applied to the steel core to inhibit bonding with the grout. Specimens were tested under uniaxial compression up to failure. Through strain data the contribution of each component of the system to the overall load carrying capacity was calculated. It was found that at the yielding point the steel core carries on average 86% of the load with the grout and FRP carrying only 13.5% and 0.5%, respectively. A simple linear elastic model was created in order to predict the failure mode of the FRP-BRB system that can also be used to design an optimized system. The model accurately predicted the failure mode for all 27 reinforced specimens. Overall, provided the FRP-BRB system was sufficiently sized, as determined by the model, the system was successful in changing the failure mode of the steel core from buckling to yielding.

LIST OF ABBREVIATIONS AND SYMBOLS USED

Abbreviations

ASTM	American Society for Testing and Materials
B	Buckling
BRB	Buckling Restrained Brace
CFRP	Carbon Fibre Reinforced Polymer
CSA	Canadians Standards Association
CSCE	Canadian Society for Civil Engineering
DNR	Data Not Recorded
EI	Flexural Rigidity
FRP	Fibre Reinforced Polymer
FRP-BRB	Fibre Reinforced Polymer Buckling Restrained Brace
GRFP	Glass Fibre Reinforced Polymer
LP	Lateral Potentiometer
OD	Outer Diameter
PVC	Polyvinyl Chloride
SCC	Self Consolidating Concrete
SCG	Self Consolidating Grout
SG	Strain Gauge
SHS	Square Hollow Section
Y	Yielding

Symbols

A	Cross-sectional Area
A_s	Cross-sectional Area of Steel Core
E	Young's Modulus of Elasticity
E_f	Young's Modulus of Elasticity of FRP Shell

E_g	Young's Modulus of Elasticity of Grout
EI_{crit}	Critical Buckling Flexural Rigidity
EI_f	Flexural Rigidity of FRP Shell
EI_g	Flexural Rigidity of Grout
EI_s	Flexural Rigidity of Steel Core
E_s	Young's Modulus of Elasticity of Steel Core
f'_c	Compressive Strength of Concrete
f'_g	Compressive Strength of Grout
f_r	Rupture Stress
I	Moment of Inertia
K	Modification Factor for End Conditions
L	Length
N_c	Number of CFRP Layers
P	Axial Load
P_{crit}	Critical Buckling Load
P_f	Total Calculated Axial Load in FRP Shell
P_g	Total Calculated Axial Load in Grout
P_s	Total Calculated Axial Load in Steel Core
P_t	Total Calculated Axial Load
P_y	Axial Yielding Load
ε	Strain
ε_r	Rupture Strain of Concrete
λ	Modification Factor for Concrete Density

ACKNOWLEDGEMENTS

The author acknowledges the financial support of Dalhousie University, the Nova Scotia Graduate Scholarship (NSGS) and the National Sciences and Engineering Research Council of Canada (NSERC). This project would not have been possible with out the help of lab technicians, Blair Nickerson, Brian Kennedy, Jesse Keane and Jordan Maerz of Dalhousie University. Support from Dr. Sadeghian and the students in his lab group was also greatly appreciated. The author also acknowledges QuakeWrap Inc. (Tucson, AZ, USA) for providing GFRP laminate and adhesive for the experimental program.

CHAPTER 1 INTRODUCTION

1.1 MOTIVATION

As of 2016, close to 35% of Canadian infrastructure was in need of repair or replacement (CSCE 2016). In the United States of America, 9.1% of the bridges were considered to be structurally deficient in 2016, with 39% of all bridges being at least 50 years old (ASCE 2016). With that number increasing yearly, solutions for efficiently and economically improving the state of infrastructure (e.g. buildings and bridges) is critical. Germany in 2006 was 1st in the category of infrastructure in the World Economic Forum's Global Competitiveness Report and in the 2018 version of the report had slipped to 7th in overall infrastructure and 19th for quality of roads (Porter and Lopez-Claros 2006; Schwab 2018). As of 2016, 20% of Germany's road networks were in need of repair and 15% of the municipal bridges required complete replacement (Schulze 2016). Since 2006 in Italy there have been 12 bridge collapses and there are another approximately 300 bridges on the verge of collapse as of 2018 (Tondo 2018).

Age, deteriorating conditions, and potential applied load changes of slender members, columns, bracing and piles have led to various market solutions that improve resistance to buckling. More conventional methods of reinforcing slender members include bulking the structures up with additional material such as steel, concrete or fibre-reinforced polymers (FRP) (Ekiz and El-Tawil 2008; El-Tawil and Ekiz 2009; Gao et al. 2013; Harries et al. 2009; Kim and Choi 2015; Sadeghian et al. 2009; Shaat and Fam 2009; Vild and Bajer 2017; Wu and Grondin 2002). Recently a more advanced method of increasing the buckling capacity of slender members was developed called a buckling restrained brace (BRB)

(Almeida et al. 2017; Black et al. 2004; Carden et al. 2004; Tremblay et al. 2006). These are currently shop fabricated, field installed systems that consist of steel members encased in a steel tubing filled with concrete or mortar. For these systems to function properly a lubricant is applied to the member to allow free expansion and contraction as well as eliminate friction and shear transfer (Black et al. 2004). The BRB system is applicable for either adding additional bracing or fully replacing old bracing in existing structures as well as for installing in new structures. These systems are currently custom-designed and manufactured for specific projects (Kersting et al. 2015). For cases where the existing bracing or column need to be kept and upgraded, the BRB system is not applicable.

The solution investigated in this paper can be applied in the field through keeping the existing member and increasing its buckling capacity. This method is like the BRB system but involves the wrapping of thin FRP laminate around members in the field instead of steel sections fabricated in a shop that would require removal of the existing member. This system will be referred to as a fibre-reinforced polymer buckling restrained brace (FRP-BRB). The FRP laminate is glued shut to form a cylindrical formwork that will remain as part of the structural system. Similar to the BRB system described, a lubricant will be applied to the steel to allow its movement to be independent of the grout. Once cured, the tubing will be filled with a cement-based self consolidating grout (SCG) or concrete (SCC). This technique, when properly sized, can provide lateral buckling support while allowing the restrained member to reach its yielding capacity. It is noted that the concept of the FRP-BRB explored in this thesis is as per U.S. Patent Number 9,719,255 B1 for buckling reinforcement for structural members by Mohammad Reza Ehsani, Tucson, AZ (US) (Ehsani 2017).

The application of this method ideally allows the failure mode of the member to switch from a brittle failure to a ductile failure with yielding. It will also increase the load capacity of the structure significantly. This method can be used in adverse or challenging locations such as waterfront structures and locations with severe salt exposure. This sustainable, cost effective solution will increase the durability of the structure while lengthening life span and service. This process can be designed to use cost effective materials as well as materials that produce a smaller environmental footprint. Cementitious by-products and other waste materials such as fly ash may be used in the concrete or grout as it is not required for its high strength (James et al. 2011). As cement production emits significant amounts of CO_2, any reduction in the amount of cement will contribute to lowering the environmental footprint (Heede 2014; Vargas and Halog 2015). Moreover, the FRP shell protects the concrete or grout against harsh environments increasing the durability of the system. The FRP shell also confines the grout and increases its strength and ductility (Harries and Kharel 2003; Vincent 2015). Minimal labour and training are involved in the installation of the system and no heavy equipment is required. As there is no need to remove the existing brace with this technique the planning is minimal helping make this system more economical. Conventional steel BRB's are a proprietary item and are custom fabricated in a shop for each job, whereas the FRP-BRB system can be modified to fit any shape using the same materials from one member to the next.

1.2 OBJECTIVES

The objectives of this research are:

- To determine the behaviour and structural capabilities of the proposed FRP-BRB strengthening system at a small scale.
- To investigate the feasibility of the FRP-BRB system in real-life applications.
- To help establish a solid platform to develop reliable design procedures applicable for aging infrastructure including bridges, buildings, and waterfront structures.

1.3 RESEARCH SCOPE

In order to achieve the outlined objectives, a number of small-scale models of the proposed system with various lengths and diameter of FRP shells were prepared and tested under pure axial loading to determine strength properties and behaviour. A self-consolidating grout was used for filling the FRP shells. A model was created in order to allow for ease of design of the FRP-BRB system and was verified using the experimental results.

1.4 THESIS LAYOUT

The general layout of this thesis consists of an introduction to the rehabilitation of slender compression members with a literature review, followed by an in-depth explanation of the experimental program, a review and discussion of the results of the testing, an analytical study of the system, ending with conclusions and recommendations for further research. The literature review, Chapter 2, will investigate various rehabilitation techniques for strengthening slender members including conventional buckling restrained braces as well as different techniques for strengthening with fibre reinforced polymers. Current research on strengthening techniques similar to the FRP-BRB studied in this thesis will be reviewed.

Chapter 3 covers the experimental program that reviews the test matrix as well as the material properties for each component of the FRP-BRB system. This section will also explain the fabrication of the specimens, the instrumentation and test set-up. Following the explanation of the experimental program the results from the testing will be provided and discussed, examining various components of the behaviour of the system. The analytical study, presented in Chapter 4, will include a detailed description of the model as well as a parametric study and design example. Finally, conclusions will be presented and recommendations for future research, as well as for practical implementation, will be provided in Chapter 5.

CHAPTER 2 LITERATURE REVIEW – REHABILITATION OF SLENDER MEMBERS

With the amount of rapidly aging infrastructure growing worldwide, it is becoming increasingly more important that rehabilitation techniques be developed and tested. From an economic and environmental sense, it is rarely more efficient to replace a structure rather than repair or rehabilitate. There are three main factors that can be said to drive the increasing need for economically and structurally efficient rehabilitation and strengthening techniques, as described by Ekiz and El-Tawil (Ekiz and El-Tawil 2008). These factors are:

- Rehabilitation for increased loads or performance (deficient bridges, buildings and other structures)
- Strengthening for extreme loading conditions (over sized or special loads)
- Seismic upgrading

Compression members are defined as rigid linear elements inclined at any angle where loads are applied only to the ends of the member (Schodek 2008). Columns and braces are two common types of compression members. A member is considered short when the failure mode under axial compression is a material or crushing failure. A member is referred to as long (or slender) when under axial load its first failure mode is by buckling with material rupture only occurring once buckled (Schodek 2008). Slenderness of a member is defined as the ratio of effective unsupported length to the radius of gyration (CSA Group 2014a). As the slenderness of a member increases, the likelihood of a buckling failure mode increases as well. This ratio is limited by codes to ensure that sufficient stability exists post-buckling (Schodek 2008). Increasing a member's resistance to buckling can allow it to reach its material failure, which for slender members, is at a higher

loading than a buckling failure. When considering Euler's critical load equation (2-1) that defines the axial load a member can take before buckling (P_{cr}), it can be seen that the load required to buckle a section increases proportionally with the flexural rigidity (Schodek 2008). Flexural rigidity (EI) is defined as the product of modulus of elasticity (E) and the moment of inertia (I) along the weak axis. A member will tend to buckle about its weak axis (Schodek 2008). From this equation it is also noted that the critical load is inversely proportional to the square of the length (L) of the member. The end conditions of a member also have an impact on the load required to buckle the member. This is represented in the equation by an adjustment factor, K. In order to strengthen a member against buckling, assuming length of member can not be altered, the flexural rigidity must be increased. This is most commonly done by increasing the moment of inertia of the member along its weak or buckling axis.

$$P_{crit} = \frac{\pi^2 EI}{(KL)^2} \tag{2-1}$$

where: P_{crit} is the critical buckling load
E is the modulus of elasticity
I is the weak-axis moment of inertia
L is the un-supported length of the steel
K is the end-condition modification factor (pin-pin = 1.0)

A common use of a slender member is in the lateral load resistance system of a structure, as bracing. Some bracing is designed as tension only bracing and is typically designed to be less stocky that tension-compression bracing. This bracing exhibits less energy dissipation, but larger inelastic deflections can result. Energy dissipation increases as the slenderness ratio decreases (CISC 2016). The Canadian Standards Association (CSA) S6-

14 limits the slenderness of all compression members to 200 in order to minimize any fluttering of members under oscillating loading. This limit is increased to 300 for tension only members (CSA Group 2014a). Slender columns may also be designed or come about from damage to the original member, but in general they are not an ideal or efficient design and are typically only designed for aesthetic purposes or space requirements.

Regardless of how a member became slender or was designed as slender, reasons for increasing its capacity can be due to a need for increased bearing capacity if loading conditions are changing. The member could potentially need to be strengthened for an extreme loading condition or simply require updating to meet a new code or requirements such as for seismic activity in the area. There has been an increase in demand for solutions to protect structures during seismic events in high seismic risk countries such as Italy and the USA (Almeida et al. 2017). Braces are used to dissipate energy in these situations which is crucial to maintain safety and the stability of structures under the conditions. The ability of a system to dissipate energy can be defined by the area under the load – deformation curve (CISC 2016).

2.1 CONVENTIONAL BUCKLING RESTRAINED BRACES

In recent years a new system has been developed and researched in order to be used in structures to increase the buckling capacity of slender compression members in new construction and rehabilitation scenarios. This method is referred to as a BRB and is most commonly used to strengthen against horizontal earthquake motions and increase energy dissipation in these cases (Almeida et al. 2017). The general design of such a system comprises of a tube or formwork surrounding a steel core infilled with a grout, concrete or another filler material (Almeida et al. 2017). A traditional BRB configuration is shown in

Figure 2-1. The steel core is modified in a way to inhibit the bonding of the steel and filler, typically by the means of a lubricant or low friction material (Almeida et al. 2017). This allows relative axial deformations between the steel core and infill material (Almeida et al. 2017). The system effectively provides lateral support to the steel core and increases the overall moment of inertia of the section, thus increasing its flexural rigidity. The idea is for the steel core, which works efficiently in tension, to also be able to work effectively in compression scenarios, thus reaching its yield strength, rather than buckling in compression (Almeida et al. 2017). The tube and filler material do not receive any, or little load in these set-ups, acting only as lateral support. Effectively, the unsupported length of the steel member is reduced to zero (López and Sabelli 2004).

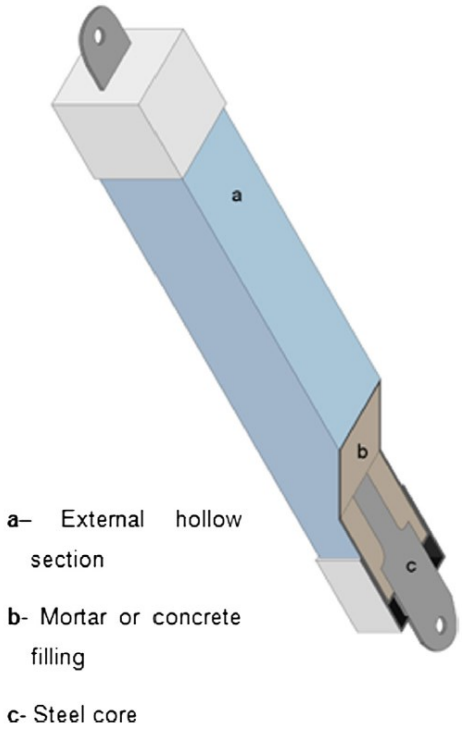

Figure 2-1 Traditional buckling restrained brace configuration (Almeida et al. 2017)

Many configurations of this design have been studied, however they all share the same goal of preventing global and/or local buckling of the steel core, allowing for equal tensile and compressive strength and optimal performance in hysteretic scenarios (Almeida et al. 2017). The ability of BRB's to dissipate energy is best demonstrated when comparing a load-deformation graph of a conventional steel brace to one of a BRB. Under stable hysteretic loading Figure 2-2 shows the resulting stress-strain diagram. As previously described, dissipation of energy is the area under the load deformation curve. It can be seen that for the same loading pattern, the BRB is able to cover more area, representing better ability to dissipate energy. One important difference is the ability for the BRB to reach the same stress in compression as it does in tension, where as the conventional brace buckles under much lower load in compression. Conventional steel braces in concentrically braced frames exhibit inelastic seismic response typically governed by buckling of the brace which in turn triggers a degradation in the stiffness and strength of the frame (Kersting et al. 2015).

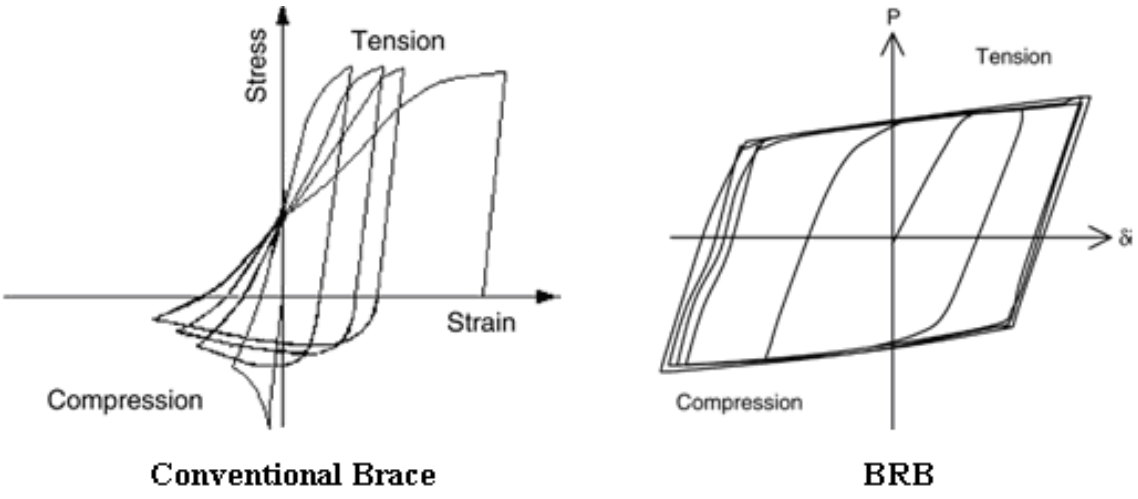

Figure 2-2 Stress-strain comparison of conventional brace and BRB (Ghassemieh and Kari 2013)

BRB's fabricated with a steel shell is currently the most common and most researched type. One of the main concerns when it comes to this design is that in order for it to be installed, it must either be built with the structure, or the existing member of the structure must be removed and replaced. This may not be ideal for all scenarios and requires careful planning. Conventional BRB's are designed using an equivalent lateral force method (López and Sabelli 2004). BRB's are designed based on a reduced seismic load applied using a linear elastic model that determines the required strength and stiffness (López and Sabelli 2004). In USA BRB's are a proprietary product and therefore are currently custom manufactured to the specific project (Kersting et al. 2015). The various manufacturers typically provide design guidance to aide in appropriately sizing the BRB.

While the use of BRB's is currently mostly limited to steel structures, Almeida et al. (2017) conducted a study to determine the feasibility of the seismic retrofit of reinforced concrete building structures with steel buckling restrained braces through non-linear static and dynamic numerical analysis. Through this analysis they were able to come up with a design method that allowed for optimizing dimensions of these buckling restrained braces, leading to improved structural performance. All together, this solution limits structural damage to the building. Figure 2-3 and Figure 2-4 show the numerical model and the outputs for the capacity of the original structure along with the capacity with the BRB's installed, respectively. Almeida et al. (2017) concluded with their study that the use of these BRB's as a seismic retrofit in a reinforced concrete structure allowed for a significant increase in strength as well as limiting deformations and increasing the capacity of the structure to dissipate energy (Almeida et al. 2017).

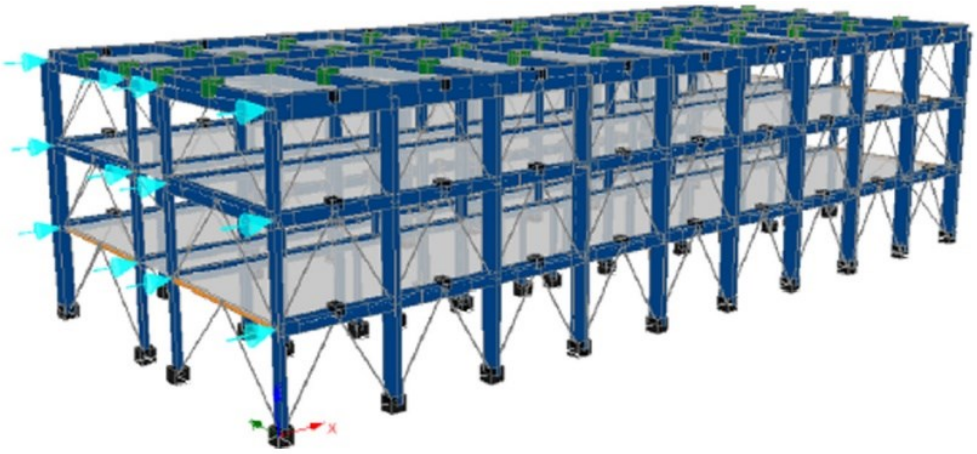

Figure 2-3 Numerical model (Almeida et al. 2017)

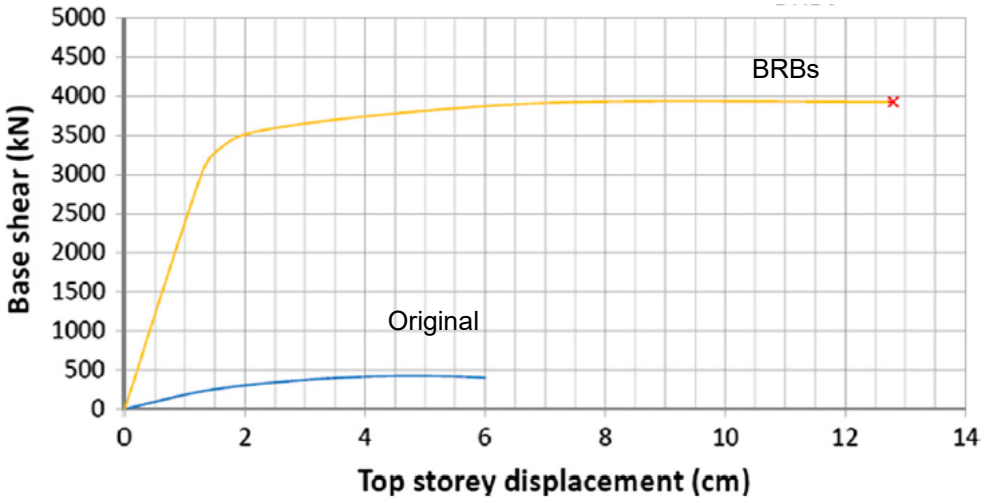

Figure 2-4 Capacity curves of original modelled structure and retrofit structure (Almeida et al. 2017)

Black et al. (2004) conducted testing on steel BRB's with cruciform steel cores in order to confirm theoretical predictions on the axial behaviour and structural stability of the braces as well as to validate their inelastic capacity under seismic conditions and calibrate a hysteretic model of the braces. For the BRB configuration considered, Black et al. (2004) found that plastic torsional buckling of the inner cruciform steel core was the most critical stability mode. Through testing and modeling it was determined that the BRB is an ideal alternative to the conventional bracing systems as it was able to improve resistance to

seismic events in new and existing structures. The BRB was able to provide the necessary rigidity to minimize and satisfy structural drift limits as well as offer considerable and repeatable energy absorption capability (Black et al. 2004).

While typically used as a reinforcing technique in buildings, Carden et al. (2004) conducted research into the use of steel BRB's aiding in the performance of steel girder bridges with ductile cross frames under seismic conditions. Steel BRB's were compared to angle section cross braces, hoping to prevent buckling as well as reduce the need for replacement post earthquake. BRB's provided better energy dissipation, lower end cross frame displacement, at a comparable level of base shear, than steel cross braces (Carden et al. 2004).

Tremblay et al. (2006) investigated two configurations of the BRB, one being the classic steel tube filled with grout, and the second being a hollow steel tube design as seen in Figure 2-5. For each configuration two core lengths were tested, 1001 mm and 2480 mm. Un-bonding material was used between the grout and the steel core for the concrete sections, however, no un-bonding material was used for the steel tube specimens. Two different loading scenarios were applied, a qualifying quasi-static cyclic test with step-wise incremental displacement amplitudes as well as dynamically applied seismic loading. Conventional bracing was also tested for comparison. While the tested conventional brace was able to withstand the qualifying quasi-static cyclic testing with incremental displacement amplitudes, it's energy-dissipation capacity was only 13% of that of the concrete filled BRB's. Both concrete filled BRB's showed elastic response and stable inelastic response under the same testing (Tremblay et al. 2006).

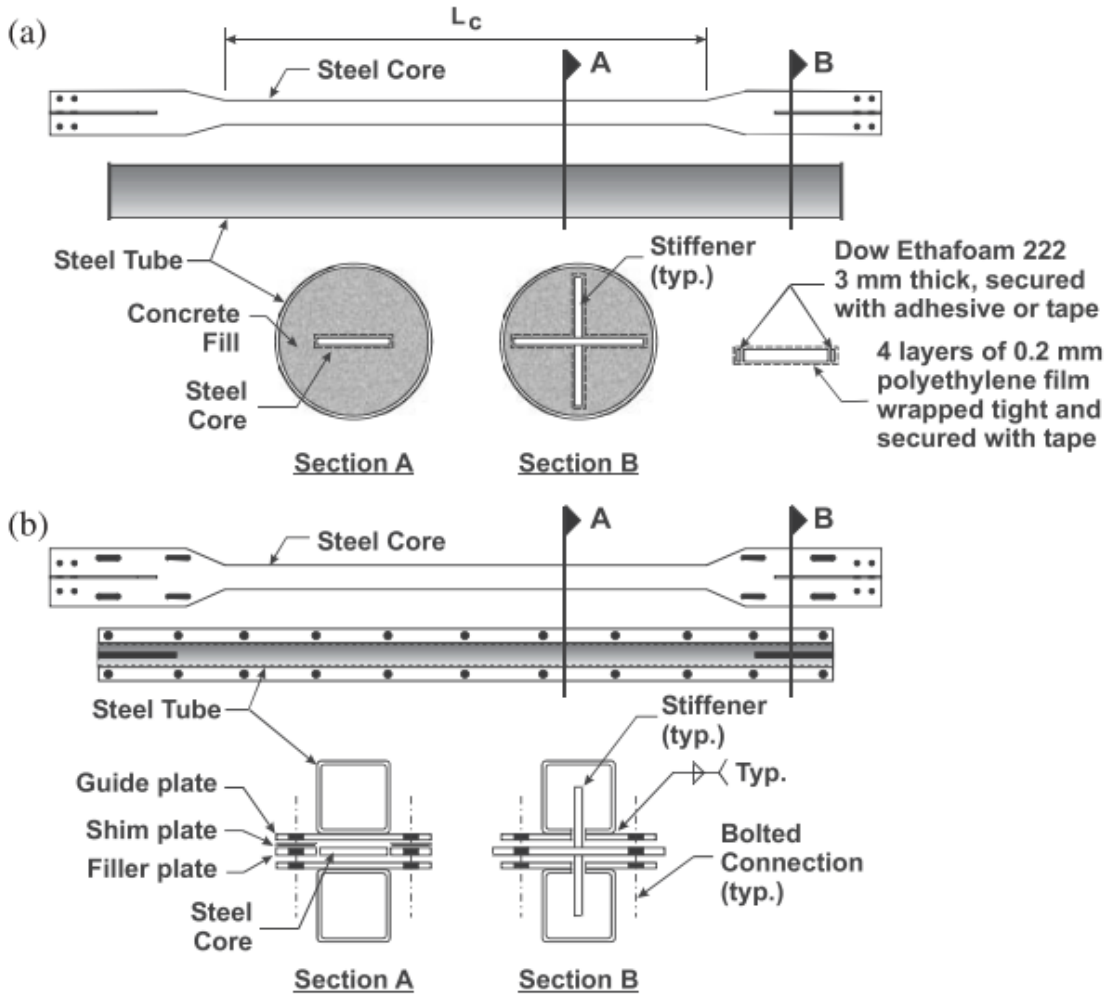

Figure 2-5 Two configurations of a BRB: (a) concrete filled tube design and (b) hollow steel tube design (Tremblay et al. 2006)

Overall, Steel-BRB's are an effective way to increase energy dissipation, ductility and over all increase the capacity when compared to a conventional slender brace. This system is known to be effective for structures in highly seismic zones and is gradually being accepted for use in bridges as well. One main downfall of this system is that it does not rehabilitate the existing structure as it is a shop fabricated solution that then must be installed in field, whether that be by removing the existing brace or installing in a new structure.

2.2 REHABILITATION WITH FIBRE REINFORCED POLYMERS

Most of the methods used to strengthen steel or concrete structures using various types of FRP involve directly wrapping the structure or member with the fabric in order to increase the strength and buckling resistance. FRP's are most commonly used to strengthen and rehabilitate reinforced concrete structures and as a result, that is where the majority of research has been focused (Ekiz and El-Tawil 2008). Although, it is becoming more commonly used and being researched more frequently on steel structures as well (Bambach et al. 2009; Ekiz and El-Tawil 2008) . This research typically investigates the use of FRP's directly bonded to concrete or embedded into the concrete as an attempt to improve flexural resistance, shear resistance, increase confinement or improve fatigue life and minimize deflections (Khorramian and Sadeghian 2019; Sadeghian et al. 2009, 2010a; b). Research has been done to investigate not only the strengthening measures mentioned, but also the performance and durability of FRP's used in these circumstances under extreme conditions, including their bond strength and fire resistance (Ekiz and El-Tawil 2008).

Bambach et al. (2009) investigated the use of carbon fibre reinforced polymer (CFRP) to strengthen thin walled steel square hollow sections (SHS) and its impact on axial capacity and design of these structures. This study was done on short SHS, with lengths three times the section dimension, in order to increase local buckling capacity, rather than on slender members requiring additional global buckling restraint. Two different CFRP layups were investigated, the first having one layer in the transverse direction (hoop) and one in the longitudinal direction. The second layup consisted of the first layup repeated twice, totaling four CFRP layers, two in each direction. Bambach et al. (2009) discuss the effect of plate slenderness on the efficiency of this strengthening technique finding that the optimum

benefit was seen around a slenderness ratio of approximately 2.5. It was found that the technique allowed for an increase in axial capacity of up to twice the steel section alone along with increase in strength to weight ratios of up to 1.5 times (Bambach et al. 2009).

Gao et al. (2013) investigated the benefits of slender tubular circular steel braces reinforced by CFRP with regards to their resistance to buckling. Gao tested seven hot-finished steel specimens with a diameter of 88.9 mm, wall thickness of 4 mm, yield strength of 355 MPa and tensile strength of 490 MPa with different number of layers of CFRP layers bonded (2, 4, 6, or 8). In order to mitigate galvanic corrosion between the CFRP and steel braces, a layer of glass fibre reinforced polymer (GFRP) was applied as a barrier between the two materials. All specimens, including two un-strengthened control specimens were tested under compression with free rotation allowed at one end. Gao insured the primary mode of failure of his specimens would be buckling by choosing a length of 2.4 metres for the specimens, or a slenderness ratio of 80. An increase in axial capacity of 24% to 84% for the 2 and 8 layers of CFRP, respectively, was reported (Gao et al. 2013). It was found that the axial load capacity (P) increased with respect to the number of CFRP layers (N_c) linearly by Equation (2-2). The CFRP layers also appeared to have increased the axial stiffness and lateral stability, seen through the increase in slope in Figure 2-6 (Gao et al. 2013).

$$P\ (kN) = 28.924 N_c\ kN + 301.81\ kN \qquad (2\text{-}2)$$

where: P is the axial load capacity

N_c is the number of CFRP layers

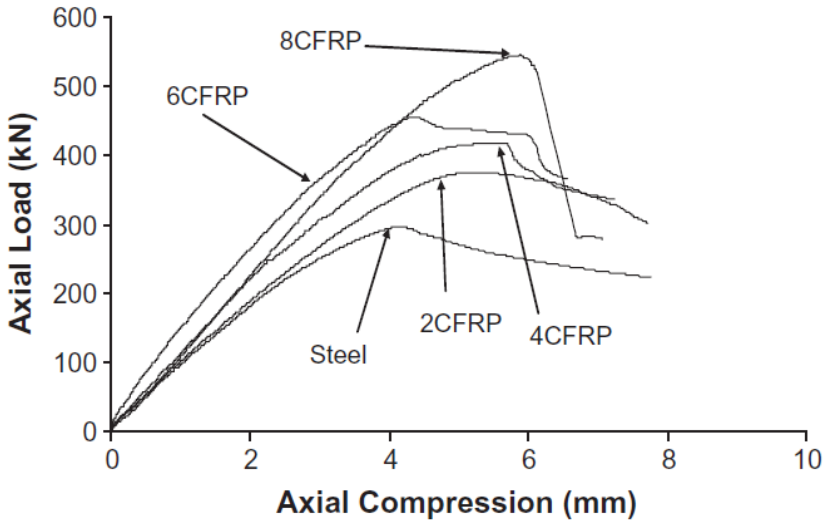

Figure 2-6 Axial load vs axial displacement of steel tubular circular specimens strengthen with CFRP (Gao et al. 2013)

Shaat and Fam (2009) investigated the behaviour of slender steel columns that had been retrofit using high-modulus CFRP plates in order to increase buckling control. Eighteen slender SHS columns at three different slenderness ratios of 46, 70 and 93 were reinforced and loaded concentrically until failure. Unidirectional CFRP plates were bonded on the two opposite sides of the SHS as shown in Figure 2-7. During testing the specimens were braced against the un-reinforced sides of the SHS to promote in-plane buckling as shown in Figure 2-8. It was found that load capacity increase ranged from 6% to 71% with an increase in stiffness ranging from 10% to 17% with the most benefit being recorded for more slender members (Shaat and Fam 2009). It was found that the CFRP could fail in crushing or debonding prior to overall system buckling, which was seen with the lowest slenderness ratio.

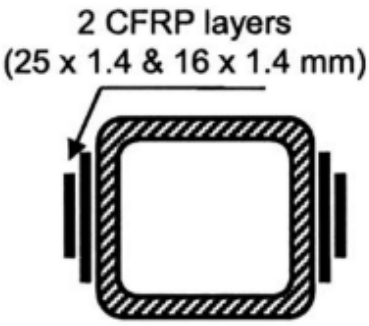

Figure 2-7 High modulus CFRP retrofitting of slender SHS columns (Shaat and Fam 2009)

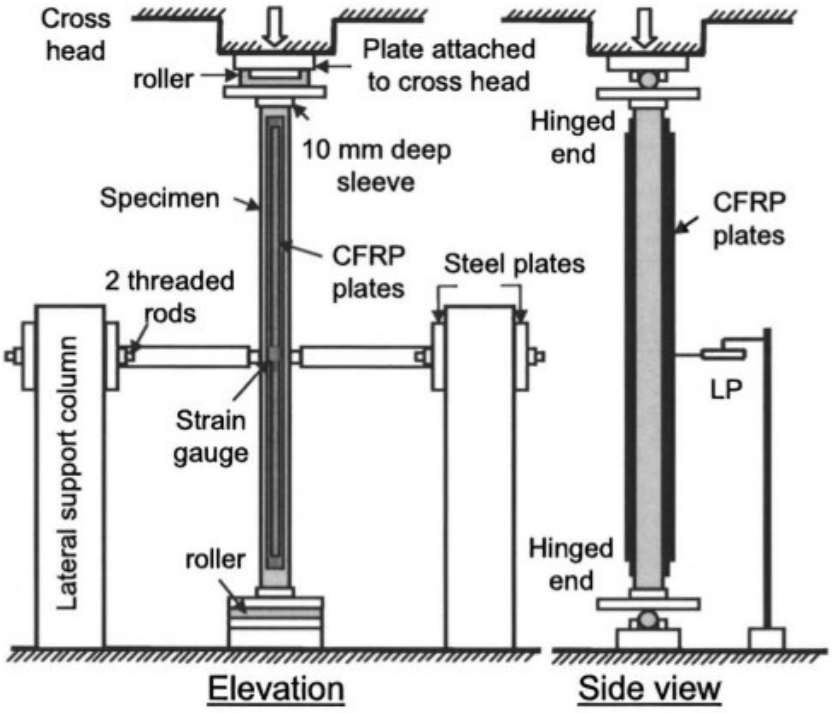

Figure 2-8 Shaat and Fam (2009) test set-up

Harries et al. (2009) conducted axial compression testing on 7 - 1.664 m long steel WT 155x10.5 sections retrofit with high strength CFRP strips or ultra high modulus GFRP strips applied along the stem of section (Harries et al. 2009). Two variations of their application were considered, first in a single layer 2-inch-wide strip or double layer 1-inch-wide along the length of the member centered 38 mm from the tip of the stem. Loading

was applied cyclically until failure occurred by either major lateral deflection or the FRP debonding. Harries (2009) found that the addition of the FRP layers had little to no effect on axial capacity, however, did allow for better control of weak-axis displacement. More load was found to be needed to achieve similar lateral displacements as the control specimens. The load required to cause a 2.5 mm deflection increased between 5% - 46% for retrofitted sections and 6% - 20% for 7.5 mm deflection (Harries et al. 2009).

Khorramian and Sadeghian (2019) investigated the use of high-modulus FRP laminates mounted near the surface of short concrete columns for the purpose of strengthening concrete columns. The columns were reinforced with four longitudinal CFRP laminate strips and loaded under various eccentricity to width ratios to combine single curvature bending and axial load. It was concluded that this technique can improve the capacity of short columns without premature buckling, debonding, or crushing of the FRP laminates. For a reinforcement ratio of 0.21% it was found that the capacities of the short columns increased by 7.7% and 10.9% for plain concrete and a 10% eccentricity to width ratio, respectively (Khorramian and Sadeghian 2019). The authors also note that this technique has potential applications for slender columns with hopes of increasing lateral stiffness and controlling buckling (Khorramian and Sadeghian 2019).

Sadeghian et al. (2009) studied the stress and strain behaviour of unreinforced slender concrete columns reinforced with various configurations of fibre orientations of unidirectional CFRP composites. 30 specimens were axially loaded in compression until failures. Strength and ductility of the columns prior to wrapping was found to decrease 38% and 60%, respectively, when increasing the slenderness ratio from 2 to 10. This was reduced to 9% and 42%, on average, when specimens were wrapped (Sadeghian et al.

2009). It was determined by the authors that CFRP composites can effectively improve the ultimate strength of the slender columns as well as improve ductility (Sadeghian et al. 2009).

The technique of FRP wrapping of both steel and concrete compression members is an efficient way to increase the strength of the member while only slightly increasing the overall weight on both concrete and steel structures. FRP wraps were seen to increase ductility as well as strength, making them a plausible solution for short compression members and slender sections. Other applications such as near surface mounting of FRP has also been seen to improve these features.

2.3 FIBRE REINFORCED POLYMER BUCKLING RESTRAINED BRACES

As fibre-reinforced polymer buckling restrained braces are not as common as steel BRB's, and therefore not always directly referred to as such, this section will discuss rehabilitation solutions with an FRP wrapping system around a core material used to provide a similar strengthening mechanism.

El-Tawil and Ekiz (2008; 2009) conducted various studies based around preventing buckling of steel braces using an FRP-BRB system comprised of CFRP wrapping blocks of sandwich material that are surrounding the steel core. Various configurations for this technique are seen in Figure 2-9. The idea behind this technique is that it would be possible for a single worker to apply this technique in the field with minimal training. It is noted that the core materials are not bonded to the steel core in these tests other than tape used to hold the blocks in place while constructing (Ekiz and El-Tawil 2008; El-Tawil and Ekiz 2009).

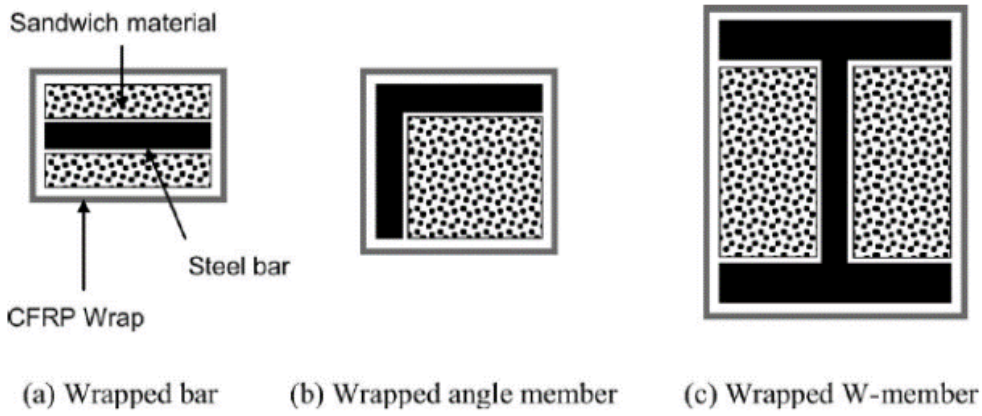

Figure 2-9 Various configurations for FRP-BRB's with CFRP wrapping (Ekiz and El-Tawil 2008)

In a series of small-scale testing (22 specimens) and computational studies Ekiz and El-Tawil (2008) investigated the behaviour of these FRP wrapped buckling restrained braces with polyvinyl chloride (PVC) and mortar block cores. Fixed end conditions were used for axial compression testing of specimens with a slenderness ratio similar to what would be found in a typical slender brace. The variables for these tests include:

- Number of longitudinal CFRP layers (1-5) paired with one transverse layer
- Core type (PVC and mortar)
- Core thickness (6.35 mm, 12.7 mm, 19 mm)
- Steel type (flat bar with three different heat treat levels)
- Steel shape (two lengths of flat plate with and with out a tapered center – as shown in Figure 2-10)
- Core and steel core bond (either bonded or unbonded)
- FRP and block core bond (either bonded or unbonded)

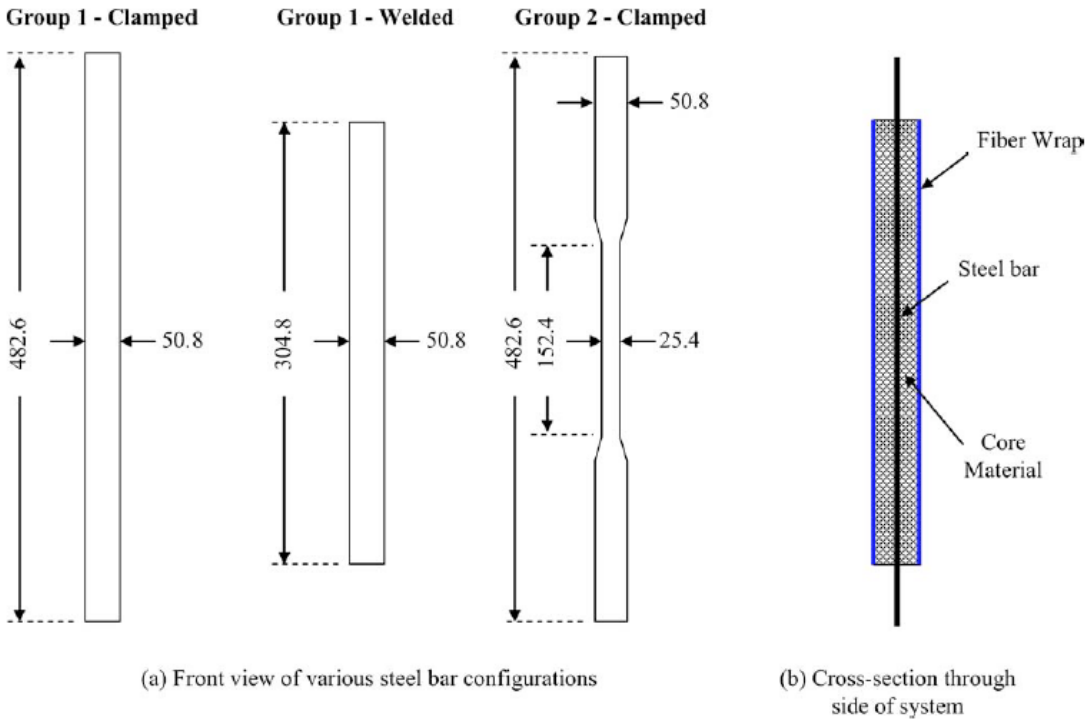

Figure 2-10 Variations in steel core for Ekiz et al. tests (Ekiz and El-Tawil 2008)

At total of 19 variables and 22 total tests, including three control specimens with no strengthening, it means that at most each combination of variables has only one specimen tested. It is assumed that this study was used to gain a broad understanding of which techniques warrant additional testing. Test outcomes were defined as yielding before buckling and buckling before yielding with the prior being considered a successful system. In addition to the experimental results, a finite element model was created to mimic the experimental scenarios tested and more conclusions were taken from the model data (Ekiz and El-Tawil 2008).

In order to investigate the effect of the number of longitudinal CFRP layers on the performance of the system the model was run holding the mortar core thickness constant at 12.7 mm with the CFRP wraps assumed to be fully bonded to the mortar core (Ekiz and El-Tawil 2008). It was concluded that buckling occurs when less than two layers of

longitudinal CFRP is used (Ekiz and El-Tawil 2008). The relationship between number of CFRP layers and system performance is shown in Figure 2-11. A similar technique was used to investigate the effect of the mortar core size as well as the effect of the bond between the CFRP layers and the mortar core. These relationships are shown in Figure 2-12 and Figure 2-13. It is seen that increasing core thickness increases strength and in the case of three CFRP layers, can change the mode of failure from buckling to yielding (Ekiz and El-Tawil 2008). The bond of the CFRP to the core has a significant impact on the strength of the system as well, changing the failure mode from buckling to yielding. The bond between the block core and the CFRP fibres was essential to prevent premature buckling of the CFRP wrap itself (Ekiz and El-Tawil 2008). Ekiz (2008) determined that the material used for the core also had an impact on the performance of the system, finding that the mortar blocks were best as they had a higher strength and stiffness than the PVC blocks. It was also determined that compressive ductility worsened when there was a bond between the steel core and the block core (Ekiz and El-Tawil 2008).

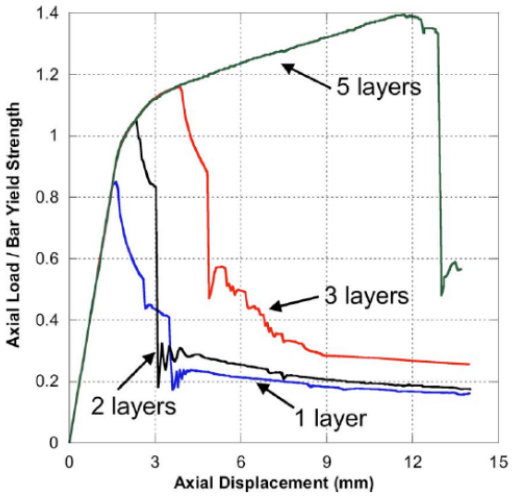

Figure 2-11 Effect of CFRP layers on FRP-BRB system response (Ekiz and El-Tawil 2008)

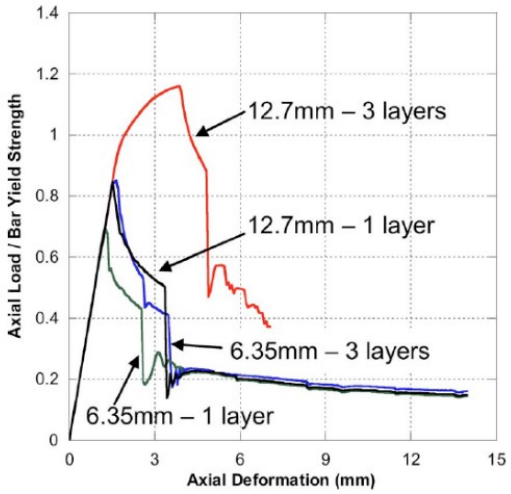

Figure 2-12 Effect of mortar block core thickness on FRP-BRB system response (Ekiz and El-Tawil 2008)

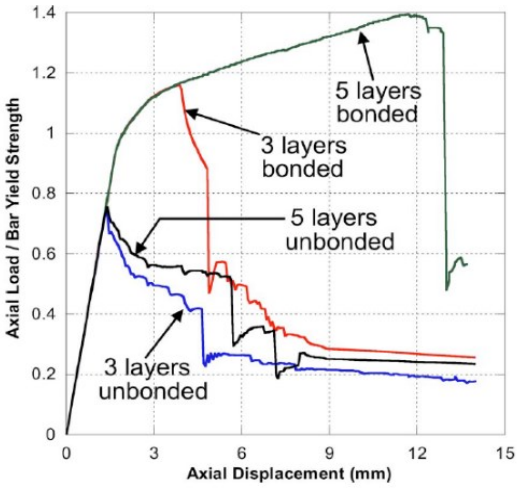

0

Figure 2-13 Effect of CFRP core bond on FRP-BRB system response (Ekiz and El-Tawil 2008)

El-Tawil and Ekiz (2009) continued this research at a larger scale with a study of seven large scale specimens fabricated using mortar blocks as the core, configuration shown in Figure 2-14, and tested under reversed axial loading in the test frame shown in Figure 2-15. El-Tawil (2009) observed that the layers of CFRP, size of core material, the bond between the CFRP and core as well the bond between the CFRP and core all had an impact on the performance of the proposed system. Double angle braces were found to benefit

more from the system compared to single angle braces with regards to early out-of-plane buckling (El-Tawil and Ekiz 2009). Buckling restrained response was achieved for up to 2% inter-story drift in testing, however the authors note that this likely requires more investigation to solidify its safety in seismic loading scenarios. The conclusion from this study on large scale braces was that the strengthening system did provide an increase in performance and energy dissipation, however, they fell short of the traditional steel-BRB system (El-Tawil and Ekiz 2009). The system does have the ability to successfully provide strengthening in situations where the member is not expected to buckle and its contribution in compression is typically ignored such as in wind bracing application (El-Tawil and Ekiz 2009).

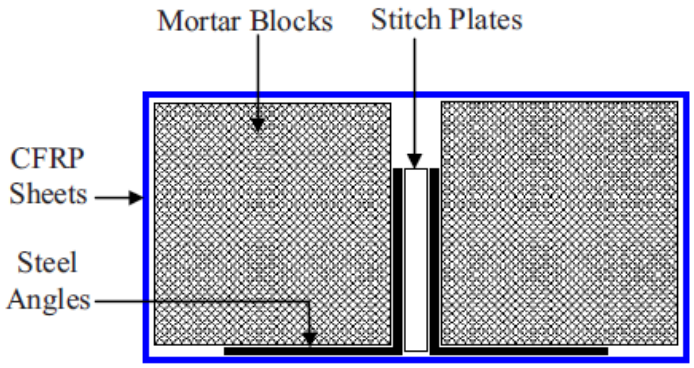

Figure 2-14 El-Tawil proposed F FRP-BRB strengthening system (El-Tawil and Ekiz 2009)

The key differences between the research of El-Tawil and Ekiz and the research presented in this thesis is that blocks of material were used for the filler, rather than a continuous pour of SCG. This study also applied a CFRP fabric after securing the filler blocks, compared to the pre-cured flexible GFRP sheets that doubled as formwork for the SCG.

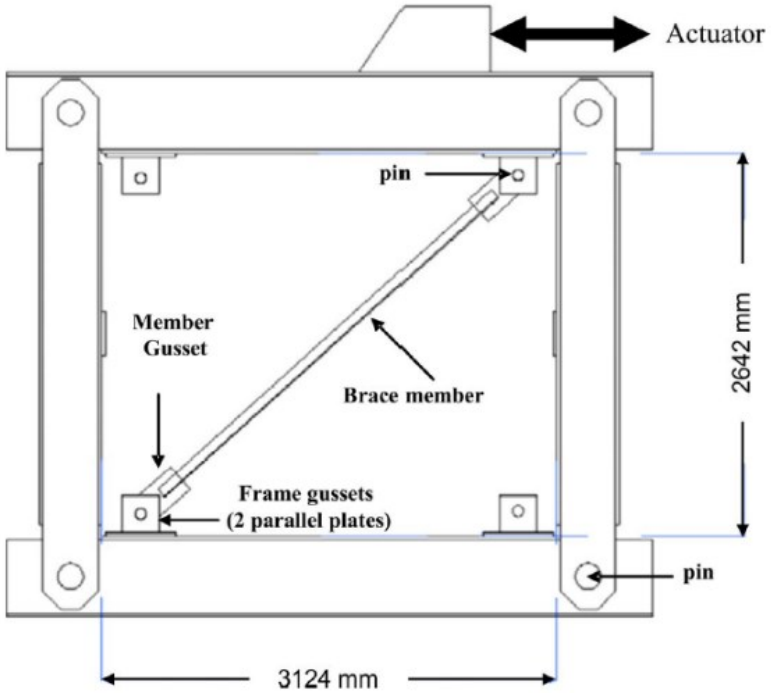

Figure 2-15 El-Tawil FRP-BRB testing configuration (El-Tawil and Ekiz 2009)

Feng et al. (2013) conducted similar research on what can be considered an FRP-BRB with the goal of strengthening steel cores with an FRP shell filled with expansive high fluidity mortar (36 MPa) (Feng et al. 2013). 18 specimens with either cross, I-shaped, circular (hollow) or square (hollow) steel cores with shell lengths corresponding to slenderness ratios of 70, 105, 140 and 175 were tested. The effect of adding layers (0, 2, or 5) transverse FRP fabrics to the ends of the GFRP tubes was also considered (Feng et al. 2013). Test end conditions were fixed and pinned as Feng (2013) noted this would simulate a case in the field where the pinned end could be released in order to allow for the GRFP tube to be added. Three failure modes were observed in these tests:

- GFRP tube splitting
- Local deformation at steel ends
- Global buckling

As the GFRP tubes used were un-directional fabric, it appears as though the splitting could be avoided or minimized if a bi-directional fabric or transverse layers in a laminate were used. Local deformation or local buckling at the ends could be mitigated by reducing un-strengthened length at the end of the system. It can be seen in Figure 2-16 that the grout did not extend to the full extents of the GFRP tube, meaning more steel at the ends was left un-supported. Feng (2013) concluded that the proposed FRP system, when used correctly provided improved bearing capacity by up to 215% and ductility increased by 877% in comparison to the un-strengthened specimens. Two layers of transverse GRFP fabric at the ends was determined to be sufficient in order to limit GRFP tube splitting. Using anymore than two layers did not provide any additional strength and were deemed redundant (Feng et al. 2013).

Figure 2-16 Cross-shaped specimen showing local buckling at ends (Feng et al. 2013)

A few differences between Feng's research and El-Tawil and Ekiz is that Feng used a solid uni-directional GFRP tube fabricated through pultrusion that is placed around the steel core where the others made use of a CFRP fabric, wrapping the core. Feng filled the FRP tube with a mortar, allowing for a continuous core bonded to the steel, where as El-Tawil and Ekiz stacked smaller mortar blocks left un-bonded to the steel core. In order to use the technique described by Feng in the field to strengthen a member, the member must be first released from one end to allow for the GFRP tube to be slid into place. This may limit the cases where it can be used as other precautions must then be taken to ensure the member can be safely released.

Han et al. (2010) conducted testing on a system with aspects similar to both El-Tawil, Ekiz and Feng. Circular tubular steel members were braced with a concrete core wrapped in bi-axial CFRP layers (1 or 2) and tested under a combined constant axial load and a cyclically increasing flexural load. Specimens were fabricated by first fitting a steel tube, either circular or square, around the member as a formwork to pour the concrete (30 MPa), followed by the removal of the steel tube and application of the CFRP. The test conditions simulated pin-pin conditions and there was no mention of a bond-release between the concrete and steel core. Han (2010) found that at the peak load for this system, longitudinal rupture of the CFRP wrapping occurred. Increasing the number of FRP layers applied had little influence on the elastic stiffness of the specimens, however it increased the elastic-plastic stiffness (Han et al. 2010). Ultimate lateral strength was found to increase 20.2% for circular specimens with two CFRP layers when compared to specimens with one layer. This relationship is less prominent for square specimens, seeing only 12.2% increase in strength (Han et al. 2010). Specimens showed energy dissipated at high levels before peak

load rupture in the longitudinal CFRP followed by a drop in the load capacity (Han et al. 2010). While this solution provided good results, it seems that this option is lacking in the sense that it would be very difficult to implement in field due to the steel tube formwork. One solution to that would be a two-part steel jacket to form the formwork.

Kaya et al. (2015) researched the possibility of repairing previously buckled and corroded short steel I-shape columns with concrete filled GFRP jackets. The GFRP used in this research was previously cured sheets able to hold their own shape, making it possible to create a tubular shell around the damaged steel section, doubling as formwork for the concrete. This allows for this rehabilitation method to be used in field as an emergency fix. Kaya (2015) tested 13 strengthen specimens at various lengths and levels of corrosion under axial compression. It was found that the buckled columns were able to regain between 69% and 104% of their original undamaged column strength (Kaya et al. 2015). This method of reinforcing is practical for use in-situ as the shell duals as formwork and can be wrapped around the damaged member. This technique is similar to the rehabilitation technique investigated in this research with the exception that it was tested on short columns. Kaya et al. (2015) also installed additional reinforcing steel in the concrete encasing the damaged member for six of the 13 specimens. The concrete in the study was also permitted to bond to the steel.

In similar research to Kaya et al. (2015), Liu et al. (2005) investigated the use of GFRP pipes filled with light-weight concrete used to rehabilitate corroded steel compression members. Seven specimens were tested with notched steel cross sections to represent corroded sections, along with various lengths of FRP tube and either expansive or non-expansive concrete. The concrete was permitted to bond to the steel core. The failure mode

for all specimens was buckling at different loads and locations. All reinforced sections buckled at the end of the jacketed reinforcement, as opposed to the unreinforced controls which buckled around the midpoint. All reinforced specimens successfully increased the load capacity of the notched specimens by 58% to 233%, with all but one, strengthened to sustain more load than the un-notched control specimens (Liu et al. 2005). Liu et al. (2005) found that the specimens retrofit with expansive concrete withstood 15% higher loads than the specimens with non-expansive concrete. This was suspected to have been as a result of active confinement. This research implied that it could be used as a retrofit technique for corroded steel compression members. It was not noted how the FRP tubes would be jacketed over the steel members in-situ.

From this research it can be seen that an FRP-BRB system provides an ideal solution, comparable to the steel-BRB system, for use in rehabilitation scenarios. All systems were capable of increasing the overall strength and ductility of the steel core, whether damaged or not, which resonates with the goals of the standard BRB system. Systems were able to dissipate energy well, making it a feasible option for seismic upgrade. Another key feature of the FRP-BRB system is that there are ways to install the system such that the existing member doesn't need to be removed or released from the structure. Drawing on various successful techniques and improving on mistakes made in some of the research investigated, the study completed in this thesis was formed. This concluded with a system that would be applicable for in-field rehabilitation, similar to El-Tawil, Ekiz and Kaya, but using a continuous core of self consolidating grout, unbonded to the slender steel core, in conjunction with a pre-cured flexible GFRP sheet that doubled as formwork for the grout.

2.3.1 Sustainable Grout and Self Consolidating Grout

One important component of any BRB or FRP-BRB is the material used to fill the gap between the core and the tubing or shell. This material must provide sufficient lateral support to the core brace. While many options exist for this material, grout or concrete is the most common choice as it can easily be modified to suit the conditions. Due to space and accessibility constraints, regular concrete may not be practical as tamping or vibrating for adequate consolidation may not be possible. An alternate to standard concrete or grout is self-consolidating concrete (SCC) or self-consolidating grout (SCG). Self-consolidating concrete or grout eliminates the need for vibration of the concrete in order to achieve good consolidation as it is highly flowable (Pedersen 2004).

In order to have a highly fluid concrete a filler is commonly used, which in turn allows the concrete to be more economically and environmentally friendly all the while meeting its required technical properties (Pedersen 2004). Fillers can be efficiently used to enhance the viscosity of SCC (Elyamany et al. 2014). Fillers are materials that are added to the mixture to reduce the use or need for another more expensive material, or to improve or vary other properties of the concrete. There are a wide variety of fillers that can be used for these purposes. The majority of these are derived from industrial processes, making the use of fillers environmentally and economically sustainable. More information and investigation on the impact and behaviour of fillers in concrete is provided in Appendix A.

CHAPTER 3 EXPERIMENTAL PROGRAM

This section will outline the experimental program for the testing of the small-scale specimens. The test matrix will be described for the small-scale specimens. All materials and their properties will be outlined along with a detailed explanation of the fabrication and testing of the specimens. The failure modes will be demonstrated and test results, including load-stroke behaviour, load-lateral displacement behaviour and load-strain behaviour will be provided and discussed. The contribution of each component of the specimen to the total load will also be calculated and discussed.

3.1 TEST MATRIX

A total of 27 FRP composite shells were prepared with three different lengths (300 mm, 600 mm, and 900 mm) and with three different diameter molds, leading to three different inner diameters. These three molds corresponded to outer diameters of 41 mm, 53 mm and 65 mm. Hot rolled steel bars (25.4 mm x 6.35 mm) were cut at lengths 30 mm longer than their corresponding shell lengths. Bars were prepared with 45 mm long tapered tabs on all ends. The steel was grouted inside the corresponding shell length. Fabrication of each component will be further discussed in Section 3.3. For each diameter and length shell, three identical samples were made as shown in Table 3-1. The test samples are identified with the specimen identification (ID) as LX-DY(Z), where X stands for the length of the FRP shell of 300 mm (L300), 600 mm (L600) and 900 mm (L900); Y stands for the size ranking of the outer diameter of the FRP shell with D1 corresponding to the smallest diameter and D3 to the largest for that group; and Z is the sample number of either 1, 2 or

3. As an example, L300-D2(2) is a specimen with a 300 mm long shell, a 53 mm outer diameter shell and is the 2nd of three identical samples.

Along with the 27 reinforced specimens, 9 plain steel samples were fabricated and tested. These specimens were identical to the steel cores of the reinforced specimens and three of each length were tested. Specimens are identified by the length of the FRP shell that they would have been reinforced with, as well the sample number of the size (1, 2, or 3). For example, the second of its kind plain steel specimen with overall length of 630 mm is identified as L600(2). Table 3-1 provides a summary of all specimens. It should be noted that the unsupported length of all specimens is 10 mm shorter than the overall steel core length. This is due to the test set-up and will be further explained in Section 3.4.

Table 3-1 Small scale specimen test matrix

Group ID	Steel Core Length (mm)	Slenderness Ratio of Steel Core	FRP Shell Length (mm)	FRP Shell Outer Diameter (mm)	FRP Shell Inner Diameter (mm)	Number of Specimens
L300	330	180	N/A	N/A	N/A	3
L300-D1				41	34.5	3
L300-D2	330		300	53	49	3
L300-D3				65	61	3
L600	630	343	N/A	N/A	N/A	3
L600-D1				38	34.5	3
L600-D2	630		600	53	49	3
L600-D3				65	61	3
L900	930	507	N/A	N/A	N/A	3
L900-D1				41	34.5	3
L900-D2	930		900	53	49	3
L900-D3				65	61	3
					Total	36

It is noted that due to difficulty in fabricating the smallest diameter, the L600 specimens were observed to have outer diameters of 38 mm rather than 41 mm.

3.2 MATERIAL PROPERTIES

All materials used in the fabrication of the small scale FRP-BRB specimens and their properties will be outlined in this section. Manufacturer details and test results from tests done to confirm the properties will be provided. The three main components of the small-scale test specimens include glass fibre-reinforced polymer shells, hot rolled 1018 mild/low carbon steel and a self-consolidating grout.

3.2.1 Fibre Reinforced Polymer Shell

FRP shells were fabricated of PipeMedic PG16.15, a glass fibre biaxial pre-impregnated laminate in conjunction with QuakeBond™ J201TC Tack Coat structural epoxy (adhesive) (QuakeWrap Inc. n.d., n.d.). Shells were constructed to have two layers of the laminate with approximately one quarter of the circumference in overlap. The manufacturer (QuakeWrap Inc., Tucson, AZ, USA) reports that the FRP laminate in the longitudinal (warp) direction of the roll has a tensile strength of 431 MPa, a modulus of elasticity of 24,140 MPa , and an ultimate elongation of 1.31% (QuakeWrap Inc. n.d.). It is reported that in the transverse (fill) direction of the roll the FRP has a tensile strength of 418 MPa, a modulus of elasticity of 25,250 MPa, and an ultimate elongation of 1.06% (QuakeWrap Inc. n.d.). The material is reported to have a ply thickness of 0.66 mm (QuakeWrap Inc. n.d.), however this was measured to be approximately 0.35 mm.

Five identical coupons in both the warp (i.e. longitudinal direction of roll) and fill (i.e. transverse direction of roll) directions of the FRP were prepared and tested in tension. Coupons consisted of 4 layers of the FRP with approximately 1 mm of adhesive between layers and were prepared and tested as per American Society for Testing and Materials

(ASTM) D3039 (2014) and ASTM D7565 (2010a). In the warp direction, the test results showed an average modulus of elasticity of 17.16 ± 0.47 GPa (using longitudinal strain range 1000 – 3000 με), average rupture stress of 192.79 ± 1.54 MPa, average rupture strain of 0.01330 ± 0.00037 mm/mm and a secant modulus of 14,504 ± 285.15 MPa. The secant modulus is the slope of the stress-strain curve assuming the behaviour was linear up to the rupture, calculated by dividing the rupture stress by the rupture strain. In the fill direction, the test results showed an average modulus of elasticity of 14.14 ± 0.20 GPa, average rupture stress of 141.16 ± 16.06 MPa, average rupture strain of 0.01162 ± 0.00167 mm/mm and a secant modulus of 12,191 ± 392.6 MPa. Two of the five identical coupons in the warp direction were excluded from the results as they did not fit the trend. Figure 3-1 shows the experimental stress-strain relationship for both the warp and fill directions of the FRP laminate. The test set-up and tested specimens are shown in Figure 3-2.

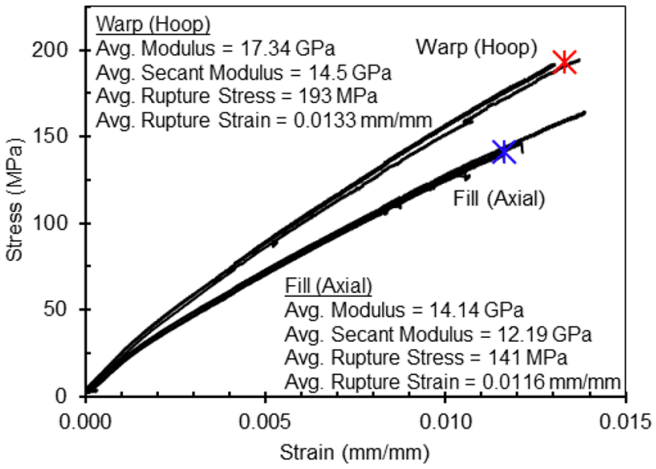

Figure 3-1 FRP laminate stress-strain behaviours in the fill and warp directions (Note: nominal thickness of 0.35 mm was used). The stars noted on each curve mark the average rupture point.

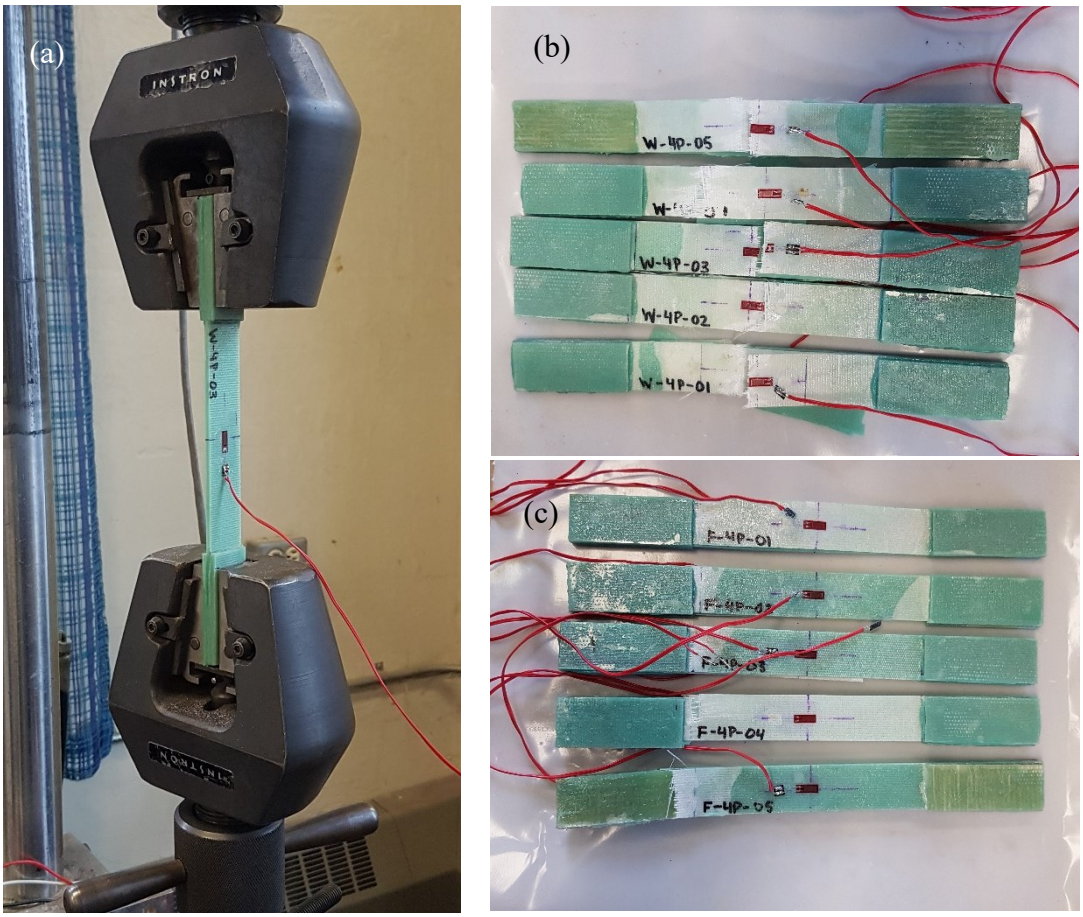

Figure 3-2 FRP tension testing: (a) test set-up; (b) tested warp specimens and L-3; and (c) tested fill specimens.

3.2.2 Steel Core

The hot rolled steel bars used for the specimens were 1018 mild/low carbon steel with a manufacturer recorded tensile yield strength of 310 MPa (Alro Steel n.d.). Steel dog-bone coupons were fabricated and tested in tension as per ASTM A370-17a (ASTM 2017). Specimens L-1, L-2 and L-3 had an overall length of 215 mm and S-3 had an overall length of 190 mm. It should be noted that specimen S-3 had identical gauge length to the other three specimens, but had 50.8 mm tab lengths, rather than 63.5 mm. Two strain gauges were applied to the steel bar, one on either side at the middle of the coupon. An extensometer was also installed for testing, but the data was determined to be unreliable

due to calibration problems and therefore the modulus and yield stress were calculated by the strain data. Coupons were tested in tension at a constant strain rate of 2 mm/min on an Instron 8501 Universal Testing Machine. The modulus of elasticity of the steel was found by analysing the slope of the linear portion of the stress-strain diagram. Yield strength was determined by two methods, the first being a visual peak and the second using a 2% offset in the linear section. The results from these two methods were similar. The visual yield stress was reported as inconclusive when there was no obvious peak (L-1 and L-3), this was likely due to the strain gauge being slightly outside of the region where yielding occurred. Tests concluded that the steel core material has a modulus of elasticity of 194.8 GPa and a yield strength of 353 MPa. The summary from these tests is provided in Table 3-2. L-3 data was excluded when calculating the yield stress for the steel as it was deemed unreliable through observation of the graph and comparison with other specimens. The test stress strain diagram is provided in Figure 3-3 and the test set-up and tested steel coupons are shown in Figure 3-4.

Table 3-2 Steel dog bone tensile test summary

Specimen	Modulus by Steel Strain (GPa)	Visual Yield Stress (MPa)	2% Offset Yield Stress (MPa)
L-1	194.0	Inconclusive	350
L-2	196.8	362.6	362
L-3	192.4	Inconclusive	401
S-3	196.0	346.5	347
Average	**194.8**	**354.6**	**353***

* excluding L-3 yield stress

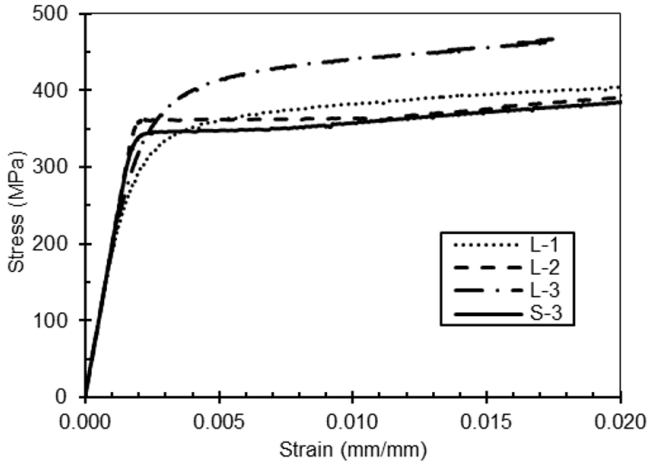

Figure 3-3 Steel tension test stress strain diagram

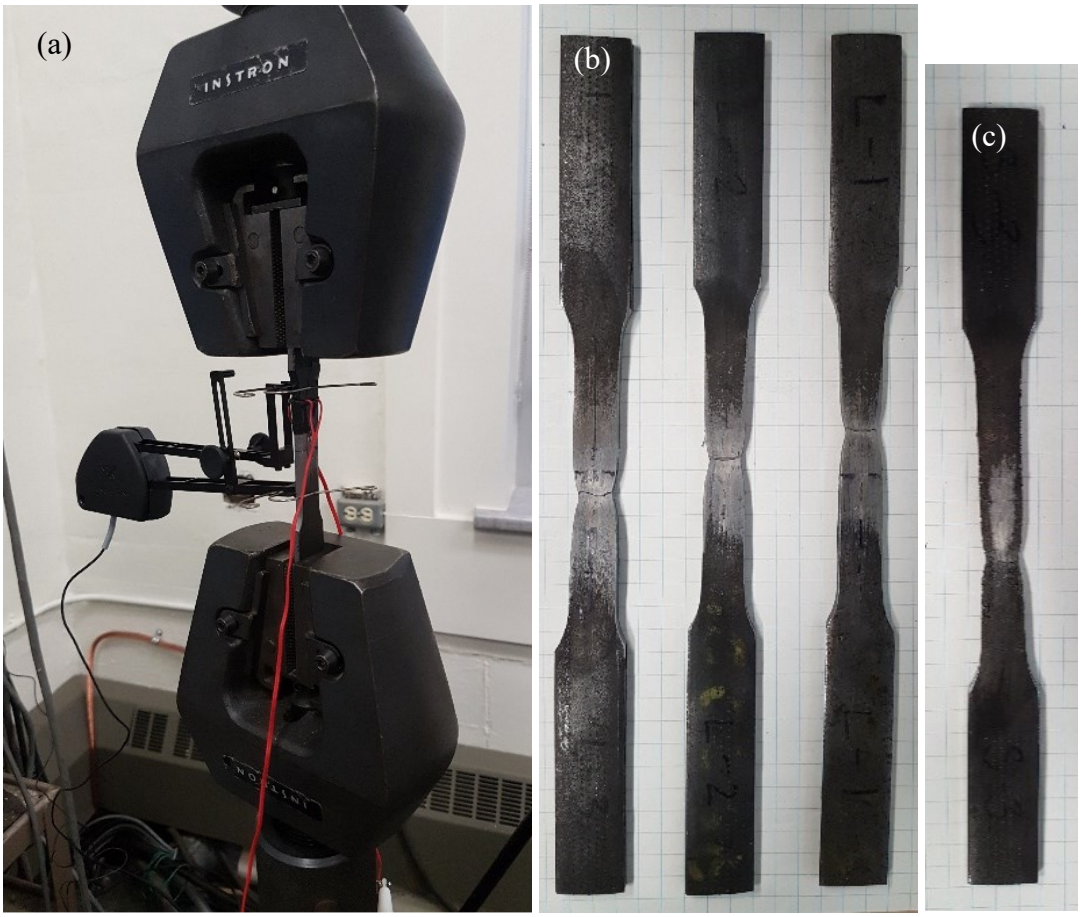

Figure 3-4 Steel tension testing: (a) test set-up; (b) tested specimens L-1, L-2 and L-3; and (c) tested specimen S-3.

3.2.3 Self Consolidating Grout

The self consolidating grout was designed to have a 28-day compressive strength of approximately 35 MPa with a high slump to allow for the grout to flow easily into the FRP shells with no vibration or consolidation required. The grout is composed of masonry sand (Shaw Resources), CRH Type N cement, Euclid Plastol 6400 superplasticizer, and water with the proportions for 1 m^3 batch shown in Table 3-3.

Table 3-3 Grout mix design for 1 m^3 batch size

Item	Bulk Density (kg/m^3)	Volume (m^3)	Percent by Volume	Weight (kg)	Percent by Weight
Water	1000	0.18	17.96	179.66	12.78
Cement	1365	0.50	49.00	668.83	47.57
Sand	1694	0.33	32.67	553.35	39.36
Superplasticizer	1090	0.0037	0.37	4.04	0.29
Total	-	1.00	100.00	1405.88	100.00

The L300, L600, and L900 specimens were fabricated with grouts having compressive strengths of 34.7 MPa, 19.5 MPa, and 34.4 MPa, respectively. The goal was to have a grout strength of 35 MPa for all specimens and the mix was designed as such, however, due to unforeseen problems, this was not achieved. The discrepancy between the L600 grout strength and the L300 and L900 batch is not fully understood. All batches of grout for each length were cast with the same proportions, only varying volume in order to fill the appropriate shell length. As all three batches of the L600 grout were similar grout strengths, it seems less likely that there was an error in the measurement of the various components. As the L600 batches were cast much later over the course of the experiment and new sand

was used, it is possible that the moisture content of the sand was higher than when the L300 and L900 specimens were cast, thus weakening the grout. Other discrepancies may come from the curing phase of these specimens. Each batch was cast at a different time in the year, which may have led to variations in the temperature and humidity of the room in which the specimens were cured. Another possibility for the discrepancy is a possible issue with the scale used for measuring the components. As the only component that was not weighed is the water, which was measured by volume with a graduated cylinder, if the scale was reading a higher value than what was being measured the grout would be weaker than excepted. As high grout strength was not required for the FRP-BRB system to be effective, the difference in the grout strength was not an issue.

3.2.3.1 Oyster Shell Powder Self Consolidating Grout

As a high strength grout was not required for the fabrication of these specimens, a study was conducted with regards to an environmentally sustainable self consolidating grout. This study investigates the addition of fine ground oyster shells as a filler used to replace sand in self-consolidating grout. The concept investigated was not used for the small-scale specimens. The paper, provided in Appendix B, was published in the 2018 Canadian Society for Civil Engineering (CSCE) Conference proceedings.

3.3 SPECIMEN FABRICATION

The following sections will outline the process of fabricating the small-scale specimens for testing. This includes fabrication and curing of the FRP shells, the preparation of the steel cores and finally casting and curing of the complete system.

3.3.1 FRP Shell Fabrication

The FRP laminate was cut to the appropriate length and width allowing for 2 layers and ¼ overlap, where the warp direction of the roll of material was the hoop direction of the shell. The two-part adhesive, in the respective required quantities, was mixed manually until a uniform colour was achieved. Adhesive was then applied at approximately 1 mm thickness over all but one circumference in width of the sheet, as shown in Figure 3-5. PVC pipes of outer diameters 33.5 mm, 48.1 mm and 60.2 mm were covered in a thin layer of plastic to inhibit accidental bonding to the pipe and facilitate removal of the FRP shell once cured. One, two or three people, depending on the length of the shell being wrapped, slowly wrapped the FRP around the PVC tubing with constant pressure. It was important to ensure that consistent and minimal force was placed on the tube while wrapping to ensure that the adhesive was not pushed out between the layers. A plastic sheet was then wrapped around the wet shell and fully taped to ensure the shell did not come un-wrapped or loosen during curing. Photos of this process are provided in Figure 3-5. After 24 hours of curing the shells were unwrapped and removed from the PVC. Excess adhesive was sanded from the ends of the shells where necessary.

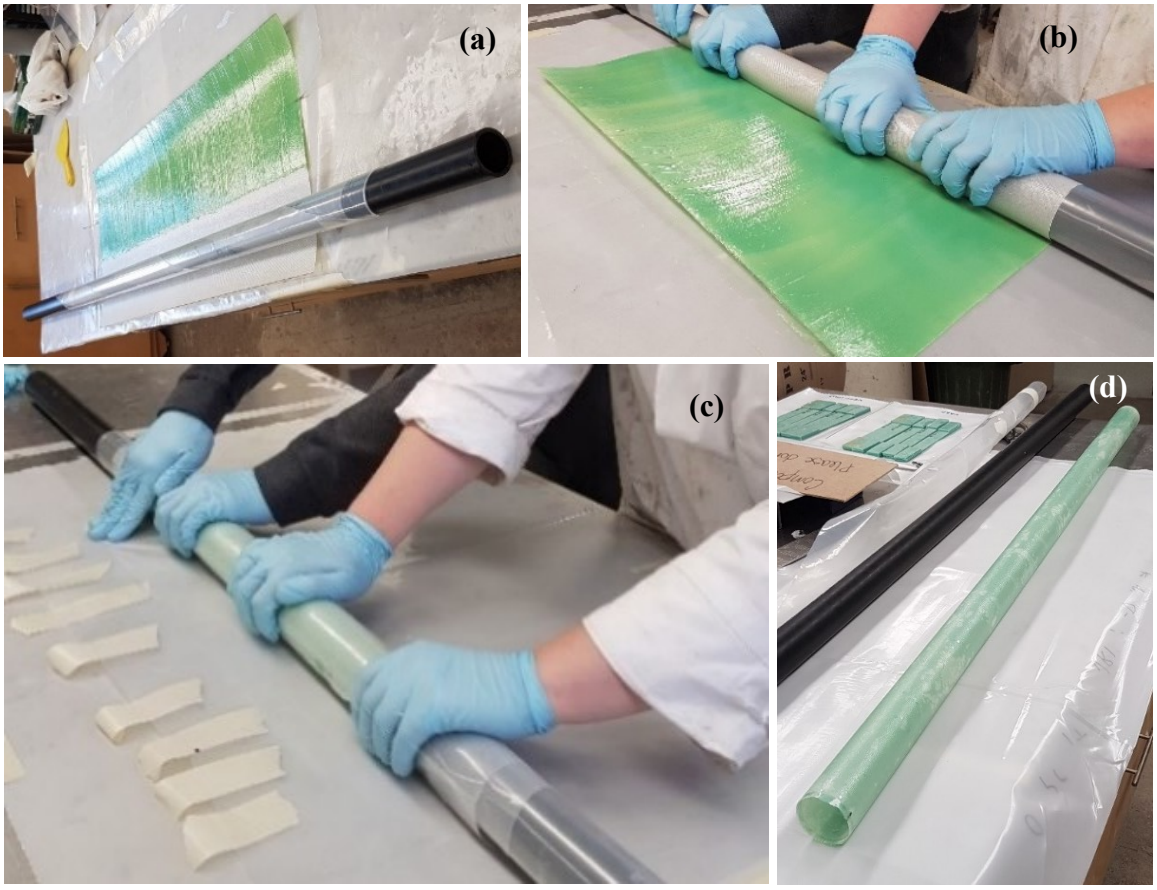

Figure 3-5 FRP shell fabrication: (a) FRP sheet cut to size, two-part adhesive mixed and applied in 1 mm layer; (b) shell is wrapped around PVC tube; (c) plastic layer is wrapped around shell and entire length of shell is taped; (d) once shell is cured, shell is removed from PVC tube and unwrapped.

3.3.2 Steel Core Preparation

Steel cores were prepared with 45 mm long tapered tabs, as seen in Figure 3-6 and Figure 3-7, in order to avoid premature local buckling at the fixtures during testing. Small pieces of expanded polystyrene were glued to the steel tabs at the ends of the steel cores to limit the transfer of force into the grout during testing. The cores were then coated in a thin layer of petroleum jelly, allowing the concrete and steel to act independently of the grout. Photos of the preparation of the steel cores are included in Figure 3-7.

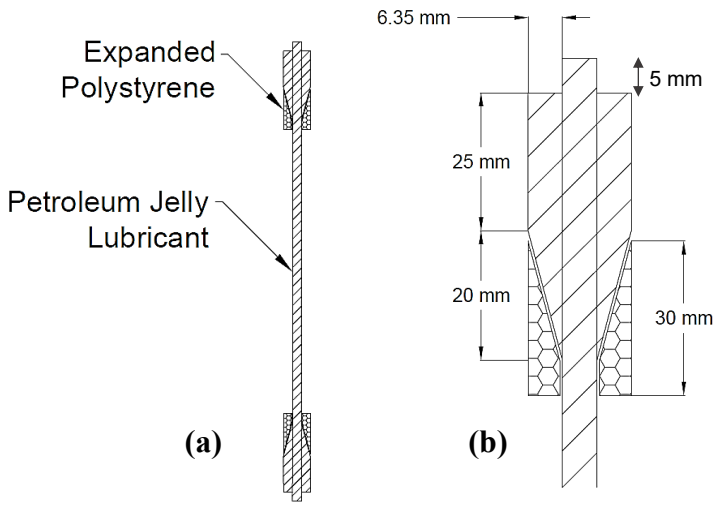

Figure 3-6 Drawing of (a) prepared steel core and (b) close up of end details

Figure 3-7 Details of steel cores: (a) expanded polystyrene on steel tabs; and (b) steel core coated in petroleum jelly.

3.3.3 Casting and Curing

A wood stand was designed to keep the steel centered within the FRP shell while casting and curing the grout. Figure 3-8 shows the frame used for casting the small-scale FRP-

BRB specimens. The stand was fabricated to allow for one specimen of each diameter at equal height to be cast at one time. The top cover of the stand allowed for adjustment to the three different heights. To ensure that the steel remained centered in the shell while curing, cut outs on the top cover and bottom were cut and aligned to restrict movement. As the shell outer diameters vary slightly the shells were shimmed to be centred around the steel core on top and bottom. A clear piece of plastic was used as the top cover so alignment could be visually confirmed.

Figure 3-8 FRP-BRB casting frame

The FRP shells were placed into the base of the stand and the steel cores were locked into their aligning slots. The middle top layer of the frame was secured at the appropriate height by four wood blocks screwed into the frame. The self consolidating grout was then funnelled into the shell until it reached the top and the clear plastic cover was lowered onto

the specimens. The alignment of the steel core and FRP tube was confirmed visually and using a level. This process is shown in Figure 3-9. All composite samples were cured in plastic bags at room temperature for a minimum of 28 days.

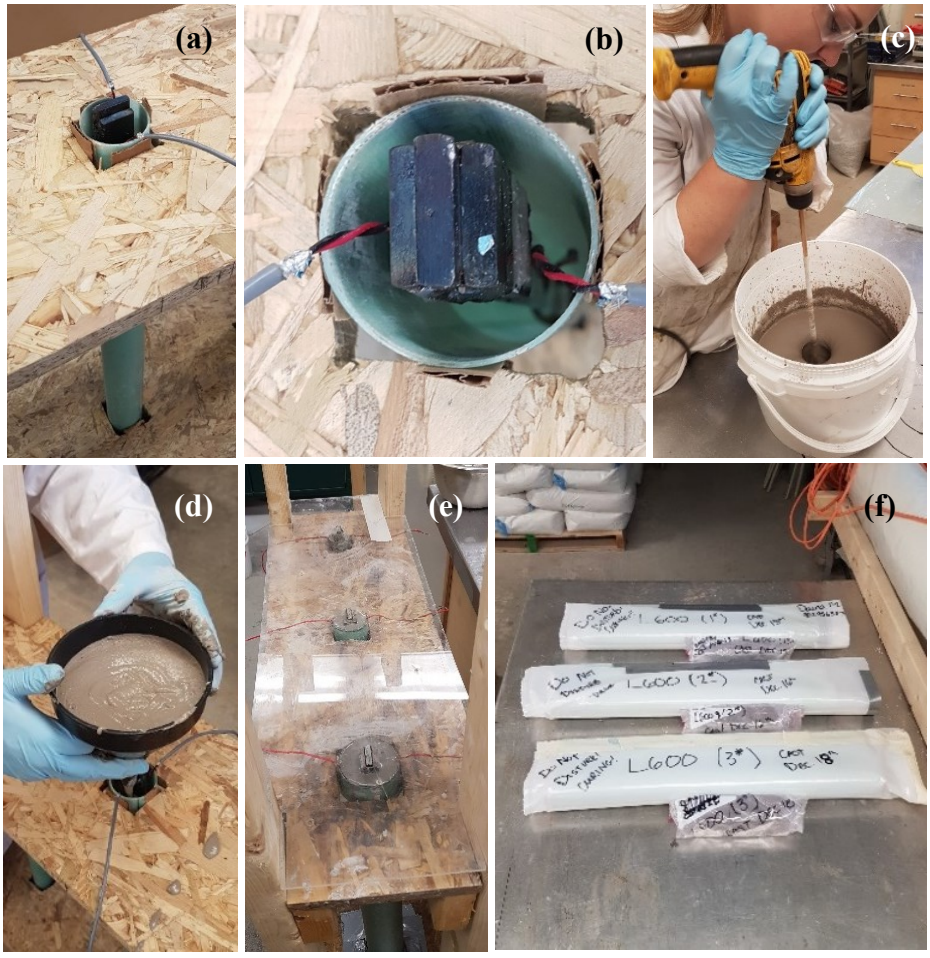

Figure 3-9 Specimen fabrication: (a) & (b) tube is shimmed to ensure steel core and FRP tube are aligned; (c) self-consolidating grout is mixed; (d) grout is funneled into FRP tube; (e) fiberglass cover is placed; (f) specimens removed after 24 hours and cured in plastic bags at room temperature.

3.4 INSTRUMENTATION AND TEST SET-UP

Both ends of each specimen were wrapped with a 75 mm width of basalt fiber using an epoxy resin as the matrix. Two layers were applied with the fibres in the axial direction and two and a half layers were applied with fibres in the hoop direction. This ensured the

test results would not be governed by imperfect end conditions of the test fixture or bursting at the ends. Pin-pin conditions were simulated with test fixtures that allowed for 5 mm of steel to be slotted into the plate on either end, preventing slip out but allowing for small rotation. Before being cast into the FRP shells, two strain gauges (SG1 and SG2) were installed at mid-height on each steel core as shown in Figure 3-10. These were used to measure the axial strain on the internal steel core. Once the specimens were prepared and cured two more strain gauges were installed at the mid-height on the surface of the FRP shell. These strain gauges (SG3 and SG4) were installed to measure the axial strain of the FRP shell. In addition to the strain gauges, two lateral potentiometers (LP1 and LP2) were set up along the longitudinal axis of the specimen to measure the extent of the lateral displacement at mid-height. In order to ensure the lateral potentiometers did not slip off during testing, and to allow the placement to be directly over the strain gauges, small aluminum plates were installed bridging the strain gauges. In addition to the equipment mentioned, the tests were recorded with a camera and a ruler was placed just behind the specimen at mid-height to allow for verification of the test data if the need arose. The test set up is shown in Figure 3-10 and Figure 3-11. Once specimens were fully prepared and cured, they were tested in compression using a 2 MN universal testing machine. The loading rate of the machine was set to have an overall strain rate of 2 mm/min. Load, displacement, and strain data were collected by a data acquisition system with 10 Hz frequency for the L300 specimens and 100 Hz frequency for the L600 and L900 specimens.

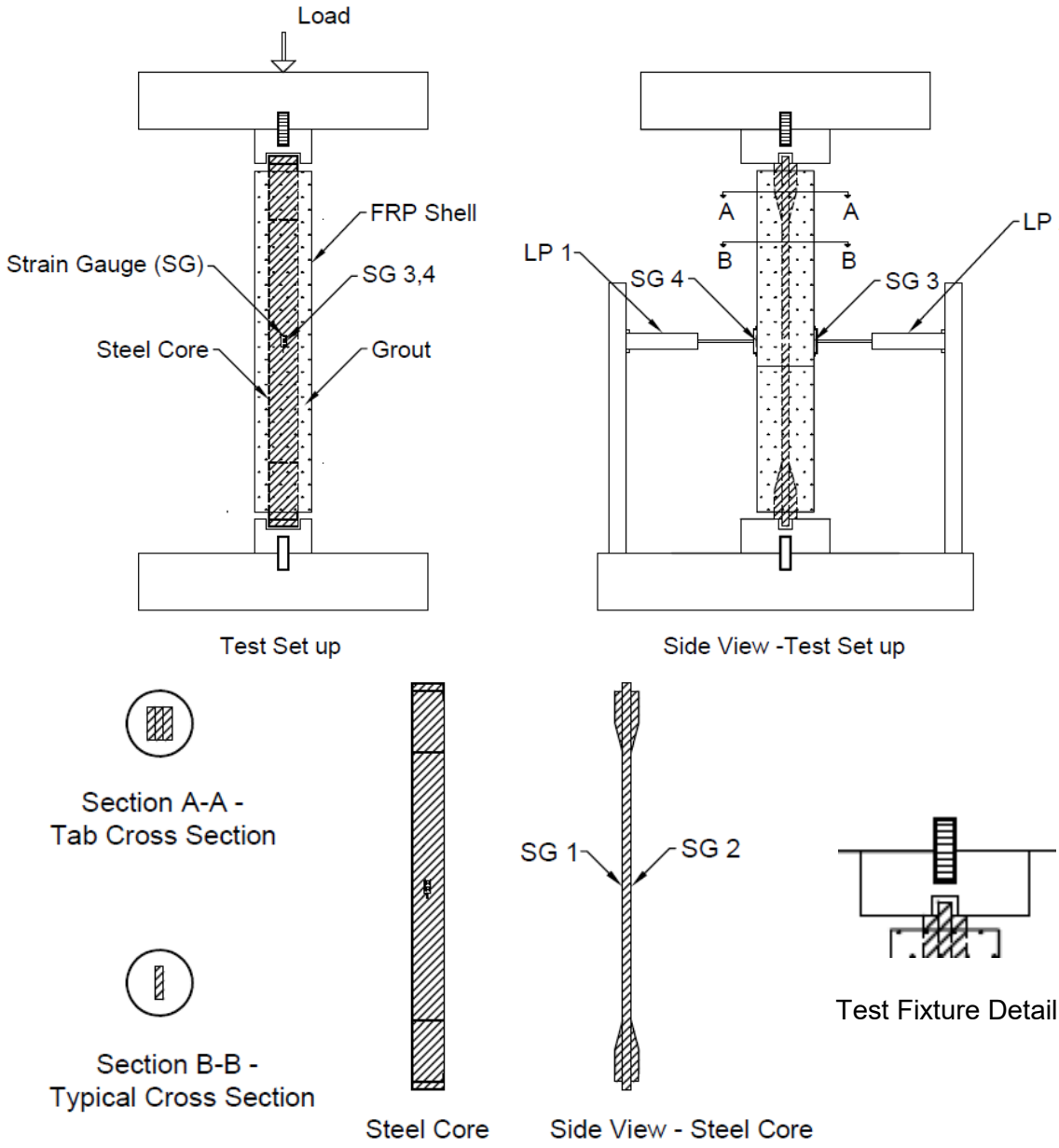

Figure 3-10 Drawing of test set-up

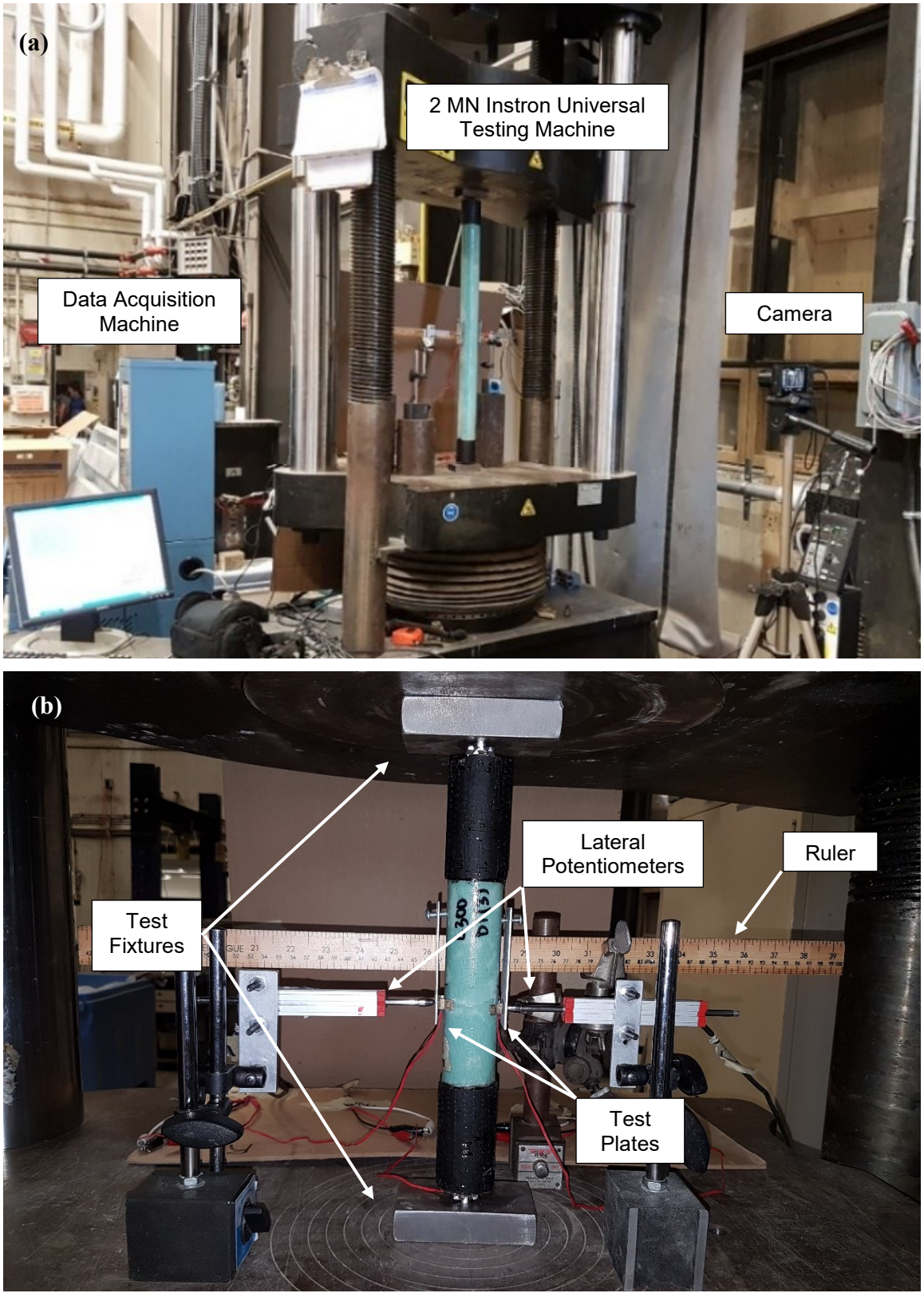

Figure 3-11 Picture of test set-up: (a) overview and (b) close up of set-up (L300 D1(3) photographed)

3.5 TEST RESULTS AND DISCUSSION

The following section will present the results from the testing of all small-scale FRP-BRB specimens. The failure modes, load-stroke behaviour, load-lateral displacement behaviour, and load-strain behaviour will be analyzed. In addition, the contribution of each component to the overall load capacity through the test will be discussed.

3.5.1 Failure Modes

Two methods of failure were considered for the compression testing of the small scale FRP-BRB specimens, yielding of the steel core and overall system buckling. The failure mode was not necessarily the ultimate failure mode of the specimen, in particular for the specimens that yielded, more load was often taken by the specimen until ultimate rupture or buckling. A photo of all tested specimens is provided in Figure 3-12 and a summary of all test results is provided in Table 3-4. All but L300 D2 and D3 specimens ultimately failed with the whole system buckling which failed by the FRP and grout rupturing as is seen in Figure 3-12.

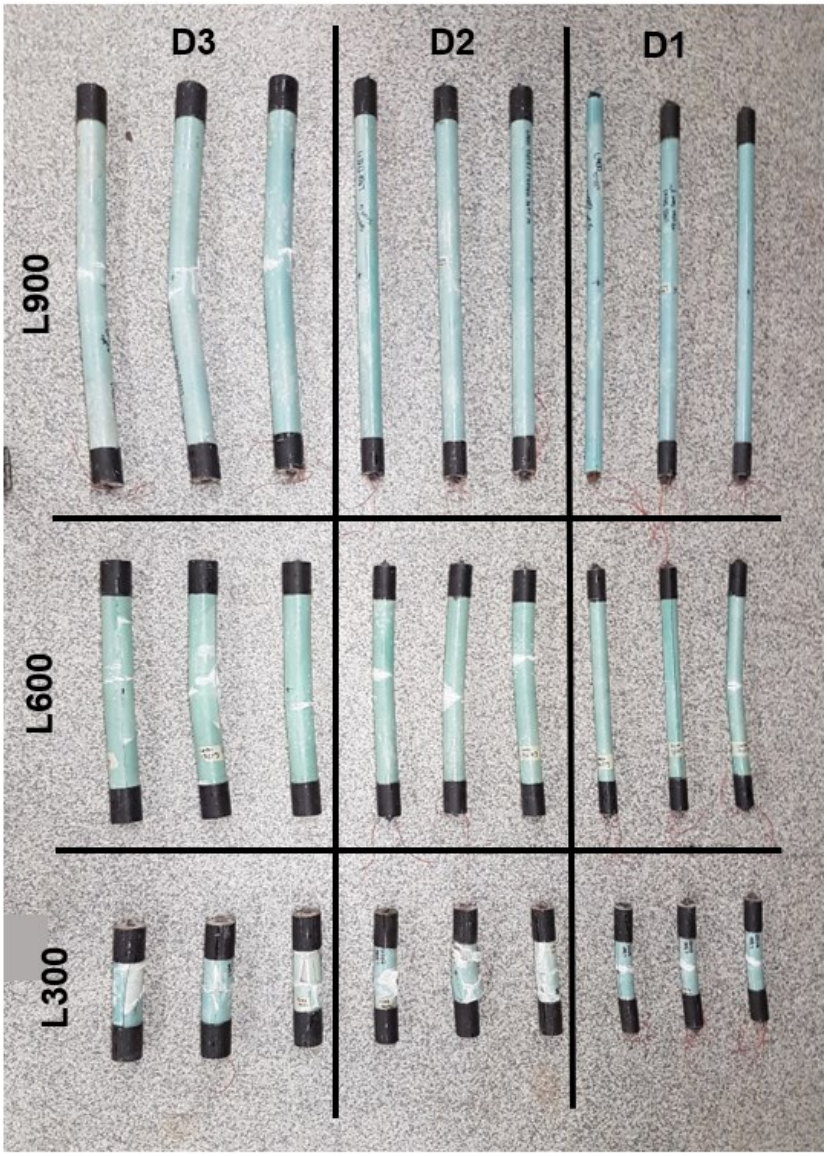

Figure 3-12 Photo of all tested specimens

Peak load was taken as the ultimate failure load of each specimen, for specimens that buckled without yielding this was taken as the buckling load and for specimens that experienced yielding of the steel core this was taken as the ultimate load. The yield load was determined using two methods. The first method was by comparing the strain in the steel, recorded by the strain gauges, to the yield strain as per Hooke's law and the experimental yield stress and modulus of elasticity. The yield strain is calculated to be

0.0018 mm/mm. When compared to the steel strain, the corresponding load was taken to be the yielding load. On occasion the steel strain gauges failed prematurely, likely due to complications with being cast in grout, and these situations have been noted in the table. When the specimen buckled prior to yielding this strain and corresponding load was also not recorded. The second method used to calculate the yielding load was by visually locating the first peak on the load-stroke diagrams shown in Figure 3-13. This method was only possible for graphs that had a definite peak. Specimens that buckled very close to what was considered a yielding load were marked as inconclusive as it was not possible to determine whether buckling or yielding occurred first. The buckling load for specimens was recorded as the peak load when no obvious yielding had occurred. Using a combination of these three loads, the failure mode was described as either yielding of the steel core or buckling. Specimens where steel strain data was not available and/or visual yield peaks were inconclusive, the failure mode was marked as such. Predicted failure modes presented in this table will be further explained in Chapter 4.

The yielding load for all specimens ranges from 51.8 kN to 69.4 kN with an average of 62.5 kN. Based on the yield stress of the steel and cross-sectional properties, the yield load for the steel would be approximately 56.9 kN. The difference in loads is thought to be due to some of the test load being directly taken by the grout, likely at the top and bottom of the specimen where the steel tabs are located. The system was deemed to be successful if the system as able to reach yielding of the steel core. Systems that ultimately failed shortly after or seemingly simultaneously with the yielding load imply that the system diameter was close to optimal for that slenderness ratio of steel core. Specimens that carried more load past that point were less efficient as failure was still decided by the yielding load.

Table 3-4 Summary table of test results

	ID		Peak Load (kN)	Avg. (kN)	Std. Dev. (kN)	Yield Load by Yield Strain (kN)	Avg. (kN)	Std. Dev. (kN)	Visual Yield Load (kN)	Avg. (kN)	Std. Dev. (kN)	Buckling Load (kN)	Avg. (kN)	Std. Dev. (kN)	Failure Mode	Predicted Failure Mode	f'_g (MPa)
L300	Plain Steel	1	19.0	**21.0**	2.40	-	-	-	-	-	-	19.0	**21.0**	2.40	**B**	**B**	N/A
		2	19.6			-			-			19.6			**B**		
		3	24.3			-			-			24.3			**B**		
	D1	1	89.9	**68.8**	14.89	DNR *	**51.8**	1.09	60.7	**60.7**	0.00	-	**58.3**	0.32	**Y**	**Y**	34.7
		2	58.0			50.7			**			58.0			**Y/B**		
		3	58.6			52.9			**			58.6			**Y/B**		
	D2	1	154.7	**153.1**	2.85	DNR	**58.4**	0.00	58.4	**59.7**	2.06	-	-	-	**Y**	**Y**	
		2	155.4			58.4			62.6			-			**Y**		
		3	149.0			DNR *			58.1			-			**Y**		
	D3	1	205.7	**202.0**	10.94	62.2	**59.0**	2.82	62.3	**63.6**	0.87	-	-	-	**Y**	**Y**	
		2	213.1			59.4			64.1			-			**Y**		
		3	187.1			55.3			64.3			-			**Y**		

L600	Plain Steel	1	5.1	**5.5**	0.65	-	-	-	-	-	-	5.1	**5.5**	0.65	**B**	**B**	N/A
		2	6.4			-			-			6.4			**B**		
		3	4.9			-			-			4.9			**B**		
	D1 ***	1	52.5	**41.9**	9.41	DNR	-	-	**	-	-	52.5	**41.9**	9.41	**Y/B**	**B**	19.5
		2	29.7			DNR			-			29.7			**B**		
		3	43.6			DNR			-			43.6			**B**		
	D2	1	65.7	**77.1**	9.21	60.24	**59.5**	0.53	**	**65.8**	2.86	65.7	**65.7**	0.00	**Y/B**	**Y**	
		2	77.1			59.4			68.6			-			**Y**		
		3	88.3			59.0			62.9			-			**Y**		
	D3	1	137.8	**136.8**	5.35	58.7	**59.2**	1.00	71.6	**67.9**	4.18	-	-	-	**Y**	**Y**	
		2	129.8			58.3			62.1			-			**Y**		
		3	142.8			60.6			69.9			-			**Y**		

L900	**Plain Steel**	1	1.1	**1.8**	0.52	-	-	-	-	-	-	1.1	**1.8**	0.52	**B**	**B**	N/A
		2	2.0			-			-			2.0			**B**		
		3	2.3			-			-			2.3			**B**		
	D1	1	27.1	**30.8**	3.52	DNR	-	-	-	-	-	27.1	**30.8**	3.52	**B**	**B**	
		2	35.5			DNR			-			35.5			**B**		
		3	29.7			DNR			-			29.7			**B**		
	D2	1	78.9	**76.6**	4.79	72.4	**69.4**	2.10	64.1	**65.2**	2.13	-	-	-	**Y**	**Y**	34.4
		2	80.9			68.1			68.2			-			**Y**		
		3	69.9			67.8			63.3			-			**Y**		
	D3	1	99.621	**114.9**	19.71	69.3	**67.9**	1.35	64.9	**66.8**	1.46	-	-	-	**Y**	**Y**	
		2	142.695			DNR *			68.5			-			**Y**		
		3	102.292			66.6			66.9			-			**Y**		

DNR	Data not recorded	*	Axial steel strain gauge failure
B	Buckling Failure	**	Inconclusive visual yielding load.
Y	Yielding Failure	***	L600-D1 specimen diameters were approximately 38 mm

3.5.2 Load – Stroke Behaviour

Load and stroke were recorded during testing of all 36 specimens. Although it is understood that stroke is not a reliable form of information, the data was used to gain a general understand of the behaviour of the FRP-BRB systems. The data from the stroke was not used in any calculations. The load-stroke graphs are provided in Figure 3-13.

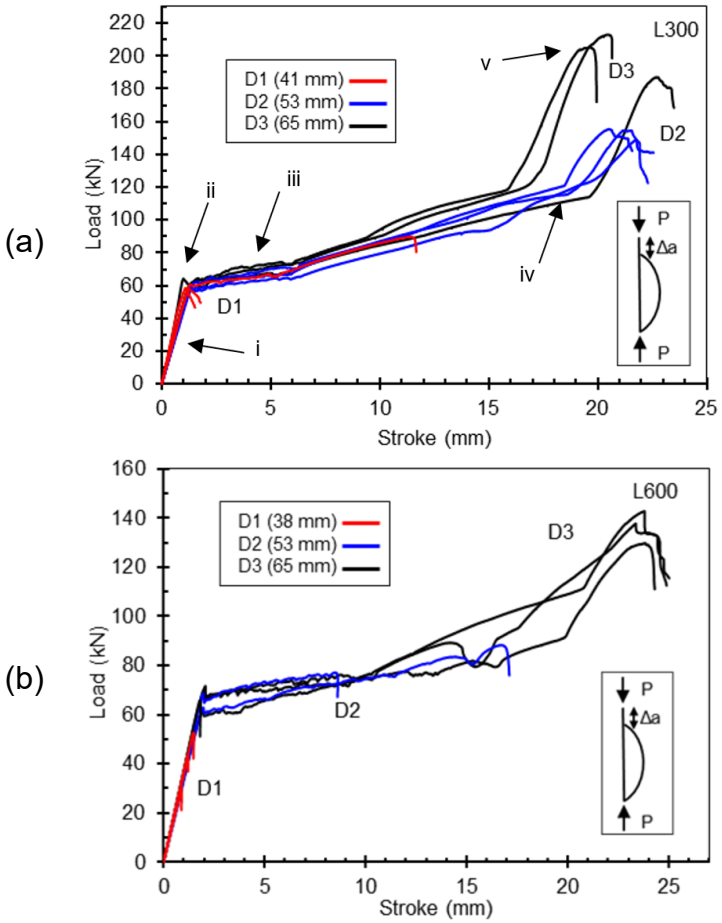

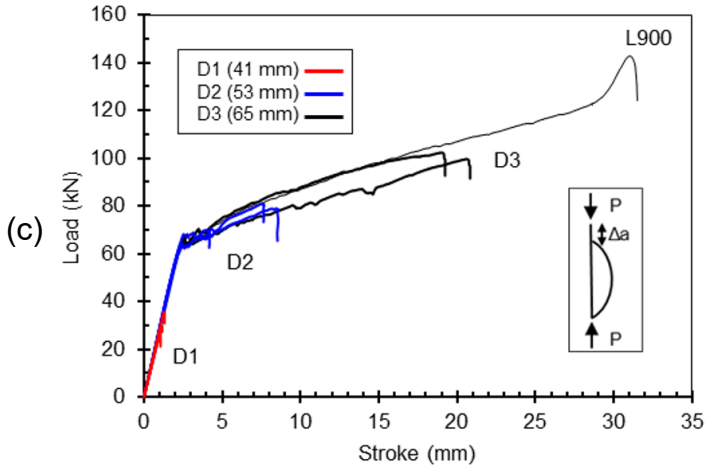

Figure 3-13 Load – stroke diagrams for: (a) L300, (b) L600 and (c) L900

There are various regions that are similar in all graphs, labelled i-v on the graph for L300. The first region, i, is the linear region of the graph. Region ii is the visual yield point of the specimens, this is the first peak seen on the graph. This region does not occur in specimens that buckled prior to yielding as described previously. Region iii corresponds to the relatively flat plateau of the graph that shows increasing load with a much lower incline compared to the initial slope in region i. Region iv is the point at which the load begins to be applied to the grout and shell. This occurs around 15 to 20 mm of stroke which is approximately the amount of free steel outside of the shell. This means the steel has been compressed to the length of the shell and now the Instron is loading the entire specimen. The final region noted, v, is the rupture point of the specimens. This region varies for each size and length specimen and is the point of ultimate failure.

For the L300 specimens, two of the D1 diameter specimens buckled or ultimately failed close to the common yielding point. These specimens were noted as having inconclusive visual yielding loads, as visually is it not possible to determine whether the specimen yielded first or buckled. The fact that these occurred so close together leads to the

conclusion that the diameter of these specimens is close to an optimal value. The optimal condition being that the load required for yielding is equal to the load required to buckle the system. As the system is consider to have failed once yielding occurs, any additional load carried past that point would be a "bonus" or safety net. The idea behind the design of the system is to reach yielding, which is a ductile failure, rather than the ultimate failure of these specimens which was a brittle failure. Understanding that factors of safety must be applied in the design of structural systems, L300-D1, while close to optimal diameter, would not be a safe choice for design as it does not allow for any room for error in installation or fabrication.

The steel core was also tested in compression in order to determine the buckling load corresponding to each length to be used in the small-scale FRP-BRB's. Three of each length were tested in compression at a rate of 2 mm/min on a 100 kN Instron 8501 Universal Testing Machine and data was recorded at 100 Hz frequency. The test parameters were identical to the reinforced sections; however, they were tested on a smaller machine to ensure precision in the data. A summary of results from these tests are provided in Table 3-5 and the load-stroke graph is provided in Figure 3-14. The results from this test allows for comparison with the proposed strengthening system and for the increase in strength to be evaluated.

Table 3-5 Summary of steel core compression buckling loads

	Buckling Load (kN)		
	L300	L600	L900
1	19.0	5.1	1.1
2	19.6	6.4	2.0
3	24.3	4.9	2.3
Average	**21.0**	**5.5**	**1.8**
Standard Deviation	2.4	0.7	0.5

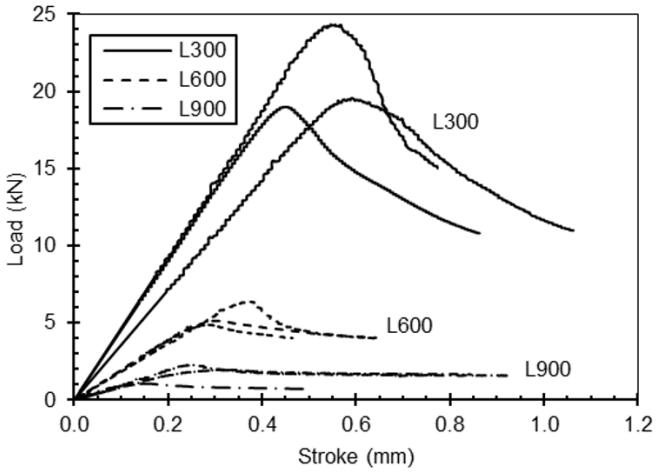

Figure 3-14 Load-stroke diagram for steel compression tests

The failure load of the FRP-BRB system is described as either the yielding load of the specimen, or the buckling load if the system was unable to reaching yielding. The ultimate or peak failure load of the specimen is the load at which the specimen was unable to carry any additional load, typically experiencing an overall system buckling and/or rupture. Table 3-6 presents the ratio of the average failure load and average ultimate failure load of each size specimen to the failure load of the plain steel specimens tested in compression. At a minimum, the system allowed for 2.84 times the load carrying capacity of the plain steel. As can be expected the larger the diameter of the specimen, the larger the increase in

load carrying capacity. Systems that did not sufficiently reach the yielding load of the steel core, such as L600-D1 and L900-D1, still saw an increase of 7.63 and 17.10 times the plain steel, respectively.

Table 3-6 Summary of average strength increase due to FRP-BRB system

Specimen Group		Y or B Load / Steel Failure Load	Ultimate Failure Load / Steel Failure Load
L300	D1	2.89	3.28
	D2	2.84	7.29
	D3	3.03	9.62
L600	D1	7.63	7.63
	D2	11.96	14.01
	D3	12.34	24.87
L900	D1	17.10	17.10
	D2	36.21	42.56
	D3	37.09	63.82

Y or B – Yielding or Buckling Load
Values are average of that specimen group

3.5.3 Load – Lateral Displacement Behaviour

Two lateral potentiometers were located at mid-height during the testing of all specimens. These recorded the lateral displacement of the specimen as it went through the process of buckling. It is important to note that the specimens did not always buckle exactly at the location of the gauges therefore the data may not fully catch the extend of the buckling, but it gives a good approximation. The graphs shown in Figure 3-15 show the extent of this movement, providing the average between the two LP's. The graphs were cut off at either their failure or when the test plates, shown in Figure 3-11, fell off and the data became un-reliable. The peak of each curve corresponds to the peak failure load of each specimen. It

is seen that the longer the specimen, the larger the lateral displacement is at buckling or its peak load. L300-D2 and L300-D3 specimens experienced little to no lateral displacement during the test. The movement they did experience was due to the rupturing and expansion of the FRP shell and grout.

(a)

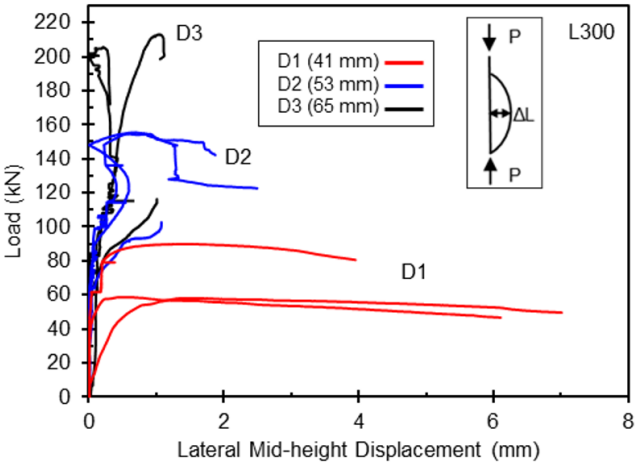

(b)

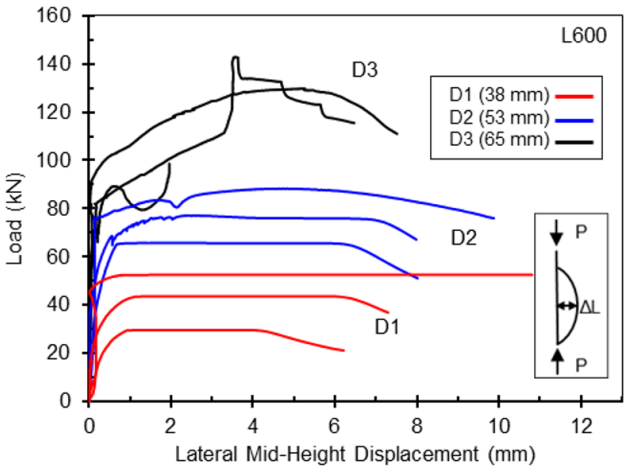

(c)

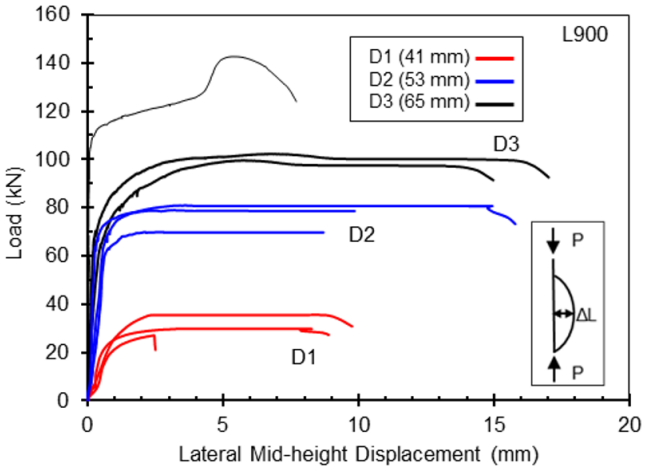

Figure 3-15 Load – lateral mid-height displacement diagrams: (a) L300, (b) L600 and (c) L900

For comparison, two lateral potentiometers were placed at mid height on the plain steel specimens, one on either side, during testing in order to collect data on the lateral displacement during buckling. The graph of the collected data is provided in Figure 3-16. At or near the peak load for most reinforced specimens a plateau occurs where the specimen is displacing laterally, while maintaining its load. This is less prominent in the plain steel specimens where once the peak load occurs the load drops with increased displacement.

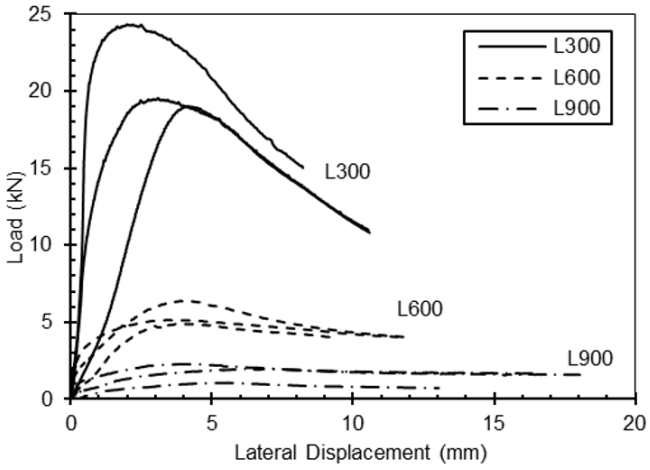

Figure 3-16 Load – lateral displacement diagram for plain steel compression tests

3.5.4 Load – Strain Behaviour

The load-strain behaviour for both the axial steel strain and the axial shell strain along the week axis of the FRP-BRB specimens will be reviewed in this section.

3.5.4.1 Steel Axial Strain

Strain gauges were carefully installed at mid height on both sides of the steel core in order to gather information on the behaviour of the steel during the tests. Although carefully installed, complications with being cast in grout led to a few of the gauges failing prior to testing. It was seen with the surviving strain gauges that once the steel core yielded the strain gauges failed, likely due to being detached by the surrounding grout. This data was used to determine the yielding load that corresponded to the yield strain of the steel.

Figure 3-17 provides the load vs strain diagrams for the steel constituent of all reinforced specimens. The average yield strain was calculated to be 1800 με based on tensile testing of the steel. This is shown on all three graphs with a dashed vertical line.

(a)

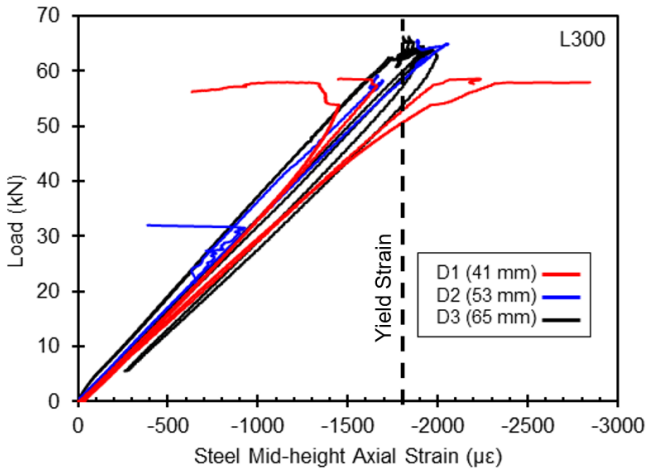

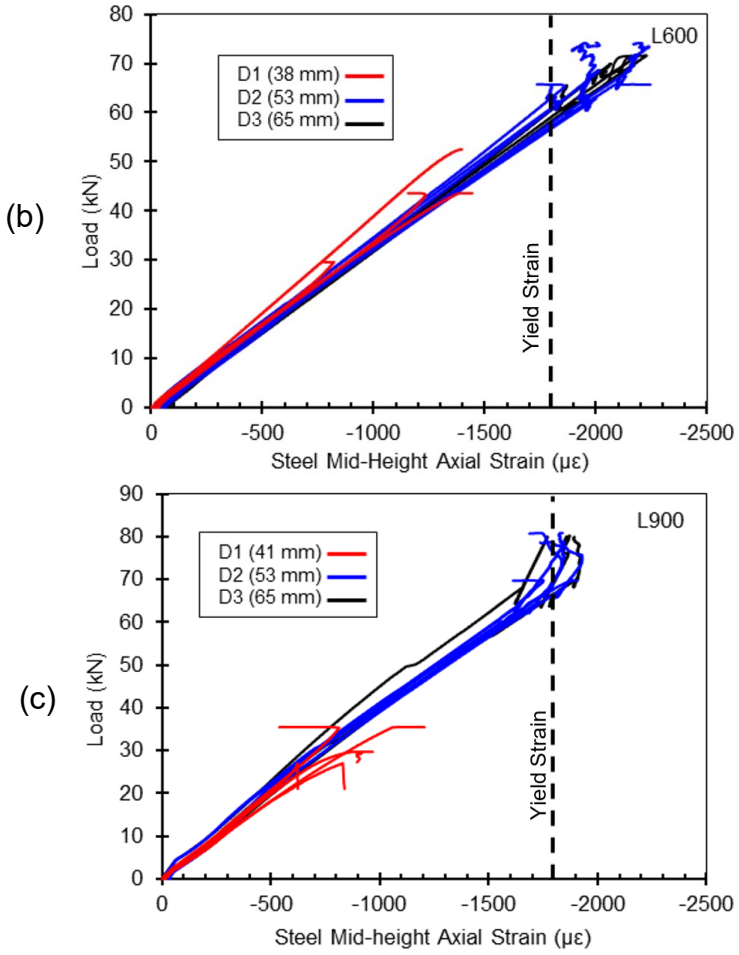

Figure 3-17 Load – axial steel strain diagrams: (a) L300, (b) L600 and (c) L900

For comparison, two of each length of the plain steel specimens were tested with axial strain gauges on either side at mid height. The load vs axial steel strain diagram for these tests is provided in Figure 3-18 with the yielding strain marked with a dashed vertical line.

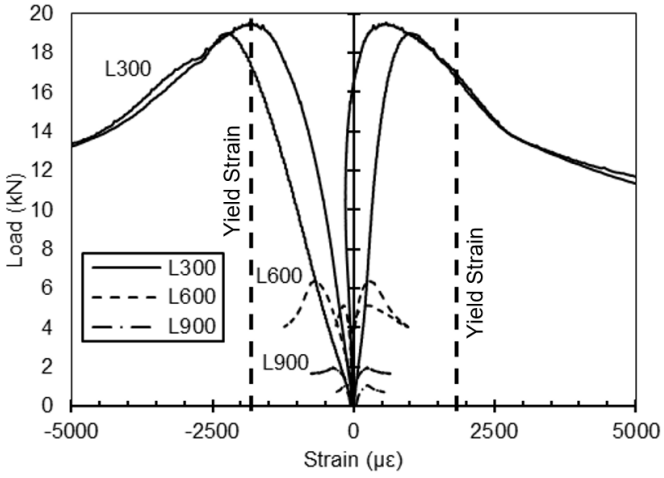

Figure 3-18 Load – strain diagram for steel compression tests

3.5.4.2 FRP Axial Shell Strain

Strain gauges were installed at mid height directly parallel to the steel strain gauges, along the weak axis. These gauges recorded strain in the FRP shells during the test. This data was also used to interpolate the strain in the grout under the assumption that the FRP shell and grout were perfectly bonded and shared the same strain data. Figure 3-19 provides the load vs axial shell strain diagrams for all three length specimens. Strain data was only plotted up until the point where it became un reliable, this typically corresponded to rupture of the specimen or debonding of the strain gauge. Based on tensile testing of the FRP material, the rupture strain in the axial direction of the specimens was found to be 11 600 με. The peaks of each curve in Figure 3-19 correspond to the peak failure load of the specimen. The strain at these peaks do not exceed 11 600 με in tension. The compression failure strain for the FRP material is unknown but is assumed to be similar to the tension strain, but likely lower. Considering this assumption, Figure 3-19 shows that the compressive axial strain of the FRP shells did not reach the crushing strain of FRP in the tested specimens. This is compatible with failure mode of the specimens pictured in Figure 3-12.

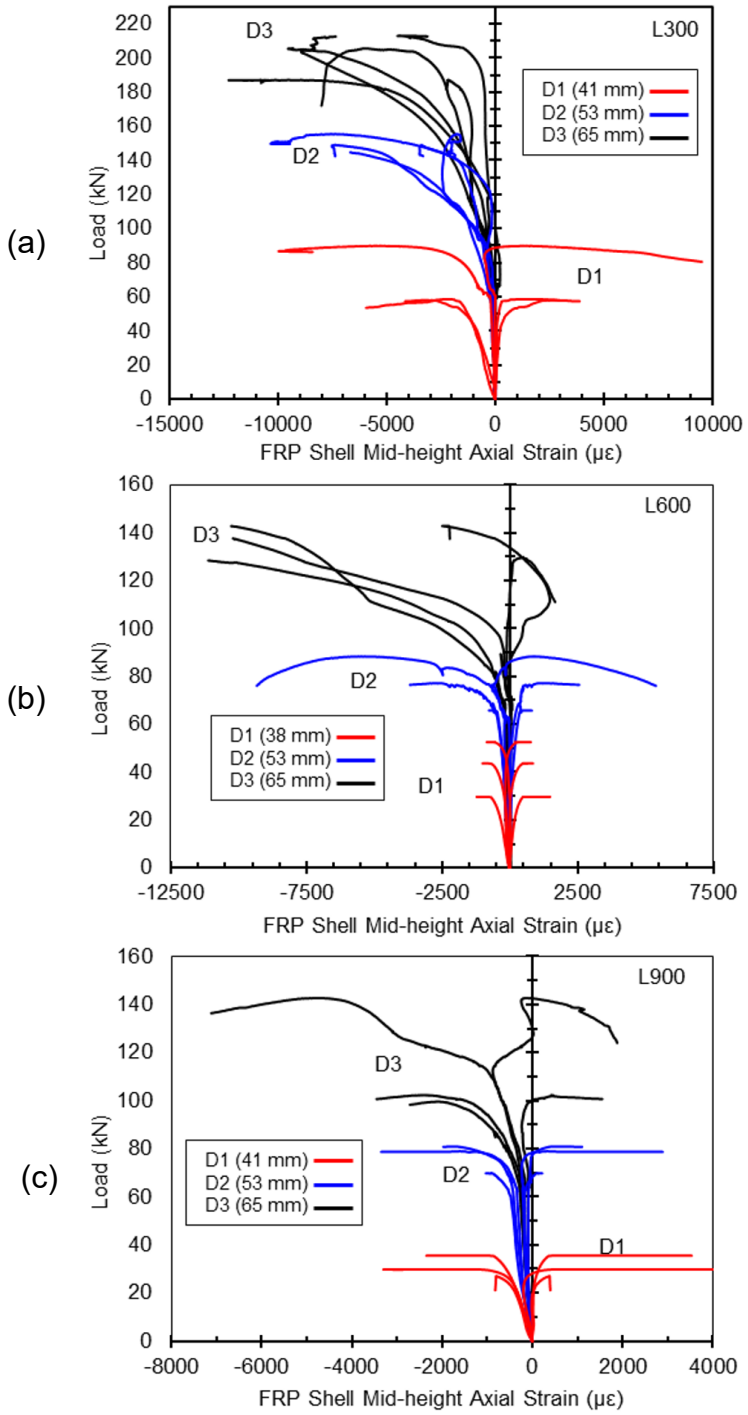

Figure 3-19 Load vs axial shell strain diagrams: (a) L300, (b) L600 and (c) L900

As much of the calculations are based on the assumption that the system is linear elastic until failure, it is important that the grout remained un-cracked for this assumption to hold. The rupture strain of concrete is calculated by a combination of Equation (3-1) of A23.3-

14 Design of Concrete Structures (CSA Group 2014b) (assumed to be valid for the self-consolidating grout used in this research) and Hooke's law to form Equation (3-2).

$$f_r = 0.6\lambda\sqrt{f_c'} \tag{3-1}$$

where: f_r is the rupture stress of concrete

λ is the modification factor for concrete density. This will be taken as 1.0 for normal density concrete

f'_c is the compressive strength of concrete, or grout in this case

$$\varepsilon_r = \frac{f_r}{E_g} = \frac{0.6\sqrt{f_g'}}{4500\sqrt{f_g'}} = \frac{0.6}{4500} = 133\ \mu\varepsilon \tag{3-2}$$

where: ε_r is the rupture strain of concrete

E_g is the modulus of elasticity of the grout

Based on this equation the rupture stress for the grout is 133 με. Table 3-7 provides the FRP strain at the visual peak loads for every specimen. Based on Table 3-7 it is seen that when the grout is in tension (positive strain values, bolded in table) this value is only exceeded when the specimen buckled prior to or very shortly after yielding such as in all D1 sized specimens and two of the L600-D2 of which buckled very shortly after yielding. This implies that the assumption that the specimens are linear elastic until yielding is reasonable.

Table 3-7 Summary of strain in grout at 1st peak

ID			Grout Strain at 1st peak	
			Compression (με)	Tension (με)
L300	D1	1	-242	**18**
		2	-3177	**2653**
		3	-6953	**2026**
	D2	1	-115	DNR
		2	-144	-127
		3	-88	-62
	D3	1	-93	-80
		2	-100	-33
		3	DNR	**4.5**
L600	D1	1	-6005	**13149**
		2	-3315	**5347**
		3	-2092	**1262**
	D2	1	-794	**1533**
		2	-630	**329**
		3	-189	-49
	D3	1	-163	**39**
		2	-86	**24**
		3	-206	**64**
L900	D1	1	-802	**381**
		2	-3036	**6820**
		3	-1141	**424**
	D2	1	-356	-211
		2	-490	-54
		3	-543	-147
	D3	1	-288	DNR
		2	-244	-179
		3	-274	-93

L900-D1 specimens did not experience any visual damage to the shell after failure as seen in Figure 3-12. These specimens returned to their original shape once the load was released. Based on the tensile strain in the grout at failure for these specimens it is very likely that the grout was cracked.

3.5.5 Contribution of Components to Total Load

The goal with these specimens is to load the steel core directly with little to no load being carried by the grout and FRP shell. In order to confirm if this was achieved, the strain in the steel, shell and grout were converted to load based on their individual moduli. Once these were calculated the total calculated load was then the sum of the three components. This allowed for a comparison between the calculated total load and the load recorded by the data acquisition system. This also allowed for an estimate of proportionally how much load was carried by each component during different stages of the testing. As the calculations are based on the assumptions that the specimens are linear elastic, the analysis is only accurate up until the yielding of the steel core. The data continues past this point; however, caution must be taken in interpreting this information.

The load carried by the individual components are all calculated by the same general equation, shown below (Equation (3-2)).

$$P_{component} = \varepsilon_{component} E_{component} A_{component} \tag{3-2}$$

where: P is the load in either the steel (s), grout (g) or the FRP (f)
ε is the strain in either the steel, grout or the FRP
A is the cross-sectional area of the component

For the steel the strain is taken to be the absolute value of the average of the two recorded strain values as both are in compression up to yielding. For both the grout and the FRP the strain was also taken to be the absolute value of the average of the two recorded strains. This is based on the assumption of super position of the strain due to the compressive force with the strain caused due to the moment as the specimens start to buckle.

A summary of the analysis at the first peak for each specimen, either yielding or buckling, is provided in Table 3-8. A sample of the graphs for this analysis was provided for one specimen of each length with diameter D2 in and the graphs for all 27 specimens can be found in Appendix C. It is important to not that this analysis was not preformed if a specimen did not have any reliable steel strain data, such as for L300D1(1) and L300D2(3).

Table 3-9 provides the ratio of each component to the calculated total load for all specimens. The contribution of steel to the total load ranges from 71% to 97% with an average of 87%, 94% and 77% for L300, L600 and L900 specimens, respectively. The overall average for steel contribution is 86%. The contribution of grout to the total load ranges from 3% to 28% with an average of 13%, 6%, and 24% for L300, L600 and L900 specimens, respectively. The overall average for grout contribution is 13.5%. The contribution of FRP shell to the total load ranges from 0.1% to 1.3% with an average of 0.3%, 0.1% and 0.6% for L300, L600 and L900 specimens respectively. The overall average contribution for the FRP shell is 0.5%.

Table 3-8 Summary of analysis of load contributions at first peak load

ID			1st Peak Test Load (kN)	1st Peak Calc. Total Load, P_t (kN)	Test Load / P_t	1st Peak Calc. Steel Load, P_s (kN)	1st Peak Calc. Grout Load, P_g (kN)	1st Peak Calc. FRP Load, P_f (kN)	Yield/ Buckle at First Peak	f'_g (MPa)
L300	D1	1	60.7	DNR *	-	-	-	-	Y	34.7
		2	58.0	63.4	0.91	52.9	10.0	0.5	Y/B	
		3	58.6	75.2	0.78	56.9	17.4	0.9	Y/B	
		Average	**59.1**	**69.3**	**0.85**	**54.9**	**13.7**	**0.7**		
	D2	1	58.4	60.0	0.97	54.4	5.5	0.2	Y	
		2	62.6	67.8	0.92	61.0	6.5	0.3	Y	
		3	58.1	DNR *	-	-	-	-	Y	
		Average	**59.7**	**63.9**	**0.95**	**57.7**	**6.0**	**0.2**		
	D3	1	62.3	66.8	0.93	60.1	6.6	0.2	Y	
		2	64.1	66.5	0.96	58.5	7.8	0.2	Y	
		3	64.3	59.9	1.07	53.0	6.7	0.2	Y	
		Average	**63.6**	**64.4**	**0.99**	**57.2**	**7.0**	**0.2**		
L300 Avg.			**60.8**	**65.6**	**0.94**	**56.7**	**8.6**	**0.3**		
Std. Dev.			**2.5**	**4.9**	**0.08**	**3.1**	**3.8**	**0.2**		
L600	D1 **	1	52.5	46.9	1.12	43.6	3.0	0.2	Y/B	19.5
		2	29.7	27.8	1.07	25.7	2.0	0.1	B	
		3	43.6	43.3	1.01	40.8	2.4	0.2	B	
		Average	**41.9**	**39.3**	**1.06**	**36.7**	**2.5**	**0.2**		
	D2	1	65.7	65.4	1.01	61.7	3.5	0.2	Y/B	
		2	68.6	71.3	0.96	65.4	5.6	0.3	Y	
		3	62.9	65.2	0.97	60.6	4.4	0.2	Y	
		Average	**65.8**	**67.3**	**0.98**	**62.6**	**4.5**	**0.2**		
	D3	1	71.6	73.2	0.98	69.3	3.8	0.1	Y	
		2	62.1	62.1	1.00	60.1	1.9	0.1	Y	
		3	69.9	68.7	1.02	64.6	3.9	0.1	Y	
		Average	**67.9**	**68.0**	**1.00**	**64.7**	**3.2**	**0.1**		
L600 Avg.			**58.5**	**58.1**	**1.02**	**54.4**	**3.5**	**0.2**		
Std. Dev.			**13.2**	**14.9**	**0.06**	**14.2**	**1.1**	**0.1**		
L900	D1	1	27.1	28.6	0.95	22.9	5.3	0.3	B	34.4
		2	35.5	35.9	0.99	29.3	6.3	0.3	B	
		3	29.7	38.4	0.77	28.0	9.9	0.5	B	
		Average	**30.8**	**34.3**	**0.90**	**26.8**	**7.2**	**0.4**		
	D2	1	64.1	66.4	0.96	52.5	13.4	0.5	Y	
		2	68.2	70.4	0.97	57.0	12.9	0.4	Y	
		3	63.3	68.2	0.93	51.4	16.2	0.6	Y	
		Average	**65.2**	**68.3**	**0.95**	**53.7**	**14.2**	**0.5**		
	D3	1	64.9	77.3	0.84	55.0	21.7	0.6	Y	
		2	68.5	68.7	1.00	52.2	16.1	0.4	Y	
		3	66.9	70.9	0.94	56.7	13.9	0.4	Y	
		Average	**66.8**	**72.3**	**0.93**	**54.6**	**17.2**	**0.5**		
L900 Avg.			**54.2**	**58.3**	**0.93**	**45.0**	**12.9**	**0.4**		
Std. Dev.			**16.8**	**17.4**	**0.07**	**13.1**	**4.8**	**0.1**		

DNR Data not recorded
B Buckling Failure
Y Yielding Failure
* Axial steel strain gauge failure
** L600-D1 specimen diameters were approximately 38 mm

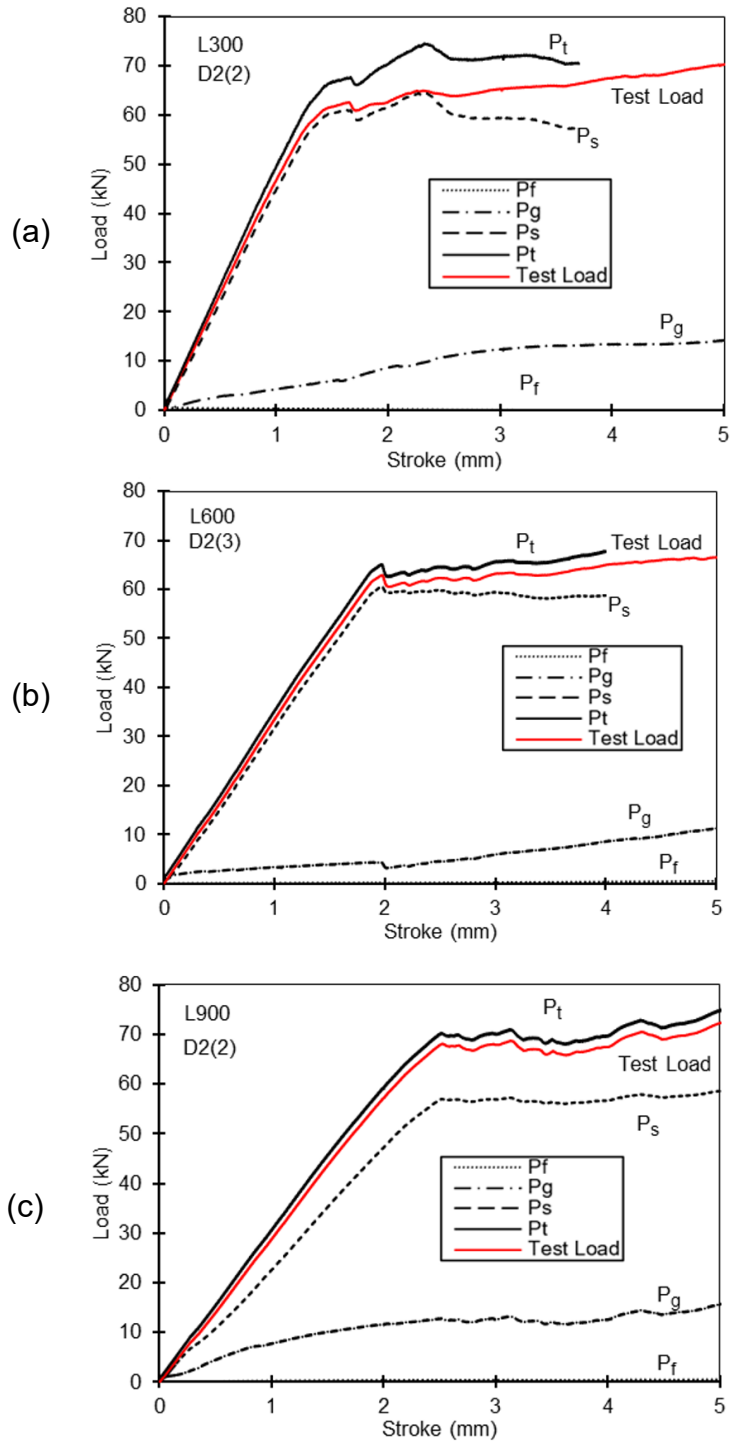

Figure 3-20 Sample graphs of contribution of components to load analysis for (a) L300-D2(2), (b) L600-D2(3) and (c) L900-D2(2)

Table 3-9 Summary of ratios of calculated load contributions to total load

ID			P_s/P_t	P_g/P_t	P_f/P_t
L300	D1	1*	N/A	N/A	N/A
		2	0.83	0.16	0.008
		3	0.76	0.23	0.012
	Average		**0.80**	**0.19**	**0.010**
	D2	1	0.91	0.09	0.003
		2***	0.90	0.10	0.004
		3*	N/A	N/A	N/A
	Average		**0.90**	**0.09**	**0.004**
	D3	1	0.90	0.10	0.003
		2	0.88	0.12	0.003
		3	0.88	0.11	0.003
	Average		**0.89**	**0.11**	**0.003**
L300 Avg.			**0.87**	**0.13**	**0.005**
Std. Dev.			**0.05**	**0.05**	**0.003**
L600	D1**	1	0.93	0.06	0.005
		2	0.92	0.08	0.005
		3	0.94	0.06	0.004
	Average		**0.93**	**0.06**	**0.005**
	D2	1	0.94	0.05	0.002
		2	0.92	0.08	0.004
		3	0.93	0.07	0.003
	Average		**0.93**	**0.07**	**0.003**
	D3	1***	0.95	0.05	0.001
		2	0.97	0.03	0.001
		3	0.94	0.06	0.002
	Average		**0.95**	**0.05**	**0.001**
L600 Avg.			**0.94**	**0.06**	**0.003**
Std. Dev.			**0.02**	**0.02**	**0.002**
L900	D1	1	0.80	0.19	0.009
		2	0.82	0.18	0.009
		3	0.73	0.26	0.013
	Average		**0.78**	**0.21**	**0.010**
	D2	1	0.79	0.20	0.007
		2	0.81	0.18	0.006
		3	0.75	0.24	0.008
	Average		**0.79**	**0.21**	**0.007**
	D3	1***	0.71	0.28	0.008
		2	0.76	0.23	0.006
		3	0.80	0.20	0.005
	Average		**0.76**	**0.24**	**0.006**
L900 Avg.			**0.77**	**0.22**	**0.008**
Std. Dev.			**0.04**	**0.03**	**0.002**

* Axial steel strain gauge failure

** L600-D1 specimen diameters were approximately 38 mm

*** Based on only one set of FRP strain data

CHAPTER 4 ANALYTICAL STUDY

A simple linear-elastic model was created in order to help justify and make sense of the experimental results, but also to create a simple design procedure for the FRP-BRB system. This model was verified by the experimental test data and various parametric studies were conducted. The effect of grout strength and the effect of the number of FRP layers in the shell on the flexural rigidity and failure mode of the system was explored. Furthermore, the effect of the grout strength and slenderness ratio on the optimal diameter for the FRP-BRB system was investigated. Similarly, the effect of the shape of the steel core and slenderness ratio on the optimal diameter was also studied.

4.1 DESCRIPTION OF MODEL

An analytical study was conducted to predict the governing failure mode for each specimen to determine whether the failure would be by system buckling or yielding of the steel core. The flexural rigidity (EI_{crit}) of the specimens could be established by equating the load required to yield the steel core (P_y) in Equation (4-1), to the load required to buckle the FRP-BRB system (P_{cr}), Equation (2-1). The result of this is presented in Equation (4-2). The steel cores all have the same cross-sectional area (A_s) with varying lengths (L). This can be modified to account for different steel core cross-sections.

$$P_y = A_s f_y \tag{4-1}$$

$$EI_{crit} = \frac{A_s f_y L^2}{\pi^2} \tag{4-2}$$

where: P_y is the yield load for the steel core

A_s is the cross-sectional area of the steel core

f_y is the yield stress of the steel core

EI_{crit} is the critical flexural rigidity

L is the un-supported length of the steel

To determine whether the composite specimens would have a yielding failure or buckling failure, the actual flexural rigidity was computed and compared to the critical values. The combined EI is calculated by adding the EI for each component of the specimen as outlined in Equation (4-3). The equation for calculating the combined EI is adopted from Xie (2005) with a term added for the FRP shell. Figure 4-1 shows the three components considered in the analysis, the steel core (s), self-consolidating grout (g) and the FRP shell (f).

$$EI = E_s I_s + E_g I_g + E_f I_f \tag{4-3}$$

where: E is the modulus of elasticity of either the steel core (E_s), the grout (E_g), or the FRP shell in the axial direction (E_f)

I is the moment of inertia of either the steel core (I_s), the grout (I_g), or the FRP shell (I_f)

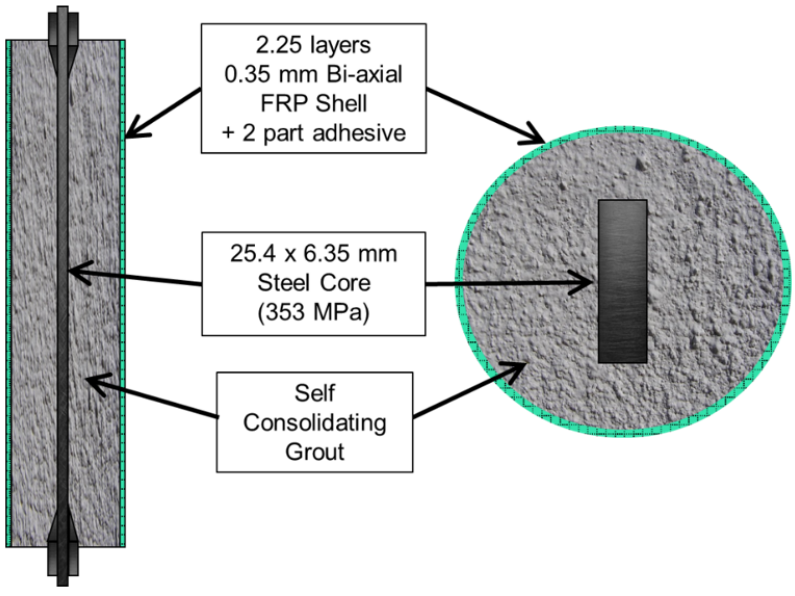

Figure 4-1 Cross-section of FRP-BRB specimens for analysis

For verification of the test data, the modulus of the steel was taken as the experimental value from Section 3.2.2. The modulus of the SCG was calculated by Equation (4-4) using the corresponding grout strength (f'_g) for each length specimen. The modulus of the FRP was take as the experimental value from Section 3.2.1 in the axial direction.

$$E_g = 4500\sqrt{f'_g} \tag{4-4}$$

where E_g is the modulus of elasticity of the grout

f'_g is the compressive strength of the grout (MPa)

The contribution of steel (EI_s) was calculated about the weak axis. For the contribution of the grout (EI_g) it was assumed that there was no cracking in the grout. This assumption is only valid up to the yield point of the specimen, assuming buckling does not take place first. The contribution of FRP shell (EI_f) was calculated using the experimental modulus of elasticity and the moment of inertia for a thin walled cylindrical shell. Once the EI was determined, it was compared to the critical EI to predict the mode of failure of the specimen. If the flexural rigidity of the composite member was greater than the critical flexural rigidity, it was predicted that the specimen would yield first. If the composite EI was less than the critical buckling EI, it was rendered that the specimen would buckle first. Predictions and actual failure modes for the specimen are presented in Table 4-1. It is important to note that this model can adequately predict if buckling would be the failure mode, however, it will not accurately predict the load associated with the buckling failure as it is no longer linear elastic and the extent of the grout cracking is unknown. As the goal of the FRP-BRB system is to achieve yielding as the first mode of failure, and ideally the systems will be designed to achieve this, it is not a problem.

Table 4-1 Predicted and actual failure modes of specimens

Shell Length	f'_g (MPa)	Outer Diameter					
		D1 (41 mm)		D2 (53 mm)		D3 (65 mm)	
		Predicted	Actual	Predicted	Actual	Predicted	Actual
300 mm	34.7	Y	Y	Y	Y	Y	Y
600 mm*	19.5	B	B	Y	Y	Y	Y
900 mm	34.4	B	B	Y	Y	Y	Y

Note: Y: Yield; and B: Buckle.
* L600-D1 specimens had 38 mm outer diameter

Using the model, it is possible to also determine the optimal diameter for the various configurations and lengths of FRP-BRB systems. The optimal diameter is simply defined as the diameter of the FRP shell that would allow the steel core to yield and the system to buckle simultaneously. This is done by setting the critical buckling flexural rigidity equal to the total flexural rigidity and solving for the diameter of system that satisfies the equation, as is shown in Equation (4-5). This equation is only applicable for the rectangular steel core sections and assumes the core is centered in the shell and loaded along this line. This equation must be modified before being applied to other cross-sections of steel. This calculation of the optimal diameter does not account for safety requirements. A reliability analysis is recommended for establishing a strength reduction factor or factor of safety for the system.

$$EI_{crit} = E_s\left(\frac{bh^3}{12}\right) + E_g\left(\frac{\pi\left(\frac{D_g}{2}\right)^4}{4} - \frac{bh^3}{12}\right) + E_f\left(\frac{\left(\pi\left(\frac{OD_{optimal}}{2}\right)^4 - \pi\left(\frac{OD_{optimal} - t_f}{2}\right)^4\right)}{4}\right) \quad (4\text{-}5)$$

where E is the modulus of elasticity of either the steel core (E_s), the grout (E_g), or the FRP shell (E_f)

b is the base dimension of the steel core

h is the height dimension of the steel core

D_g is the diameter of grout, equal to the outer diameter of the FRP shell, less the thickness of the FRP shell and adhesive

$OD_{optimal}$ is the optimal outer diameter of the FRP shell

t_f is the thickness of the FRP shell, excluding the adhesive

4.2 PARAMETRIC STUDY

In order to gain a more in depth understanding of how various components of the FRP-BRB impact the overall design and behaviour of the system, multiple parametric studies were investigated. One of the largest components of the system is the grout used for lateral support of the steel core. The effect of the grout strength on the flexural rigidity of the system was explored. The number of FRP layers was another variable that was considered in the behaviour of the system. The optimal diameter was examined for varying grout strengths and slenderness ratios, as well as different sized steel angle braces. Finally, a simple design example was completed for four different 5 m long angle steel cores. It

should be highlighted that the modulus of elasticity of steel for the parametric study was taken to be 200 GPa.

4.2.1 Effect of Grout Strength

The grout provides lateral support to the steel core in order to help inhibit buckling. As it performs such an important role, the quality of grout required to do this job successfully must be investigated. In order to do so, the flexural rigidities of the three FRP shell diameters, 41 mm, 53 mm, and 65 mm, were calculated for grouts varying from 10 MPa to 50 MPa. These flexural rigidities are represented as "X"'s in Figure 4-2. In order to compare these values directly, two FRP layers were assumed for all specimens and the steel core was the same flat plate, 25.4 mm x 6.35 mm, as used in the experimental studies.

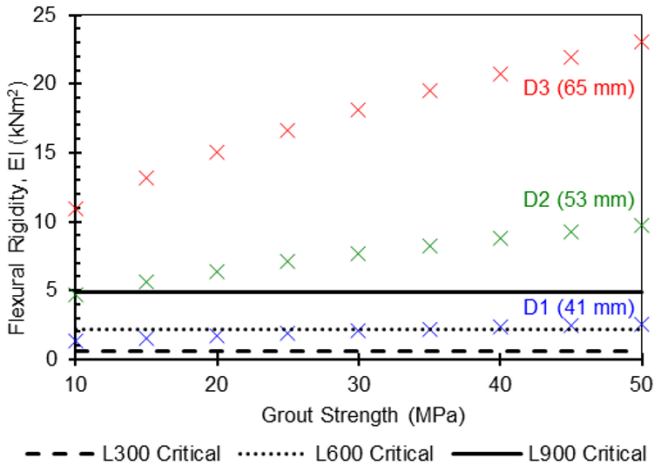

Figure 4-2 Variation of flexural rigidity as a function of grout strength, FRP shell outer diameter and length of system. Two FRP layers assumed and 25.4 x 6.35 mm flat plate steel core.

Noted on the same figure are the critical buckling flexural rigidities for the three lengths investigated, L300, L600 and L900. These horizontal lines allow for the failure mode to be predicted for each diameter and grout strength. If the "X", or flexural rigidity, for a system falls above a critical line it implies that for a specimen at that length, the composite EI is

larger than the critical EI and therefore the system (at that length) would experience yielding of the steel core. If the "X" falls below the line, it implies the opposite and a buckling failure is predicted at that length. For example, for an FRP-BRB system with a grout strength of 30 MPa, diameter D1, and length L900, the system is predicted to buckle as the "X" falls below the line. This same specimen, at length 300 is predicted to yield as the "X" falls above the L300 critical buckling line.

It is seen that the smaller the diameter of the system, the smaller the impact of increasing the grout strength is. From 10 MPa to 50 MPa grout a 90%, 106% and 110% increase in flexural rigidity is seen for D1, D2, and D3, respectively. For the smaller diameter specimens, this increase is more critical for the lengths investigated as it has the ability to switch the failure mode from buckling to yielding. This same increase in grout strength is less important for the larger diameter specimens as they succeed with even the lower grout strength and therefore any increase after that is un-necessary.

4.2.2 Effect of Number of FRP Layers

In a similar technique to the changing grout strength, the impact of increasing the number of FRP layers on a system was explored. The grout strength was held constant at 35 MPa with the same cross section of steel used in the experimental study, 25 mm x 6.35 mm flat plate. Flexural rigidities for the three diameters, D1, D2, and D3 were calculated for one to five layers of FRP shell. These flexural rigidities are noted with "X"'s in Figure 4-3 and the critical flexural rigidities are denoted with horizontal lines for each length specimen. As previously explained, if the specific "X" falls above a certain critical EI line, it means that at that length, the steel core would yield at that length. If the "X" falls below the line the system would buckle at that length.

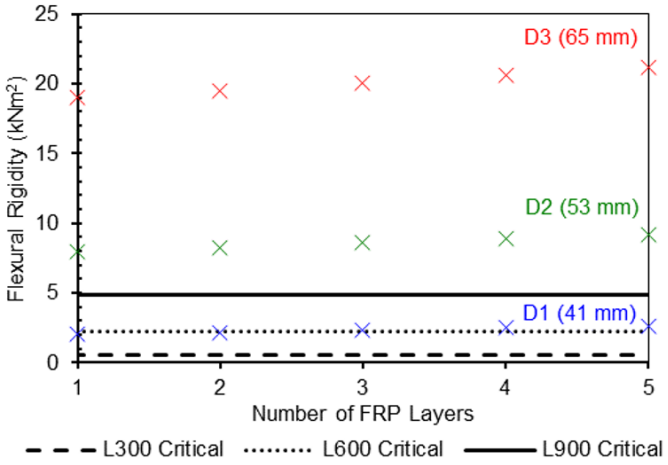

Figure 4-3 Diagram of flexural rigidity with respect to number of FRP layers, FRP shell outer diameter and length of system. Grout strength of 35 MPa assumed and 25.4 x 6.35 mm flat plate steel core.

The increase in number of FRP layers is seen to have an even smaller impact on the overall flexural rigidity compared to changing the grout strength. The largest impact is seen on the smallest diameter FRP shell. When changing the number of layers from one to five, an increase of 27%, 15% and 12% is observed for D1, D2, and D3, respectively. This increase only has an impact on D1 with respect to the L600 critical buckling line. From this study we can conclude that the number of FRP layers does not have a significant impact on the flexural rigidity of the system and therefore the number of FRP shell layers should be chosen for convenience and ease of installation. The larger the diameter of the FRP it is likely additional layers will be required for added stiffness as the FRP shell acts as formwork for the self-consolidating grout.

4.2.3 Effect of Grout Strength on Optimal Diameter

The optimal (outer) diameter for an FRP-BRB system allows for the system to buckle at the same time as the core yields. It is important to note that while this is referred to as the optimal diameter, it does not include a safety factor that would be suggested for design of

the system. In other words, the optimal diameter is the minimum allowable diameter for the design or the system. Figure 4-4 explores the effect of changing the grout strength and slenderness ratio on the optimal diameter. The graph is designed for the small-scale specimens containing the same steel core as the experimental program assuming two layers of FRP shell. It is important to consider that when reading the optimal diameter off Figure 4-4, it does not account for any space between the shell and the steel core. This means that it is important to compare the suggested size for the optimal diameter, to the dimensions of the steel core and increase the diameter if needed.

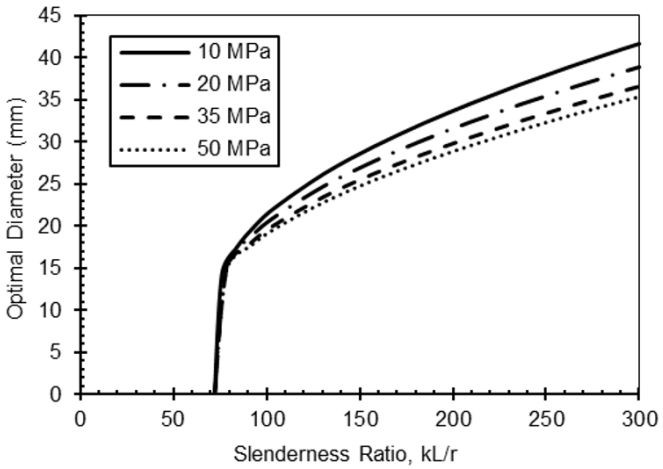

Figure 4-4 Optimal outer diameter of system with respect to grout strength and slenderness ratio. Two-layer FRP shell and 25.4 x 6.35 mm flat plate steel core was assumed.

The point at which all lines converge around the optimal diameter of 15 mm and a slenderness ratio of approximately 70 is the point at which the system is no longer needed as the steel core alone would yield prior to buckling, eliminating the need for the FRP-BRB system.

As can be expected, as the slenderness ratio of the system increases, the optimal diameter also increases. Lower strength grout requires a slightly larger diameter system, but not

significantly. For example, at a slenderness ratio of 300 a system containing 10 MPa grout requires an outer diameter of 41.7 mm and a system containing 50 MPa grout requires an outer diameter of 35.3 mm. For the case of the 50 MPa grout, it is likely that due to the maximum dimension of the steel core, 25.4 mm, and the need for a safe amount of cover between the core and the edge of the grout, that the optimal diameter would be too small. This enforces the idea that a high strength grout is unnecessary for the success of the system.

4.2.4 Effect of Steel Core Shape on Optimal Diameter

As not all braces are flat plate steel, it is important to consider more common cross-sections for the steel core. The following parametric study considers various sized angle braces at different slenderness ratios. In order of increasing size, the angles considered were 50 mm x 50 mm, 75 mm x 75 mm, 100 mm x 100 mm and 125 mm x 125 mm, all with 6 mm thick legs. For this study the grout strength was set to be 35 MPa and two layers of FRP shell were considered. The resulting graph is shown in Figure 4-5. For this study, it was assumed that the centroid of the angle is in line with the center of the system and that the entire system is loaded along this common centroid.

The point at which all lines converge around the slenderness ratio of approximately 75 is the point at which the system is no longer needed as the steel core alone would yield prior to buckling, eliminating the need for the FRP-BRB system.

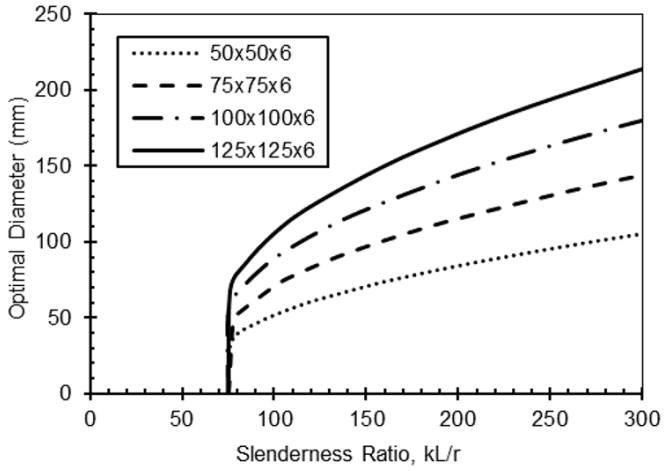

Figure 4-5 Optimal outer diameter of system with respect to steel core shape and slenderness ratio. Grout strength held constant at 35 MPa and 2 layers of FRP assumed.

Figure 4-5 shows that as the size of the angle section increases, and as the slenderness ratio increases, the optimal diameter increases as well. Once again, it is important to note that the optimal diameter does not account for any cover between the shell and the steel core, nor does it recognize when the diameter is smaller than the steel core itself.

4.3 DESIGN EXAMPLE

A practical design example has been considered. A brace with an unsupported length of 5 m was designed to be retrofit with the proposed system in order to prevent buckling. The brace is a steel angle with a leg thickness of 6 mm and yield strength of 350 MPa. The four leg lengths that have been designed for are 50 mm, 75 mm, 100 mm and 125 mm. It was assumed that the grout had a compressive strength of 35 MPa and that either two, four or six layers of FRP were used. The composite flexural rigidity of each system was calculated as shown in Section 4.1. The optimal diameter for the FRP shell was determined by equating the yielding load to the buckling load for all brace sizes. Table 4-2 summarizes the results of the designs along with three options for shell diameters, depending on how

many layers of FRP shell are used. For example, if the brace had an angle cross-section of 50x50x6 mm, an FRP shell with outer of 139.9 mm made of 2 layers of the FRP laminate would be required to match the buckling capacity of the brace to its yielding capacity. The table also shows that increasing the number of FRP layers does not decrease the shell diameter significantly. It should be highlighted that full-scale tests are needed to verify the results of the design example.

Table 4-2 Design example summary for a full-size brace with 5 m unsupported length and angle steel cross-sections

Angle Size (mm x mm x mm)	**50x50x6**	**75x75x6**	**100x100x6**	**125x125x6**
Shell made of 2 layers of FRP laminate				
EI Steel (kNm^2)	9.4	32.9	79.9	158.4
EI Grout (kNm^2)	480.2	718.9	934.9	1119.9
EI FRP (kNm^2)	10.5	14.2	17.2	19.7
EI Composite (kNm^2)	500.0	766.0	1032.0	1297.9
Yielding Load (kN)	197.4	302.4	407.4	512.4
Buckling Load (kN)	197.4	302.4	407.4	512.4
Optimized FRP OD (mm)	**139.9**	**154.5**	**164.9**	**172.5**
Shell made of 4 layers of FRP laminate				
EI Grout (kNm^2)	469.7	704.8	917.7	1100.2
EI FRP (kNm^2)	20.9	28.3	34.4	39.4
EI Composite (kNm^2)	500.0	766.0	1032.0	1297.9
Optimized FRP OD (mm)	**140.5**	**155.2**	**165.6**	**173.1**
Shell made of 6 layers of FRP laminate				
EI Grout (kNm^2)	459.3	690.7	900.5	1080.6
EI FRP (kNm^2)	31.3	42.4	51.6	59.0
EI Composite (kNm^2)	500.0	766.0	1032.0	1297.9
Optimized FRP OD (mm)	**141.1**	**155.8**	**166.2**	**173.8**

CHAPTER 5 CONCLUSION AND RECOMMENDATIONS

The purpose of the presented research was to understand the behaviour and structural capabilities of the proposed FRP-BRB system and confirm its real-life feasibility as an in-field rehabilitation technique for slender members. This research also helped to establish a platform to develop reliable design procedures that will be applicable for rehabilitation of aging infrastructure including bridges, buildings, and waterfront structures. In order to achieve these goals an experimental program consisting of 27 strengthened specimens and 9 un-strengthened specimens were prepared and tested under uniaxial compression. Specimens were fabricated using flat plate steel cores wrapped with an FRP shell and infilled with a self-consolidating grout. A simple linear-elastic model was created in order to help justify and make sense of the experimental results, but also to create a simple design procedure for the FRP-BRB system. This model was used to analyse a variety of parameters and their effects on the behaviour system.

The following conclusions were drawn from both the experimental results and analytical study:

- The linear-elastic model was successful in predicting the failure mode of all small-scale strengthened specimens.
- It is recommended that a minimum of two layers of FRP be used for the shell. More may be necessary if additional support is needed to maintain shape.
- Ends of specimens should be reinforced with additional bi-axial FRP layers to avoid premature bursting near the end supports.

- The system, when sized correctly, provided adequate lateral support allowing the failure mode to change from a sudden buckling failure to a ductile yielding failure of the steel core.
- On average, at the yielding point the steel core carries 86% of the load with the grout and FRP carrying only 13.5% and 0.5%, respectively.
- It is seen that the smaller the diameter of the system, the smaller the impact of increasing the grout strength is. From 10 MPa to 50 MPa grout a 90%, 106% and 110% increase in flexural rigidity is seen for D1, D2 and D3 respectively.
- When changing the number of layers of FRP from one to five, an increase of 27%, 15% and 12% is observed for D1, D2, and D3, respectively. This implies that the number of layers is relatively insignificant to the over all flexural rigidity of the system, particularly with a larger diameter.

In addition to the conclusions drawn based on the experimental and analytical study, the following recommendations are suggested to further expand on the research:

- Additional small-scale tests should be conducted with angle and channel cross-section steel cores that are more representative of typical braces.
- Full scale tests should be conducted in order to confirm the relationship between the small-scale specimens and real-life application, as well as to verify the conclusions drawn from small-scale tests.
- A non-linear model should be created in order to verify large scale testing & further understand how the different parameters impact the behaviour of the system past yielding.

- A reliability analysis should be conducted to propose safety requirements for design codes.

BIBLIOGRAPHY

Almeida, A., Ferreira, R., Proença, J. M., and Gago, A. S. (2017). "Seismic Retrofit of RC Building Structures with Buckling Restrained Braces." *Engineering Structures*, 130, 14–22.

Alro Steel. (n.d.). "1018 Hot Rolled Steel." <https://www.alro.com> (Feb. 27, 2019).

ASCE. (2016). *2017 Infrastructure Report Card*. *ASCE News*.

ASTM. (2003). *C33/C33M - 16 - Standard Specification for Concrete Aggregates*. ASTM International, West Conshohocken, PA, USA.

ASTM. (2009). *C1611/C1611M - Standard Test Method for Slump Flow of Self-Consolidating Concrete*. ASTM International, West Conshohocken, PA, USA.

ASTM. (2010a). *D7565/D7565M - Standard Test Method for Determining Tensile Properties of Fiber Reinforced Polymer Matrix Composites Used for Strengthening of Civil Structures*. ASTM International, West Conshohocken, PA, USA.

ASTM. (2010b). *C109/C109M - Standard Test Method for Compressive Strength of Hydraulic Cement Mortars (Using 2-in . or [50-mm] Cube Specimens)*. ASTM International, West Conshohocken, PA, USA.

ASTM. (2014). *D3039/D3039M - Standard Test Method for Tensile Properties of Polymer Matrix Composite Materials*. ASTM International, West Conshohocken, PA, USA.

ASTM. (2017). *A370-17a - Standard Test Methods and Definitions for Mechanical Testing of Steel Products*. ASTM International.

Bambach, M. R., Jama, H. H., and Elchalakani, M. (2009). "Axial Capacity and Design of Thin-Walled Steel SHS Strengthened with CFRP." *Thin-Walled Structures*, 47(10), 1112–1121.

Black, C. J., Makris, N., and Aiken, I. D. (2004). "Component Testing, Seismic Evaluation and Characterization of Buckling-Restrained Braces." *Journal of Structural Engineering*, 130(6), 880–894.

Brouwers H.J., J. J. H. and R. (2005). “Self-Compacting Concrete: The Role of the Particle Size Distribution.” *First International Symposium on Design, Performance and Use of Self-Consolidating Concrete*, (May), 109–118.

Carden, L. P., Itani, A. M., and Buckle, I. G. (2004). “Seismic Performance of Steel Girder Bridges with Ductile Cross Frames Using Buckling-Restrained Braces.” *Journal of Structural Engineering*, 132(3), 338–345.

CISC. (2016). *CISC Commentary on CSA S16-14*. CISC, Markham, ON, Canada.

CSA Group. (2014a). *S16-14 Design of Steel Structures*. CSA Group, Toronto, ON, Canada.

CSA Group. (2014b). *A23.3-14 Design of Concrete Structures*. CSA Group, Toronto, ON, Canada.

CSCE. (2016). *Canadian Infrastructure Report Card: Informing the Future*.

Dodson, V. H. (1990). “Pozzolans and the Pozzolanic Reaction.” *Concrete Admixtures*, (2), 159–201.

Ehsani, M. R. (2017). “Buckling Reinforcement for Structural Members.” *United States Patent*, USA.

Ekiz, E., and El-Tawil, S. (2008). “Restraining Steel Brace Buckling Using a Carbon Fiber-Reinforced Polymer Composite System: Experiments and Computational Simulation.” *Journal of Composites for Construction*, 12(5), 562–569.

El-Tawil, S., and Ekiz, E. (2009). “Inhibiting Steel Brace Buckling Using Carbon Fiber-Reinforced Polymers: Large-Scale Tests.” *Journal of Structural Engineering*, 135, 530–538.

Elyamany, H. E., Abd Elmoaty, A. E. M., and Mohamed, B. (2014). “Effect of Filler Types on Physical, Mechanical and Microstructure of Self Compacting Concrete and Flow-able Concrete.” *Alexandria Engineering Journal*, Faculty of Engineering, Alexandria University, 53(2), 295–307.

Feng, P., Zhang, Y., Bai, Y., and Ye, L. (2013). “Strengthening of Steel Members in Compression by Mortar-Filled FRP Tubes.” *Thin-Walled Structures*, 64, 1–12.

Fennis, S. A. A. M., Walraven, J. C., and den Uijl, J. A. (2013). “Compaction-Interaction Packing Model: Regarding the Effect of Fillers in Concrete Mixture Design.” *Materials and Structures*, 46(3), 479–479.

Ferraris, C. F. (1999). “Measurement of Rheological Properties of High Performance Concrete: State of the Art Report.” *Journal of Research of the National Institute of Standards and Technology*, 104(5), 461–478.

Gao, X. Y., Balendra, T., and Koh, C. G. (2013). “Buckling Strength of Slender Circular Tubular Steel Braces Strengthened by CFRP.” *Engineering Structures*, 46, 547–556.

Ghassemieh, M., and Kari, A. (2013). “Application of Shape Memory Alloys in Seismic Control of Steel Structures.” *Advances in Materials Science and Applications*, 2(2), 66–72.

Han, L. H., Tao, Z., Liao, F. Y., and Xu, Y. (2010). “Tests on Cyclic Performance of FRP-Concrete-Steel Double-Skin Tubular Columns.” *Thin-Walled Structures*, 48(6), 430–439.

Harries, K. A., and Kharel, G. (2003). “Experimental Investigation of the Behavior of Variably Confined Concrete.” *Cement and Concrete Research*, 33(6), 873–880.

Harries, K. A., Peck, A. J., and Abraham, E. J. (2009). “Enhancing Stability of Structural Steel Sections Using FRP.” *Thin-Walled Structures*, 47(10), 1092–1101.

Heede, R. (2014). “Tracing Anthropogenic Carbon Dioxide and Methane Emissions to Fossil Fuel and Cement Producers, 1854-2010.” *Climatic Change*, 122(1–2), 229–241.

Ho, D. W. S., Sheinn, A. M. M., Ng, C. C., and Tam, C. T. (2002). “The Use of Quarry Dust for SCC Applications.” *Cement and Concrete Research*.

James, M. N., Choi, W., and Abu-Lebdeh, T. (2011). "Use of Recycled Aggregate and Fly Ash in Concrete Pavement." *American Journal of Engineering and Applied Sciences*, 4(2), 201–208.

Katz, A., and Baum, H. (2006). "Effect of High Levels of Fines Content on Concrete Properties." *ACI Materials Journal*, 103(6), 474–482.

Kaya, A., Dawood, M., and Gencturk, B. (2015). "Repair of Corroded and Buckled Short Steel Columns using Concrete-filled GFRP Jackets." *Construction and Building Materials*, 94, 20–27.

Kersting, R. A., Fahnestock, L. A., and López, W. A. (2015). *Seismic Design of Steel Buckling- Restrained Braced Frames A Guide for Practicing Engineers About the Review Panel*. *NEHRP Seismic Design Technical Brief*.

Khorramian, K., and Sadeghian, P. (2019). "Performance of High-Modulus Near-Surface-Mounted FRP Laminates for Strengthening of Concrete Columns." *Composites Part B: Engineering*, 164(November 2018), 90–102.

Kim, S. H., and Choi, S. M. (2015). "Compressive Behavior of H-shaped Brace Strengthened with Non-Welded Cold-Formed Element." *Journal of Constructional Steel Research*, 112, 30–39.

Kronlof, A. (1994). "Effect of Very Fine Aggregate on Concrete Strength." 15–25.

Liu, X., Nanni, A., and Silva, P. F. (2005). "Rehabilitation of Compression Steel Members Using FRP Pipes Filled with Non-Expansive and Expansive Light-Weight Concrete." *Advances in Structural Engineering*, 8(2), 129–142.

López, W., and Sabelli, R. (2004). "Seismic Design of Buckling-Restrained Braced Frames." *North American Steel Construction Conference*, 1251–1260.

Mňahončáková, E., Pavlíková, M., Grzeszczyk, S., Rovnaníková, P., and Černý, R. (2008). "Hydric, Thermal and Mechanical Properties of Self-Compacting Concrete Containing Different Fillers." *Construction and Building Materials*, 22(7), 1594–1600.

Moosberg-Bustnes, H., Lagerblad, B., and Forssberg, E. (2004). “The Function of Fillers in Concrete.” *Materials and Structures*, 37(2), 74–81.

Nehdi, M., Mindess, S., and Aïtcin, P.-C. (1998). “Rheology of High-Performance Concrete: Effect of Ultrafine Particles.” *Cement and Concrete Research*, 28(5), 687–697.

Oey, T., Kumar, A., Bullard, J. W., Neithalath, N., and Sant, G. (2013). “The Filler Effect: The Influence of Filler Content and Surface Area on Cementitious Reaction Rates.” *Journal of the American Ceramic Society*, 96(6), 1978–1990.

Okamura, H., and Ouchi, M. (2003). *The Influence of Fillers on The Properties of Self-Compacting Concrete in Fresh and Hardened State*.

Olivia, M., Mifshella, A. A., and Darmayanti, L. (2015). “Mechanical Properties of Seashell Concrete.” *Procedia Engineering*, 125, 760–764.

Ollivier, J. P., Maso, J. C., and Bourdette, B. (1995). “Interfacial Transition Zone in Concrete.” *Advanced Cement Based Materials*.

Pan, J., Feng, Y., Wang, J., Sun, Q., Zhang, C., and Owen, D. (2012). “Modeling of Alkali-Silica Reaction in Concrete : A Review.” *Front. Struct. Civ. Eng*, 6(1), 1–18.

Pedersen, B. M. (2004). “Alkali-Reactive and Inert Fillers in Concrete.” Norwegian University of Science and Technology.

Porter, M. E., and Lopez-Claros, A. (2006). *The Global Competitiveness Report 2006*. World Economic Forum.

QuakeWrap Inc. (n.d.). *Product Data Sheet: PipeMedic PG16.15 for Structural Strengthening and Leak Proofing*. Tucson, AZ.

QuakeWrap Inc. (n.d.). *Product Data Sheet: QuakeBond ™ J201TC Tack Coat*. Tucson, AZ.

Sadeghian, P., Rahai, A. R., and Ehsani, M. R. (2010a). “Experimental Study of Rectangular RC Columns Strengthened with CFRP Composites under Eccentric Loading.” *Journal of Composites for Construction*, 14(4), 443–450.

Sadeghian, P., Rahai, A. R., and Ehsani, M. R. (2010b). "Effect of Fiber Orientation on Compressive Behavior of CFRP-Confined Concrete Columns." *Journal of Reinforced Plastics and Composites*, 29(9), 1335–1346.

Sadeghian, P., Shekari, A. H., and Mousavi, F. (2009). "Stress and Strain Behavior of Slender Concrete Columns Retrofitted with CFRP Composites." *Journal of Reinforced Plastics and Composites*, 28(19), 2387–2396.

Safi, B., Saidi, M., Daoui, A., Bellal, A., Mechekak, A., and Toumi, K. (2015). "The Use of Seashells as a Fine Aggregate (by Sand Substitution) in Self-Compacting Mortar (SCM)." *Construction and Building Materials*, 78, 430–438.

Schodek, D. L. (2008). *Structures*. (S. Helba, E. Francis, L. Cupp, and H. Shufeldt, eds.), Pearson Prentice Hall, New Jersey, USA.

Schulze, E. (2016). "Germany Has a Crumbling Infrastructure Problem." *CNBC*.

Schwab, K. (2018). *The Global Competitiveness Report 2018*. World Economic Forum.

Scrivener, K. L., Crumbie, A. K., and Laugesen, P. (2004). "The Interfacial Transition Zone (ITZ) Between Cement Paste and Aggregate in Concrete." *Interface Science*, 12(4), 411–421.

Shaat, A., and Fam, A. Z. (2009). "Slender Steel Columns Strengthened Using High-Modulus CFRP Plates for Buckling Control." *Journal of Composites for Construction*, 13(1), 2–12.

Siffique, R. (2008). *Waste Materials and By-Products in Concrete*. Springer, India.

Sonebi, M., Svermova, L., and Bartos, P. J. M. (2004). "Factorial Design of Cement Slurries Containing Limestone Powder for Self-Consolidating Slurry-Infiltrated Fiber Concrete." *ACI Materials Journal*, 101(2), 136–145.

Tondo, L. (2018). "Italy's Crumbling Infrastructure Under Scrutiny After Bridge Collapse." *The Guardian*.

Tremblay, R., Bolduc, P., Neville, R., and DeVall, R. (2006). “Seismic Testing and Performance of Buckling-Restrained Bracing Systems.” *Canadian Journal of Civil Engineering*, 33(2), 183–198.

Vargas, J., and Halog, A. (2015). “Effective Carbon Emission Reductions from Using Upgraded Fly Ash in the Cement Industry.” *Journal of Cleaner Production*, 103, 948–959.

Vild, M., and Bajer, M. (2017). “Strengthening Under Load: Numerical Study of Flexural Buckling of Columns.” *Procedia Engineering*, The Author(s), 190, 118–125.

Vincent, T. J. (2015). “Axial Compressive Behaviour of FRP-Confined High-Strength Concrete.” The University of Adelaide.

Wu, Z., and Grondin, G. Y. (2002). “Behaviour of Steel Columns Reinforced with Welded Steel Plates.” 214.

Xie, Q. (2005). “State of the Art of Buckling-Restrained Braces in Asia.” *Journal of Constructional Steel Research*, 61(6), 727–748.

Ye, G., Liu, X., De Schutter, G., Poppe, A. M., and Taerwe, L. (2007). “Influence of Limestone Powder used as Filler in SCC on Hydration and Microstructure of Cement Pastes.” *Cement and Concrete Composites*, 29(29), 94–102.

Yoon, G. L., Kim, B. T., Kim, B. O., and Han, S. H. (2003). “Chemical-Mechanical Characteristics of Crushed Oyster-Shell.” *Waste Management*, 23, 825–834.

APPENDIX A A REVIEW ON THE PURPOSE, PROPERTIES, AND BEHAVIOUR OF FILLERS IN CONCRETE

INTRODUCTION

On the most basic level, concrete is the combination of large aggregate (such as stone or gravel), sand, cement and water. This basic mix design has been modified and improved since the early years of concrete use, making concrete a highly versatile building material. Designers and engineers can adjust the mix design to obtain any number of desirable properties and appearances. Concrete properties are related to various factors such as cement content, type or blend of cement, water content, as well as aggregate quantity, size and surface conditions. Each constituent of concrete, on its own, has a variety of options available. For example, the cement alone can contain high concentrations of alite (C_3S), known as high early cement, which allows the mixture to reach the desired strength sooner than the standard cement. Beyond simply adjusting the mixture proportions of the previously mentioned ingredients, there are various components that can be added to further increase the range of possibilities for the design of the concrete. Some of these additives include admixtures such as accelerators, water reducers, superplasticizers, air entraining, anti-freezing and many more, all of which serve an individual purpose in the concrete mix. Further to these admixtures, concrete can be improved or be made to exhibit different properties by the addition of fillers.

Fillers are materials that are added to the mixture to reduce the use or need for another more expensive material, or to improve or vary other properties of the concrete. The most common use of fillers is in found in what is known as self-consolidating concrete and flowable concretes. Self-consolidating concrete (SCC) is a type of concrete that eliminates

the need for vibration of the concrete in order to achieve good consolidation (Pedersen 2004). In order to have a highly fluid concrete, use of filler is required, thus allowing the concrete to be more economically and environmentally friendly all the while meeting its required technical properties (Pedersen 2004). Fillers can be efficiently used to enhance the viscosity of SCC (Elyamany et al. 2014).

There are a wide variety of fillers that can be used for these purposes. The majority of these are derived from industrial processes, making the use of fillers environmentally and economically sustainable. How these fillers impact the physical and chemical properties of concrete will be discussed in this paper. It will be shown that the addition of fillers in concrete can be beneficial when used properly but will greatly complicate predicting how the material will behave.

PURPOSE OF FILLERS IN CONCRETE

Sustainability

The production of concrete has a large negative impact on the environment. The production of cement emits significant amounts of carbon dioxide into the environment (Elyamany et al. 2014; Pedersen 2004). The process of making concrete as well as the concrete mixture itself consumes a great amount of water. Any reductions and the amount of cement and water in the production of concrete without significant reductions in the quality of the concrete would increase the sustainability. The addition of fillers is an easy way to increase the sustainability of the concrete.

Many fillers, such as fly-ash, stone dust, silica fume and blast furnace slag are by-products of industrial processes (Elyamany et al. 2014). Being able to repurpose these by-products

alone is helping to decrease any environmental footprint. Many fines, or powders, are generated when stone is crushed to become the large aggregate for the concrete. These fines that are produced have been in the past considered to be waste (Pedersen 2004). In the United States annually over 100 million tons of waste fines are dumped in landfills (Katz and Baum 2006). One study found that huge amounts of oyster shell waste was being disposed of illegally at oyster farms around Korea. This is another sustainable material that can be used as a potentially beneficial filler in concrete (Yoon et al. 2003). By recycling these by-products, thus potentially reducing the cement and water usage, environmental relief is seen through reduction of hazardous emissions as well as preservation of raw materials and energy savings (Nehdi et al. 1998). How these various fillers impact the properties of concrete will be further discussed.

Alterations to Concrete Properties

Fillers may be introduced into concrete mixes in order to alter the properties of the fresh and/or hardened concrete. Some of the properties that may be affected when various fillers are added include:

- Compressive strength
- Permeability
- Freeze-thaw resistance
- Surface finish and colour
- Workability
- Durability

- Chemical resistance (chloride penetration, sulfate attack, alkali-silica reaction)
- Segregation resistance
- Bleeding resistance
- Weight reduction
- Slump
- Viscosity
- Yield Stress

An effort will be made in the following sections to review how various fillers impact some of these properties.

Limitations

Many standards have limitations on the use of fines in concrete mixes. This is due to the uncertainty, and wide variation, of how the fillers will react and their impact on the concrete properties. ASTM C33 states that fine aggregate, finer than 75 μm, must be limited to 5% for concrete subjected to abrasion and 7% for concrete not subjected to abrasion. ASTM C33 limits the use of fines in concrete mixes, unless it can be proved that the concrete will have at least equal properties to a reference concrete made with materials from a source that has been known to exhibit acceptable performance (ASTM 2003). The European code is more refined in that it allows various levels of fines, 3, 10, 16 and 22%, however, any mixes with over 3% must have further evaluation for their harmfulness (Katz and Baum 2006). In the European standard (European Pre-standard, pr ENV 197–1: 1992E) specifies

25 cement varieties where all but the standard Portland cement is made up of fillers and mineral admixtures (Nehdi et al. 1998).

Katz has states that there are various reasons that the additions of very fine fillers have been limited in the past. These reasons include (Katz and Baum 2006):

- Workability may be reduced due to increase in surface area. This can lead to more water being needed, meaning more cement would be needed to maintain strength, thus leading to an increase in shrinkage and sensitivity to cracking.
- Can prevent proper bonding between paste and aggregate as the fine particles tend to stick to the larger aggregates. This may promote cracking and weaken the concrete.
- If the fines contain any clay particles, significant volume changes can occur as they absorb water and later dry out. This can increase the sensitivity to cracking and allow for ingress of damaging substances, thus weakening the concrete.

These reasons are all about fillers in general and do not consider the fact that all fillers vary in composition, size and shape which all may have different effects on the properties of concrete. Further research is constantly being conducted that will allow designers to feel more confident in the use and benefits of using fillers in the future. As mentions in the introduction, the new generation of concrete, self-consolidating concrete, shows the contributions of fines as improving the cohesiveness of the fresh mixture. It is recommended with theses mixes to use a powder (cement and fillers) to water ratio of one (Katz and Baum 2006). Some micro-fillers can impart superior properties on cement-based materials.

TYPES OF FILLERS

This section will discuss the sources various fillers that are commonly used as well as various fillers that are not as common but are being studied. Not all listed below will be analyzed in this paper.

Industrial By-product

Fillers that are derived as a by-product of industrial processes are economically and environmentally useful in the production of concrete. The following table will outline various fillers that are by-products of industrial fillers as well as their source and composition.

Table 1 Industrial by-product fillers (Siffique 2008)

Type of Filler	Source	Composition
Ground Granulated Blast Furnace Slag (GGBFS)	By-product of iron manufacturing in a blast furnace oven where iron ore, limestone and coke (A fuel made from coal) are heated to 1500°C. The GGBFS comes from the molten slag during this process which is then granulated, dried and ground into a fine powder.	CaO, SiO_2, Al_2O_3 and MgO, which are the same as Portland cement but in different proportions
Recycled or Waste Plastic	Industrial and personal waste. There are various types of plastics. They can be melted or shredded.	Varies based on type of plastic
Scrap Tires	Old automobile tires currently deposited at landfills. Can be shredded, chopped and manufactured into ground or crumb rubber through milling.	Synthetic and natural rubber, sulfur and sulfur compounds, phenolic resin, oil, fabric, petroleum waxes, pigments, carbon black, fatty acids, inert materials and steel wires
Waste Glass	Glass is made through the melting of silica, soda ash and $CaCO_3$ at a high temperature followed by cooling. Waste glass can then be crushed into fine particle sizes.	~70% SiO_2

Coal Fly Ash	By-product of combustion of pulverized coal in thermal power plants. Removed through dust collection systems from the exhaust. Very fine spherical particles.	Determined by the composition of the coal used. Mainly silica, alumina and calcium and iron oxides. Pozzolanic
Municipal Solid Waste Ash	By-product created during the combustion of municipal solid waste. Contains high levels of toxic metals.	Very dependant on the waste source. Contains high levels of toxic metals. Mainly SiO_2, calcium and iron.
Wood Ash	Generated from the combustion of wood and wood products. Wood is burnt for fuel at pulp an paper mills, and the wood comes from everything from saw dust to wood chips and bark.	Carbon, calcium, potassium, magnesium, manganese, phosphorus and sodium
Cement Kiln Dust	By-product of cement manufacturing comprised of micron-sized particles that have been collected from electrostatic precipitators during the production of cement clinker.	Similar to Portland cement. Mainly Lime, Iron, SiO_2 and alumina
Foundry Sand	By-product of ferrous and non-ferrous metal casting industries. The sand is used as a molding material and when it is past its useful life it is termed foundry sand.	Dependant on the type of metal molded, type of binder and combustible used. Primarily SiO_2 and Al_2O_3
Crushed Rocks	By-product of the creation of coarse aggregates.	Dependant on the aggregate source
Silica Fume	By-product of production of silicon and ferrosilicon alloys.	Mainly SiO_2

Manufactured

Very few fillers exist that are manufactured for the sole purpose of acting as a filler in concrete. This is because the use of fillers allows for a cost saving as well as an improved sustainability, so manufacturing a filler would defeat both of those purposes. Metakaolin is an example of a manufacturer filler. It is manufactured by the calcination of kaolinitic clay at 500-800°C. Kaolin is a fine that clay mineral commonly used in porcelain dolls. Metakaolin is comprised mainly of $Al_2Si_2O_7$ and is a pozzolanic material (Siffique 2008).

Environmentally Sourced

Apart from fillers that have been manufactured themselves or derived from other industrial manufacturing processes there are also filler that are by-products of agricultural and environmental processes. A few environmentally sourced fillers are described in Table 2.

Table 2 Environmentally sourced fillers (Siffique 2008)

Type of Filler	**Source**	**Composition**
Rice Husk Fly Ash	Agricultural by-product created by burning of the husks of rice. When burnt, the cellulose and lignin are removed and only silica ash remains	80-85% SiO_2
Seashells	Sea food refineries, waste shells are typically disposed of in landfills.	Calcium carbonate with rare impurities (Yoon et al. 2003)
Volcanic Ash	Formed during volcanic eruptions. The ash is created when rock shatters and molten rock is separated into small particles during explosions.	Directly related to the magma source. High in SiO_2, but relative low in non-silica elements

BEHAVIOUR OF FILLERS IN CONCRETE

The Filler Effect

The filler effect occurs when fillers are added to concrete mixes and it results in an accelerate cement hydration rate. This effect is due to an increase in the water-cement ratio or dilution where the cement content is reduced and due to additional surface area being provided by the addition of fine powders, or fillers. It is thought that the increase in surface area provides additional locations for the nucleation of hydration products to occur, thus speeding up reactions and creating a more homogeneous paste (Moosberg-Bustnes et al. 2004; Oey et al. 2013). The filler effect is further accelerated by the addition of

superplasticizers which will also help to improve the particle packing (Moosberg-Bustnes et al. 2004).

Tandré Oey determined through simulations using a boundary nucleation, growth model along with a multiphase reaction ensemble, and a kinetic cellular automaton model that the extent of the filler effect and its accelerations is linked to three things (Oey et al. 2013):

- The magnitude of the increase in surface area.
- The fillers capacity to offer favorable sites for hydration product nucleation and the interfacial properties that either increase or decrease its tendency to act as a nucleant.
- The chemical composition of the filler and how likely its dissociated ions are to participate in exchange reactions with the calcium silicate hydrate product.

The Wall Effect

The wall effect is a term used in concrete that describes the interfacial transition zone. The interfacial zone in concrete is the region of cement paste that forms around the aggregates (Ollivier et al. 1995). This zone is caused by the cement grains being packed against the larger aggregate, leading to an increase in porosity and the tendency of smaller cement particles to gather in the area. The role of the interfacial transition zone is critical to the performance of the concrete (Scrivener et al. 2004). Individually the concrete and cement paste are brittle materials that exhibit elastic behaviours, where as the composite concrete material shows quasi-ductile behaviour (Figure 1). This ductile behaviour is due to microcracking, predominantly in the interfacial transition zone, which is the weakest link in the composite material. The thickness of the transition zone varies with the

microstructure of both the cement and aggregate and throughout the course of hydration (Scrivener et al. 2004). The interfacial transition zone can be modified by changing the particle size distribution of the cementitious materials, this can be done by the addition of fine fillers.

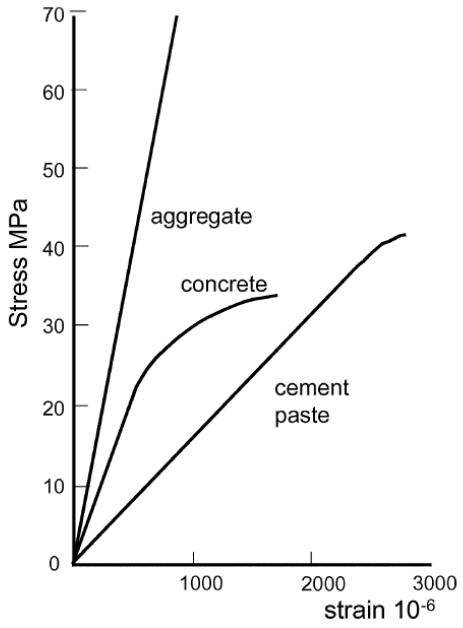

Figure 1 Stress-strain curves for aggregate, cement and concrete (Scrivener et al. 2004)

When fines are added to cement pastes they tend to have a higher density and are more homogeneous than pastes without filler. Having a high size ratio between the large and small particles allows this density to increase, however the smaller this ratio is, the more obvious the wall effect becomes (Moosberg-Bustnes et al. 2004). A microscopic study of fillers showed that the filler was well distributed within the cement paste, even around aggregates, thus proving that fillers have the ability to reduce the wall effect and improve particle packing (Moosberg-Bustnes et al. 2004). A phenomenon called the “two wall effect” can also occur when two larger aggregates lay close together and the finer cement

particles cannot get between, causing a void and a weak point, fine fillers have the ability to lessen this effect (Moosberg-Bustnes et al. 2004). This effect is shown in Figure 2.

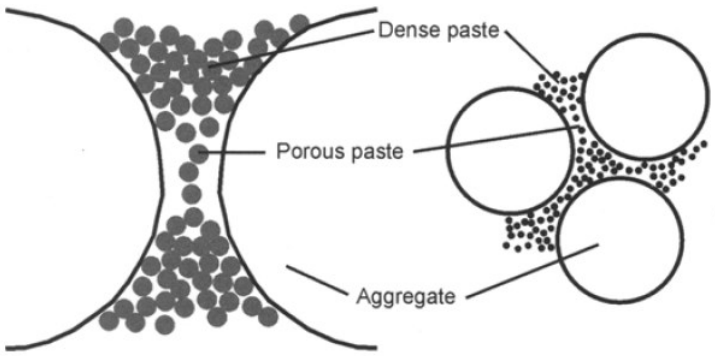

Figure 2 The "two-wall" effect (Moosberg-Bustnes et al. 2004)

Kronlöf explained the improved interactions between the paste-aggregate interface when fillers are added by identifying the following four physical factors (Kronlof 1994).

- The formation and orientation of large crystals is interfered with by the fillers at the paste-aggregate interface.
- Internal bleeding is reduced at the interfaces as large quantities of fine particles alter the rheology.
- The wall effect does not impact the contact between the fine filler and cement paste. The function of the filler then approaches the function of an unreacted cement particle core.
- The stress peaks are lowered as the concrete components are more homogenously mixed with the addition of the filler.

Reactivity

Reactivity of the constituents of concrete and the fillers that may be added is very important to the quality of the concrete being produced. The following sections will discuss two common reactions in concrete, pozzolanic and alkali-silica reactions. Inert filler choices will also be reviewed.

Pozzolanic and Alkali-Silica Reactions

A pozzolanic reaction is the reaction between siliceous and/or siliceous-alumina components, calcium hydroxide and water (Dodson 1990). The pozzolan minerals are most frequently used as mineral admixtures in concrete mixes as the pozzolanic reaction they produce is known to create cementitious properties (Dodson 1990). These fillers on their own possess no, or very little, cementitious properties, but when mixed with water in a very fine form will chemically react. Examples of pozzolanic fillers include (Elyamany et al. 2014; Pedersen 2004):

- Fly ash
- Silica fume
- Rhyolite
- Glass filler
- Metakaolin
- Granulated blast furnace slag

Alkali-silica reaction is a reaction that occurs between the alkali in cement and certain amorphous or poorly crystalline silica found in natural aggregates and minerals (Pan et al. 2012). The reaction is known to only occur if the conditions are ideal. For ideal conditions there must be the presence of a reactive aggregate, a high level of alkalinity and no less than 80% relative humidity in the concrete pores. This reaction is causes damage to concrete as over time the reaction expands, causing pressure to be exerted on the concrete around it and overall expansion of structural elements (Pedersen 2004). This then leads to cracking and damage in the concrete (Pan et al. 2012). The process of alkali-silica reactions is significantly guided by the mechanical properties of the aggregate including mineralogy, size, alkali content in pore solution, relative humidity, temperature and confining stresses (Pan et al. 2012). The Alkali-silica reaction can be summarized in two steps, the first being the rupture of the aggregate siloxane networks which is caused by the attack of hydroxyl ions to produce alkali silicate gel and silicic acid. The production of silicic acid reacts with more hydroxyl ions. The second step is where the expansion of the alkali silicate gel occurs and water is absorbed (Pan et al. 2012). This process is shown in Figure 3.

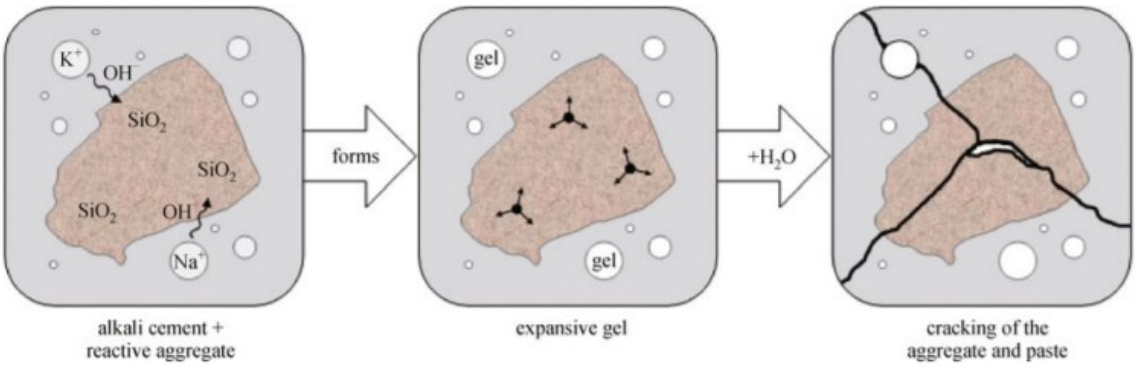

Figure 3 Alkali-silica Reaction Process (Pedersen 2004)

Pedersen found that the addition of highly pozzolanic fillers, rhyolite filler, glass filler and silica fume, in concrete mixes where alkali-silica reactions were predominant, resulted in the reduction of expansions due to alkali-silica reactions. He also found that the alkali-reactive fillers that did not exhibit pozzolanic reactions, increased the expansions when compared to a reference mix (Pedersen 2004). This study also found that pozzolanic materials showed an increase in compressive strength and its was theorized that this was due to their pozzolanic reactivity (Pedersen 2004). However, a study by Elyamany et al. found there was no significant difference in compressive strength of pozzolanic fillers in comparison to non-pozzolanic fillers. This is not to say the compressive strength was lesser than that of the control (Elyamany et al. 2014). Silica fume showed an increase in compressive strength as the filler content increased. It was theorized that this was due to a high pozzolanic effect (Elyamany et al. 2014). Elyamany found that non-pozzolanic fillers predominately showed better segregation resistance than the pozzolanic fillers that he investigated and that the pozzolanic fillers decreased the segregation resistance in comparison to a control mix. He found that the bleeding resistance was increased for both pozzolanic and non-pozzolanic fillers (Elyamany et al. 2014).

Alkali-silica reactions are very slow, taking up to 15-20 years to start to show damage. As a result of this, various tests have been developed to evaluate effects much sooner. These tests include the South-African accelerated mortar bar test and the Canadian Concrete Prism test (Pedersen 2004). The mortar bar test takes only 14 days to complete whereas the prism test tales a minimum one year to complete.

A study by Pedersen suggested that all fillers made of minerals containing silica will have a pozzolanic reaction, more or less, at temperatures as high as 80°C (Pedersen 2004). His

study concluded that test methods, such as the accelerate mortar bar test, using very high temperatures should not be used for these fillers, unless there is other evidence that the reaction will occur at lower, more reasonable temperatures. This is due to the unlikely event that these mixes would be exposed to this level of heat in real life applications. There is conflicting research on the effect of fines on alkali-silica reactions, some believe that the finest particles of alkali-reactive aggregates should not be considered dangerous in concrete. It has been reported that filler particles below a critical limit (~ 50 μm for some rocks) may give pozzolanic reactions, which are positive (Pedersen 2004). However some have reported that filler particles smaller than 20-30 μm gave very fast and negative reactions (Pedersen 2004).

Inert Fillers

Inert fillers do not exhibit any properties that will have a chemical reaction with the surrounding concrete matrix. Some inert fillers include (Ho et al. 2002; Moosberg-Bustnes et al. 2004; Pedersen 2004):

- Granite
- Gneiss
- Limestone filler
- Quartz (as a by-product and natural raw material)

Despite not demonstrating pozzolanic properties, or being able to inhibit alkali-silica reactions, inert fillers can be beneficial as an additive to concrete mixes. In a study by Pedersen, granite and gneiss fillers gave the lowest flow resistance making them a good

option for self-consolidating concrete where a high level of flow is ideal (Pedersen 2004). Non pozzolanic fillers, despite having an insignificant negative effect on compressive strength, have been found to exhibit a higher resistance to segregation when compared to pozzolanic fillers and mixes containing no fillers (Elyamany et al. 2014).

Pedersen also found that non-reactive limestone when added to a mix had no effect on the expansion during the mortar bar test. Ho et al., found that in comparison to limestone powder, incorporating inert granite fines lead to an increase in the required superplasticizer to maintain rheological properties and yield stress (Ho et al. 2002). He also noted that extremely fine granite may in fact promote durability problems. A discussion on the impact of particle size will be discussed in the following section. Kronlöf completed a study on the impact of very fine fillers in concrete and found that quartz fillers increased the compressive strength by around 4 MPa (Kronlof 1994). She concluded that this strength increase was due to an improved interaction between the paste and aggregates. Oey stated that due to limestone's properties and abilities to serve as a preferred surface and the chemical effects (ion sorption) it produces, it should be in fact considered a mineral additive rather than just a filler in cementing systems (Oey et al. 2013).

Effect of Particle Size Distribution and Fines

The grading of the materials in a concrete mix can have a significant impact on the quality of the concrete. It is known that having a relatively continuous grading of all the solids in the mix, aggregates as well as powders, will allow for a better workability and stability in the concrete (Brouwers H.J. 2005). Ensuring a good gradation of the solids will ensure that all voids in the concrete all filled. The more well graded the mix is, the higher the packing density of the concrete will be. A higher packing density means that there will be less voids

and spaces to be filled with water, thus reducing the water demand and increasing the strength (Fennis et al. 2013). Fillers tend to be either finer or of similar fineness to the cement. An example of a good particle size distribution using a limestone filler is shown in Figure 4. Fillers can be appropriately selected to help increase the packing density of the concrete. If the filler does not increase the packing density, it will increase the water demand, thus negatively impacting the properties of the concrete (Fennis et al. 2013).

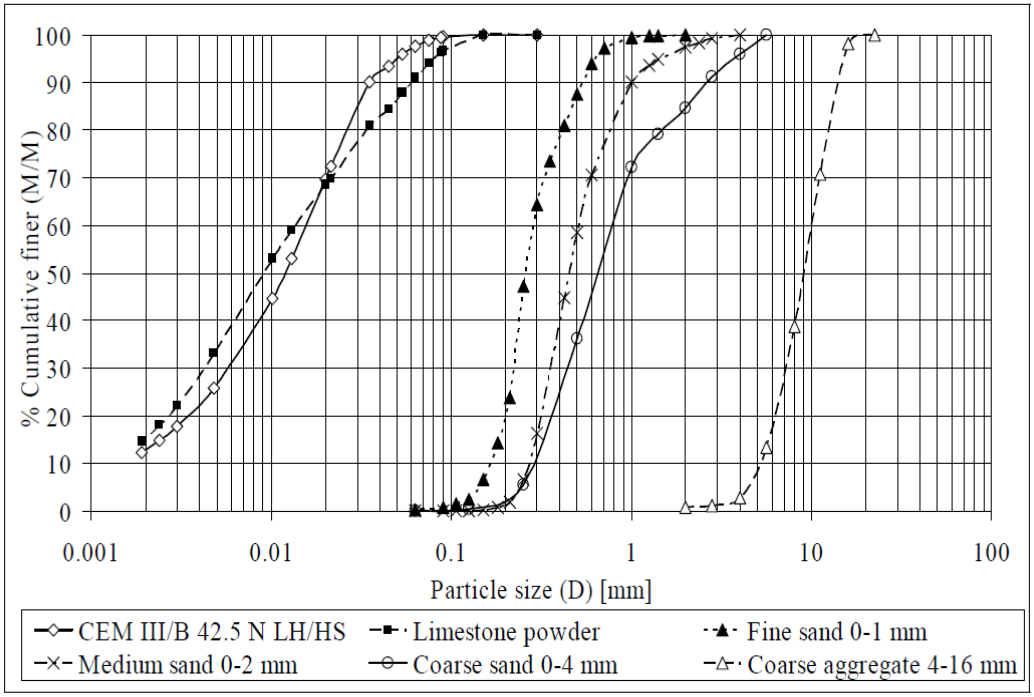

Figure 4 Particle size distribution of well graded concrete (Brouwers H.J. 2005)

Kronlöf found that good packing of all the components in concrete using fillers was an effective method of improving the quality of the concrete without having to increase the use of cement (Kronlof 1994). They found that while keeping a constant, relatively low, binder content and modifying the aggregate distribution with the use of fine aggregate increased the 91- day strength by as much as three times. This effect became less significant at higher binder contents. It was found that less water was required to maintain a constant

workability as the amount and fineness of the filler increased due to improved particle packing (Kronlof 1994). The improved gradation was found to have the positive effects of lower water requirement, increased strength, decreased porosity and better workability.

Katz studied the impact of high levels of fines of various sizes (28, 19 and 8 μm of crushed dolomite stone) on the properties of normal strength concrete. It was found that the addition of fines could improve the 28-day strength by as much as 30% (Katz and Baum 2006). The main issues were found to be that when very high quantities of the ultra-fine particles (~ 5 micron) were introduced, it tended to increase the admixture requirement which in turn had negative impacts on the concrete properties (Katz and Baum 2006). The results from Katz's experiment relative to a control mix are shown in Figure 5. This demonstrates the need for the solid constituents of the mix to be well graded. Katz concluded that large amounts of fines can be incorporated with no negative effect if workability can be adjusted with an appropriate amount of admixture.

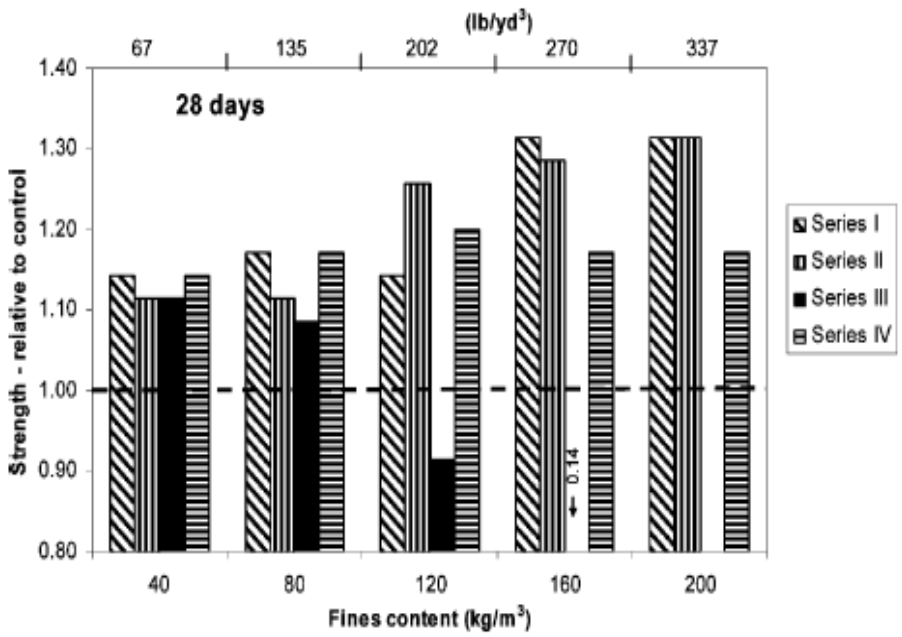

Figure 5 Relative compressive strength of mixes with high levels of fines (Katz and Baum 2006)

Rheological Properties

The rheological properties of concrete refer to the properties of the concrete in its fresh, or fluid state and how it flows or deforms. These properties are what will impact the workability, consistency and plasticity of the concrete. Rheological properties are important as they can be related to the properties in the hardened state, but also as concrete is most commonly placed in its fresh state. If the mix is too fluid, or not fluid enough problems with compaction, segregation, and consolidation can occur. The difficulty with defining the rheological properties with concrete is that many of the properties are qualitative, rather than fully quantitative. The rheological properties of concrete can be classified into three different groups, qualitative, quantitative empirical and quantitative fundamental (Ferraris 1999). Examples of these properties are shown in Table 3. Qualitative properties can only be used to generally describe the flow.

Table 3 Rheological Properties (Ferraris 1999)

Class I	Qualitative	• Workability • Flowability • Compactibility • Stability • Finishability • Pumpability • Consistency
Class II	Quantitative Empirical	• Slump • Compacting factor • Ve-be
Class III	Quantitative Fundamental	• Viscosity • Yield Stress

Various studies have been performed that investigate the impact of fillers on the rheological properties of concrete mixes. Nehdi investigated the impact of ultra fine filler particles as partial replacement of cement on the rheological properties of high strength concrete. In comparing various sized limestone fillers (LF), ground silica filler (GS), silica fume (SF) and a reference mix (OPC), Nehdi concluded that constant workability could be achieved using up to 20% replacement with silica or limestone without the need for additional superplasticizers, as seen in Figure 6 (Nehdi et al. 1998). It was found, however, that the use of silica fume increased the demand for superplasticizer in order to maintain a constant workability (Nehdi et al. 1998). Similar to silica fume, Elyamany found that granite fines also required a higher dosage of superplasticizer in order to achieve workability (Elyamany et al. 2014). Studies have also shown that lime powder, basalt powder, and marble powder can significantly improve the workability of self-compacting concrete (Elyamany et al. 2014). They also have the ability to reduce the amount of super plasticizer necessary to achieve workability (Sonebi et al. 2004).

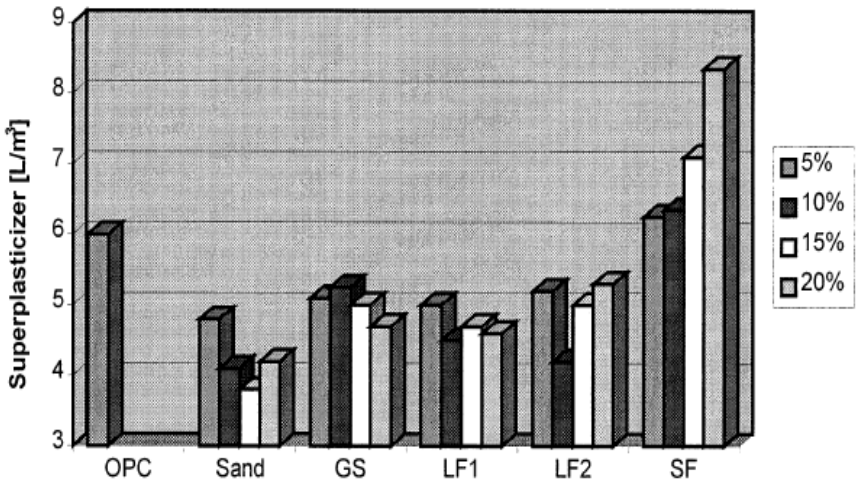

Figure 6 Superplasticizer requirement for a constant workability (Nehdi et al. 1998)

Nehdi further considered how the fillers impacted the flow resistance and slump of the concrete when comparing to a reference mix. It can be seen in Figure 7 that the addition of fillers decreases the flow resistance. The addition of fillers means an increase in wettable surface area, which should increase the flow resistance, Nehdi hypothesized that the decrease could be due to the improved gradation of the binder and a lubricating effect by the fine particles, thus reducing interlocking of the aggregates. It was concluded that the finer and more spherical the particles are, the lower the flow resistance (Nehdi et al. 1998).

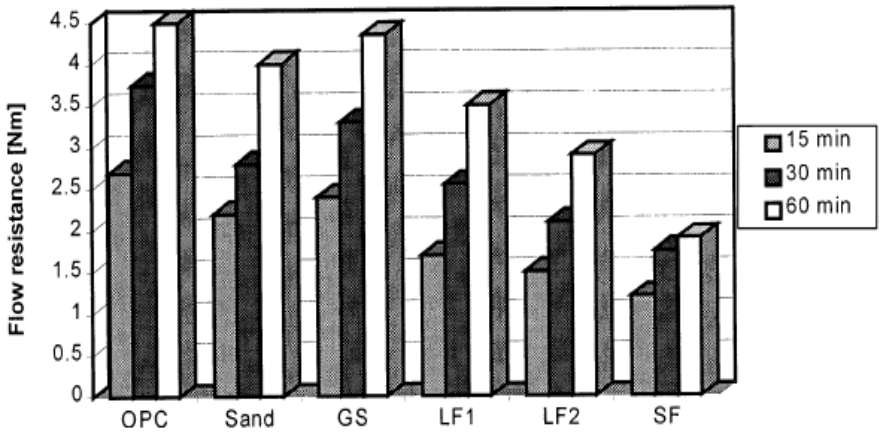

Figure 7 Flow resistance of mixes made with 15% filler at various ages (Nehdi et al. 1998)

As for the effect of fine fillers on the slump flow of the concrete mixes (with constant workability), the effect was not clear (Nehdi et al. 1998). The mixes with fillers tended to show an equal or slightly higher slump than the reference. These results of slump over time are presented in Figure 8, noting that all mixes started with a slump flow 200 ± 20 mm.

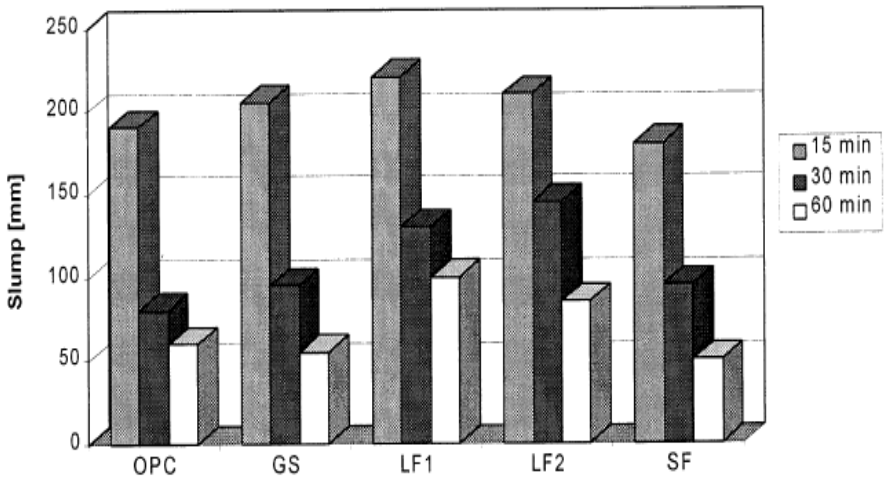

Figure 8 Slump flow variations with different fillers (Nehdi et al. 1998)

Micro fillers were found to decrease the bleeding of a fresh concrete mix, with the reduction increasing as the fineness of the particles increased. Nehdi found this to be generally true, with the exception being that the ground silica, which had the largest particle size. It was thought that this was due to ground silica changing the electrolytic environment, increasing the inter-particle interaction (Nehdi et al. 1998). Elyamany's results also showed that the type of filler used had a significant effect on the fresh properties of the concrete. He concluded that non-pozzolanic fillers were able to improve segregation and bleeding resistance in the concrete mixes he tested (Elyamany et al. 2014).

Hardened Properties

One of the main features of concrete is that it is strong in compression, but weak in tension. Finding ways to improve the strength of concrete in new and innovative ways is always being studied. With concrete one must design to optimize all the various desired properties such as resistance to cracking, resistance to shrinkage, resistance to water ingress, freeze thaw resistance, all while maintaining a required strength. Many researchers have considered how the strength and other properties of concrete in its hardened state can be improved by the addition of various shapes, sizes and types of fillers.

Okamura conducted a study on the influence of four different types of fillers, while maintaining constant water to cement ratio, fine and coarse aggregate content, on self-consolidating concrete properties in the fresh and hardened state. The four types of fillers considered were limestone, dolomite, fly ash and quartzite of varying grain size distribution. Okamura tested many properties of the mixes and concluded that, in comparison to a reference concrete, the concrete with fillers had a higher or comparable compressive strength, they showed greater shrinkage, comparable water absorption, and good freeze-thaw resistance (Okamura and Ouchi 2003). His study determined that all fillers used resulted in higher values of shrinkage, as much as double, than that of the reference self-consolidating concrete, as shown in Figure 9. Mňahončáková conducted a similar study on the hydric, thermal and mechanical properties of self-consolidating concrete with fly ash and limestone fillers. In this study it was found that heat and liquid water transport are faster in the self-consolidating concrete with limestone filler, whereas the material with fly ash showed much better water vapour transport. Mňahončáková

determined that this corresponded well with the better freeze resistance of the fly ash concrete in comparison to the limestone filler (Mňahončáková et al. 2008).

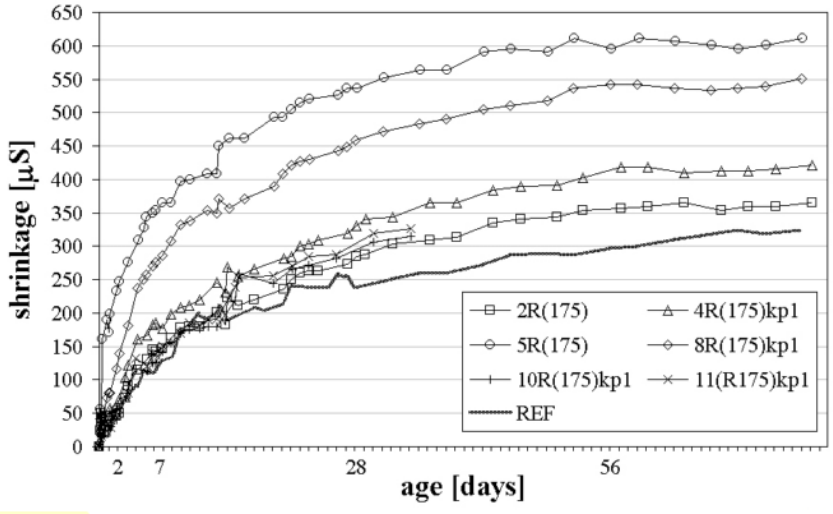

Figure 9 Shrinkage of SCC containing various fillers (REF = Reference Concrete) (Okamura and Ouchi 2003)

In Mooseberg-Bustnes's study of the effect of quartz filler in concrete he found that this filler can partially replace cement while improving the microstructure and properties of the concrete. It was concluded that the strengthening of the concrete was due to the improvement of the pore structure (Moosberg-Bustnes et al. 2004). The quantity of small pores was seen to increase while the quantity of large pores decreased which had a postitive effect on the durability and strength in the hardened state. It was believed that the increase in strength was therefore not due to the cementitious properties, but due to the improved particle packing (Moosberg-Bustnes et al. 2004). In Katz's research it was also found that with higher levels of fines in normal strength concrete, and thus an increased amount of paste, the shrinkage in the hardened state increased significantly (Katz and Baum 2006).

Elyamany found through his study that the filler type used had insignificant effect on the water absorption of flowable concrete in its hardened state. It was found that in general, non-pozzolanic fillers, such as granite and marble dust, allowed for lower water absorption and void ratios when compared to pozzolanic fillers such as silica fume and metakaolin. This study also concluded that there was no negative effect on the compressive strength of non-pozzolanic fillers when compared to pozzolanic fillers (Elyamany et al. 2014). Pedersen found in his study on alkali-reactive and inert fillers that there was no significant increase in compressive strength for rock fillers such as mylonite, cataclasite and granite/gneiss (Pedersen 2004).

Little research has been conduction on the effects of adding very fine seashell powder to concrete mixes, however studies have been done on the replacement of fine aggregate by shell fines. Yoon investigated the implications of replacing various levels of sand with crushed oyster shells with different gradations and levels of fines. It was found that there was no significant reduction in compressive strength for doses of up to 40% replacement. Yoon mentioned that in order to go through with this replacement one must also consider the salinity content of the shells, approximating that up to 20% of the granular materials can be replaced without a detrimental effect to the concrete (Yoon et al. 2003). Safi conducted a study on the replacement of the fine aggregates in mortars with sea shells. It was found that the mechanical properties of the mortars containing crushed seashells were almost the same as that of the reference mortar, only slight strength reductions were recorded (Safi et al. 2015).

CONCLUSION

It seems as though there is no general rule that works for all fillers. Various fillers bring different properties to the table, each with benefits and limitations. Their benefits and limitations are not restricted to the filler itself but also to the reactions and interactions the fillers have with other components of the cement mixture. The factors that may impact how a filler will react include:

- Chemical composition
- Reactivity
- Size
- Shape
- Surrounding matrix
- Gradation of the concrete
- Heat of curing

It is recommended that any filler be individually tested and researched prior to being incorporated in a structural mix. As there will not always be a study done on every size, shape and chemical composition of every filler it is always safer to have testing performed on the material.

There are, however, a few rules of thumb that can be used when deciding on an appropriate filler:

- Ensure all aggregates, including fine fillers, follow a good gradation. This will ensure optimal packing.

- Choosing a pozzolanic filler will likely improve or maintain strength properties while reducing cement requirement.
- Avoid fillers known to cause severe alkali-silica reactions.

As concrete and self consolidating concrete continues to evolve, and the need for sustainable, cost effective construction products increases, fillers will become more frequently used and their advantages studied.

APPENDIX B Recycled Ground Oyster Shell for Use as a Filler in Self-Consolidated Grout

Introduction

The production of concrete has a large negative impact on the environment. The cement production process emits significant amounts of carbon dioxide into the environment and the process consumes large amounts of water (Elyamany et al. 2014). Beyond simply adjusting the mixture proportions of a standard concrete mix, fillers can be added. Fillers are materials that can be added to the mixture in order to reduce the use or need for another more expensive or unsustainable material, or to vary other properties of the concrete or grout. The addition of fillers in concrete or grout mixes can help improve the sustainability, lessen the environmental impact as well as have an impact on physical properties. A very common use of fillers is in what is known as self-consolidating or flowable concretes and grouts in order to efficiently enhance the viscosity (Elyamany et al. 2014). Self consolidating concrete (SCC) and self consolidating grout or mortar (SCG or SCM) are a type of concrete and grout that has a high slump, eliminating the need for vibration to achieve good consolidation (Pedersen 2004). A few common environmentally friendly and recycled fillers include eggs shells, sea shells, lime stone rock, fly ash, stone dust, silicane fume and blast furnace slag (Elyamany et al. 2014; Pedersen 2004; Safi et al. 2015; Siffique 2008; Ye et al. 2007).

This paper will focus on the addition of waste sea shells, oyster shells in particular, to self consolidating grout. Safi et al. (2015) conducted a study to investigate the use of crushed sea shells as the fine aggregate in SCM and found that they could be used without negatively affecting the essential properties of mortar, causing only a small reduction in

compressive strength (Safi et al. 2015). The study by Safi et al. made use of larger, sand sized crushed shells of various types but did not investigate the use of shells ground more finely than the sand. Yoon et al. (2003) conducted a study on the chemical-mechanical characteristics of crushed oyster shells. In this study they looked into the composition and characteristics of various sized crushed oyster shells as well as their effect when used in soil mortar, however; they did not specify which particle size distribution they used in their mixes. It was found that the compressive strength of their mortars decreased after 20% and 40% dosage ratio for cement/soil ratio of 0.2 and 0.1 respectively (Yoon et al. 2003). Olivia et al. (2015) investigated the mechanical properties of seashell concrete by partial replacement of the cement. The shells were filtered through a #200 sieve to ensure all particles were fine and conducted trial batches with 2,4,6 and 8% replacement of cement by weight. Olivia et al. concluded that the optimum compressive strength was 4% replacement, however; adding the seashells reduced all compressive strengths in comparison to the control with none (Olivia et al. 2015).

Test Matrix

The test matrix consisted of two main batches of grout with ground oyster shells replacing sand at various levels. A control mix with no ground oyster shell was used as a base line for both batches. The first batch was designed to have the same water to cement ratio as the control batch, only varying the amount of oyster shell at intervals of 5% replacement of the sand in comparison to the control. This allowed for a comparison and analysis of the effect of the filler on the workability and slump. The second batch was designed to have a similar slump as the control mixture, by varying the water to cement ratio along with the amount of oyster shell filler. This allowed for the effect on strength to be analyzed. As it is

difficult to ensure the same slump every time, a range of ± 45 mm was allowed. Specimens were named based on the level of oyster shell in the batch (5-30) and whether they were water controlled (W) or slump controlled (S).

Material Properties

Both the masonry sand and the ground oyster shells were put through a sieve test to determine their gradation curves. The results of both tests are shown in Figure 1. Both the sand and ground oyster shells follow a similar gradation; however, the ground oyster shell is finer. This makes the ground oyster shell a good candidate to replace the sand in term of gradation.

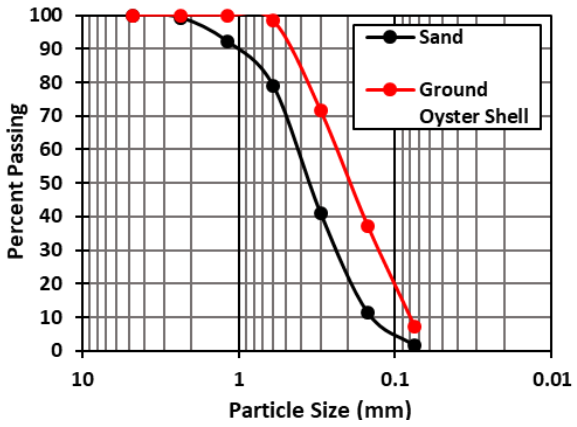

Figure 1 Gradation curve of sand and ground oyster shell

Specimen Fabrication

There were two main components to the fabrication of the test specimens. First the fresh oyster shells had to be prepared and finally the grout was mixed and cured. The oyster shells were collected from a beach in Brule Point, Nova Scotia. The shells were all empty and scoured by the tides and salt water. The oyster shells were then scoured and bathed in fresh water to remove as much salt and contaminants as possible. The shells were then

placed in an oven at 70 degrees Celsius for approximately 24 hours. Once fully cleaned and dried, small 1 kg portions were sent through the jaw crusher twice each to break the full shells down into a size the pulverizer could manage. Next, in 1 kg size batches, the broken shells were placed in the pulverizer for 4 minutes until ground into a fine powder. This powder was collected and sieved in order to determine the particle size distribution. This process is shown in Figure 2.

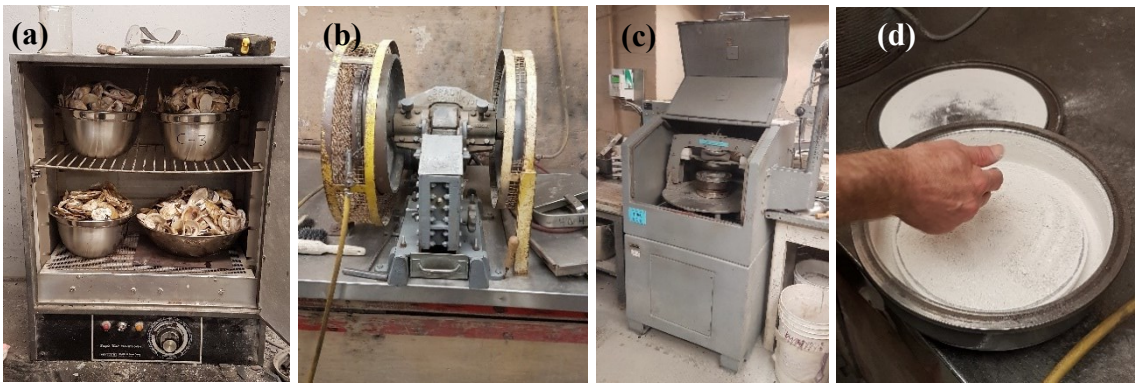

Figure 2 Ground oyster shell preparation: (a) shells are washed and dried; (b) shells are then put through jaw crusher twice; (c) shells are run through

Once the ground oyster shell fines were prepared, the grout was mixed. All mixes contained water, superplasticizer, type N cement, masonry sand and the ground oyster shells. Depending on the batch of grout, there was a different variation of ground oyster shells, while maintaining the same quantity of fine aggregates, which includes the sand and oyster shells. To ensure a consistent mixture, the cement, fine aggregates and water were added in rotation and mixed with a power drill and paint mixer attachment. For each batch of grout, a modified slump test was conducted using a smaller tube (or cone) than the ASTM Standard for self-consolidating concrete to conserve material, ASTM 1611 (2009) (ASTM 2009). A base line was set for this with the control mix. Three grout cubes were cast in

50x50x50 mm cubes for each batch of grout and cured for one day in lab before being removed from their molds and placed in the curing room. This process is shown in Figure 3.

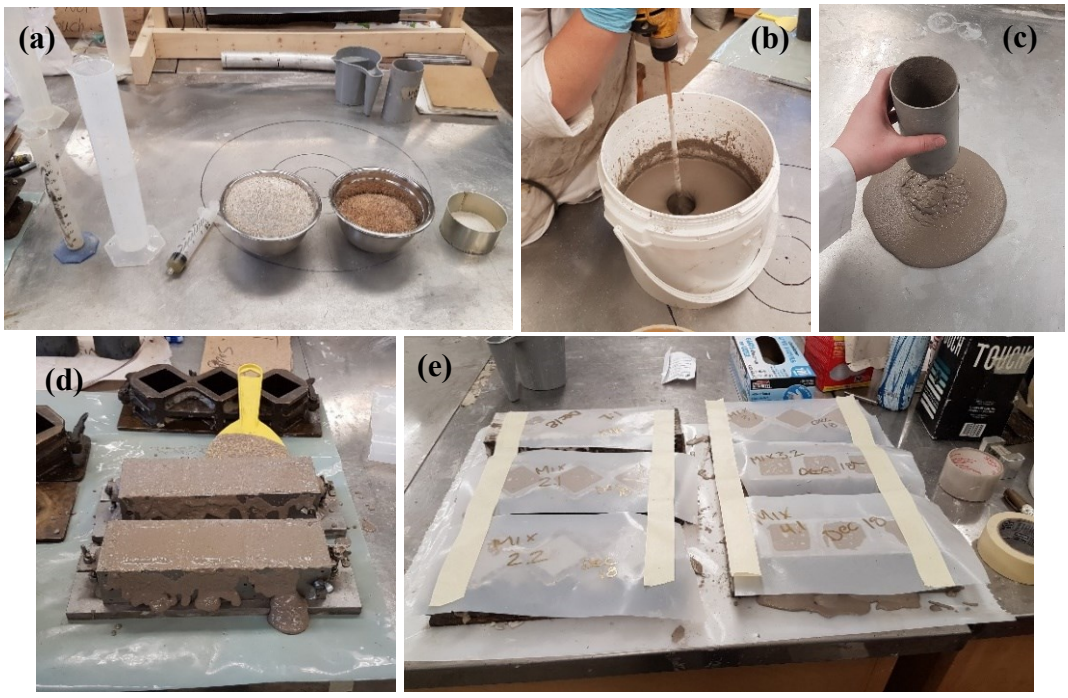

Figure 3 Specimen fabrication: (a) materials for the mix; (b) mixing materials; (c) modified slump test performed; (d) grout cubes prepared and; (e) grout cubes covered for one day of curing in lab

Test Setup

The test set up and procedure for the experiment was in accordance with ASTM C109 (2010) (ASTM 2010b). A spherical bottom fixture was used to minimize any accidental eccentricities. Final specimens were tested under compression using a universal testing machine with a constant strain loading rate of 1 mm/min. Load and stroke were recorded for all specimens until failure. Figure 4 demonstrates the test setup.

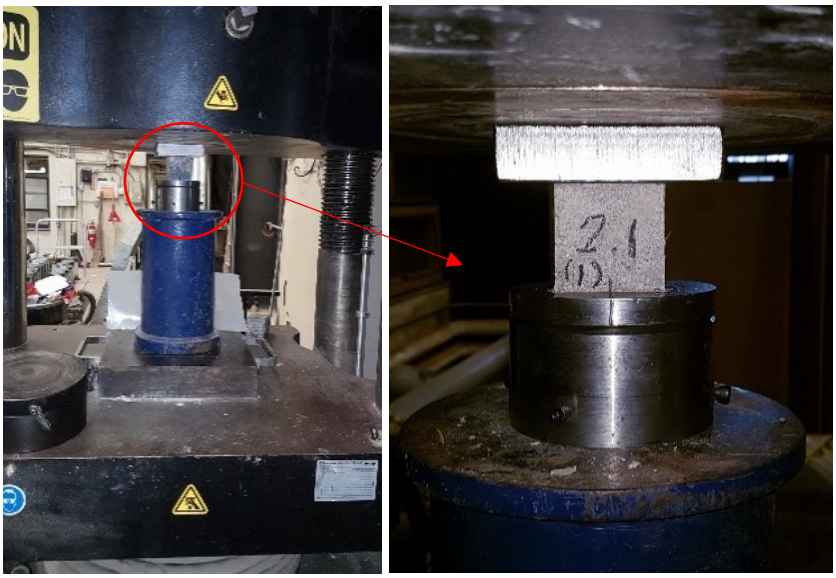

Figure 4 Test set-up

Results and Discussion

All specimens were tested under compression at 38 days after casting and their results are provided in Table 1. It should be noted that the control specimen and GO5-W were tested in compression, however only the peak load was recorded.

Table 1: Summary of test results

Specimen group ID	Mini slump flow (mm)	Compressive strength		
		Average (MPa)	Standard Deviation	Coefficient of Variation (%)
Control	250	40.85	1.85	4.52
GO5-W	330	38.50	1.07	2.79
GO5-S	295	42.32	3.14	7.42
GO10-W	348	44.41	0.81	1.81
GO10-S	235	49.32	1.94	3.94
GO15-W	363	44.92	0.72	1.60
GO15-S	235	47.84	0.51	1.07
GO20-W	363	46.09	0.51	1.11
GO20-S	238	51.15	1.86	3.64
GO25-W	310	43.88	0.98	2.23

GO25-S	220	46.14	3.11	6.74
GO30-W	295	44.13	1.37	3.10
GO30-S	223	46.40	0.46	0.98

Slump Flow Behaviour

The control mix was designed to have a mini slump flow of 250 mm, which through trial and error was determined to be a reasonable slump for a self-consolidating mix. It should be noted that the mini slump flow was obtained from small volume of grout filled in a 50x100 mm cylinder. Initially when determining a reasonable mix design, full scale slump tests were conducted as well as the modified smaller test to ensure a fair comparison. When adding the same amount of water to each batch, the slump increased, as expected. For 25 and 30% addition of ground oyster shell the slump decreased in comparison to the addition of 5% to 20%, but still increased with respect to the control. The constant slump batch was designed to maintain a slump of ± 45 mm of the control. The results of the mini slump test for the constant water samples are provided in Figure 5.

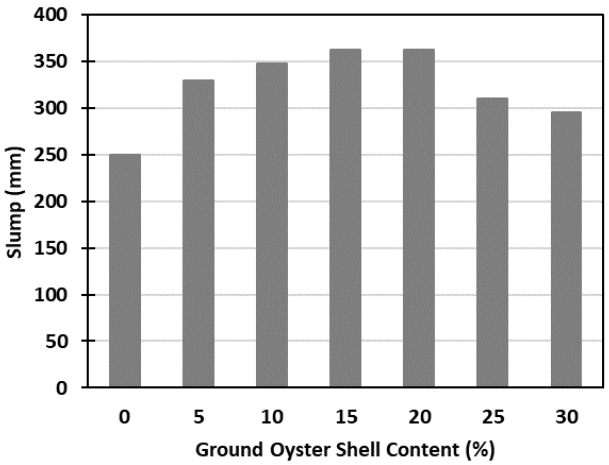

Figure 5 Variation of mini slump for constant water

Strength Behaviour

While maintaining constant slump, the results show an increase in strength in comparison to the control mix for all levels of oyster shell. The best strength results came from a 20% replacement of sand with oyster shell. The replacement of 20% of the sand corresponded to an increase in strength of almost 25% over the control. The 20% replacement was found to provide the highest strength increase for both constant slump and constant water, however; a lower strength increase was seen with constant water content. This is expected as more unnecessary water will lead to a weaker concrete; however, there is still an increase in the strength over the control mix in all but the 5% mix. The 5% ground oyster content mix, with constant water content appears to be off the trend when comparing it to the others. Figure 6 shows a compressive strength comparison for all ground oyster shell content levels tested.

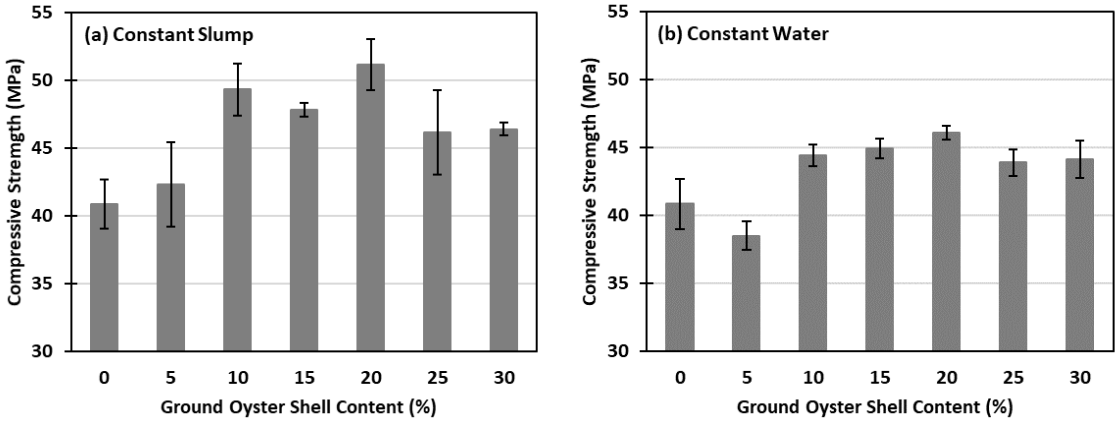

Figure 6 Variation of compressive strength: (a) constant slump mixes and (b) constant water mixes

Mix design proportions and details, for a cubic meter batch size, have been provided for the 20% ground oyster shell content mix with constant slump in Table 2.

Table 2 Mix proportions for 20% ground oyster content (by volume of sand)

Component	Quantity (1 m^3 batch)	
	Weight (kg)	Volume (m^3)
Water	170.5	0.170
Cement (Type N)	676.3	0.495
Masonry Sand	447.6	0.264
Ground Oyster Shell	60.0	0.066
Super Plasticizer	4.08	0.004
Mini Slump	238 mm	
28 Day Strength	51.15 MPa	

Load-Stroke Behaviour

Load and stroke were collected during the compression testing and the average curve for the three cubes of each constant slump batch is provided in Figure 7. Data from the 5% replacement batches has not been included as the discrepancies between the other data sets was too large. The cause of this discrepancy is unknown, however is likely due to an error in the mixing or curing stage. Further investigation is needed, including re casting and testing these specimens. Figure 7 shows that all variations followed a similar load-stroke shape, with the peak load and peak stroke varying slightly between specimens.

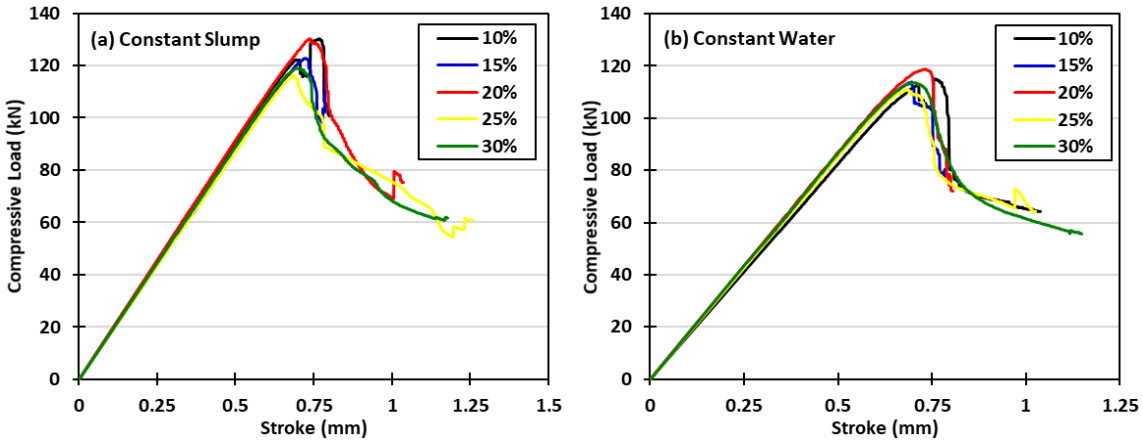

Figure 7 Comparison of load-stroke curves: (a) constant slump mixes and (b) constant water mixes

Table 3 gives the slope of the initial linear portions of these curves. It is seen that all constant slump specimens had a similar slope, with the average of all curves being 177.99 kN/mm. The constant water specimens had an average slope of 170.93 kN/mm.

Table 3 Initial slope of load-stroke curves

Ground Oyster Shell Content (%)	Average Initial Slope of Load-Stroke Curve (kN/mm)	
	Constant Slump	Constant Water
10	180.37	164.69
15	175.21	172.79
20	182.26	173.51
25	174.04	170.56
30	178.08	173.11
Average	177.99	170.93
Standard Deviation	3.07	3.28

Conclusions

Six variations of a control mix were designed to feature various levels of replacement of sand with ground oyster shell from 5-30%. Each level of replacement had two different batches, one with the same level of water as the control and the other with the same slump

measurement as the control. All specimens were cast in grout cubes and tested in compression after 38 days of curing. It was found that for both controlled water and slump 20% replacement was the optimal design. 20% replacement of sand with ground oyster shell allowed for almost a 25% increase in strength over the control mix when slump was maintained. The next stage of this study will include mixing a larger batch of the 20% mix design to obtain the slump flow based on ASTM 1611 (2009). Further work on this topic will also include investigation into the particle size distribution of the ground oyster shell by conducting a hygrometer test on the fines. Various levels of replacement will be re-mixed in order to rule out any errors that may have occurred in the first round of mixing. Higher levels of replacement may also be considered, along with more levels of replacement between the 5-30% used in this study.

APPENDIX C Contribution of Components to Total Load Graphs

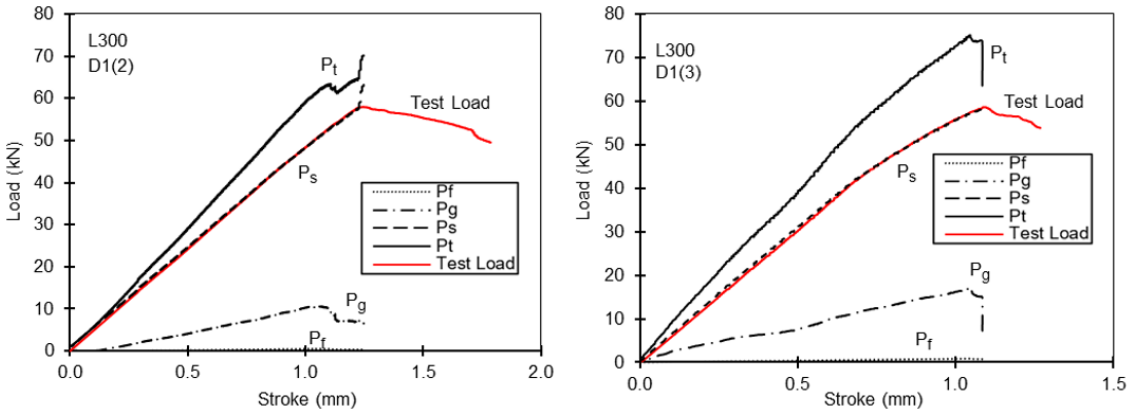

L300 D1 Contribution of materials to total load

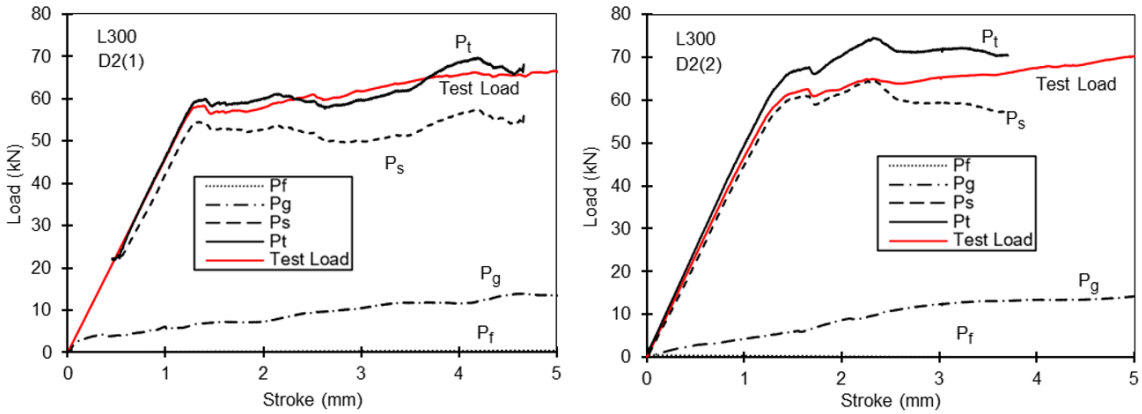

L300 D2 Contribution of materials to total load

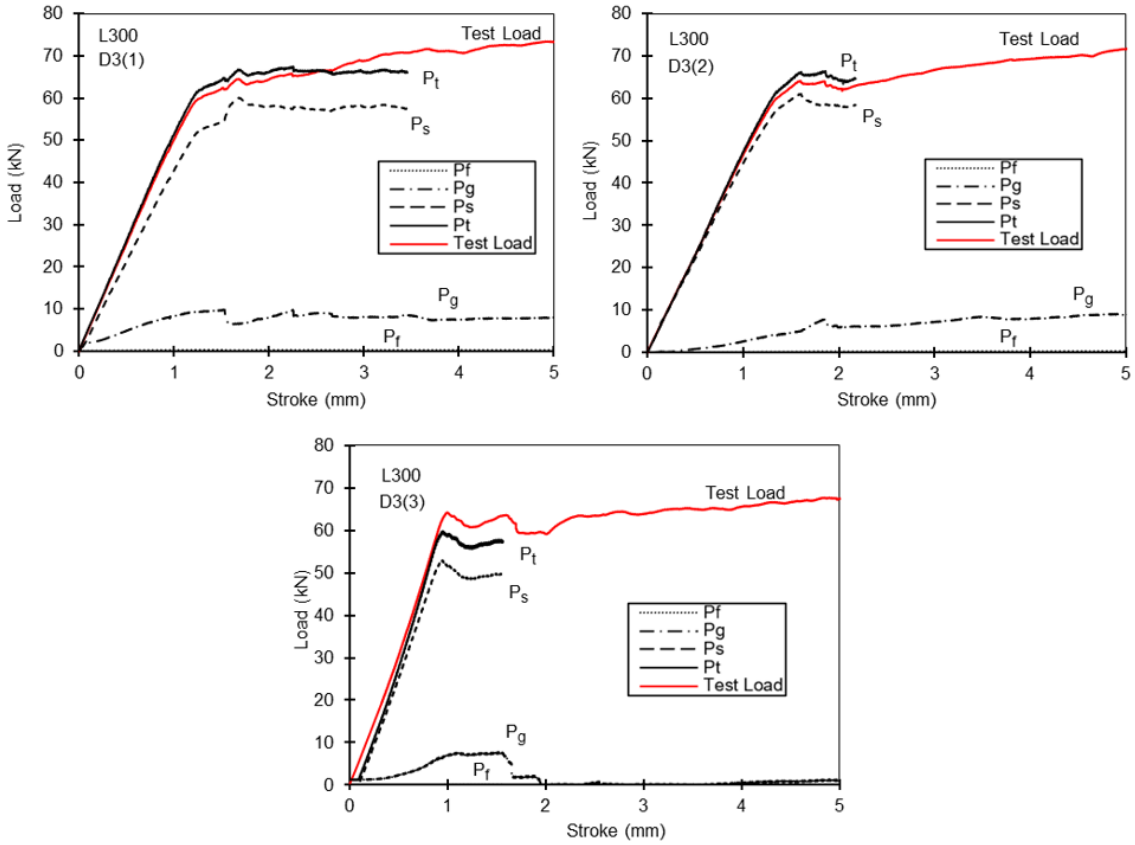

L300 D3 Contribution of materials to total load

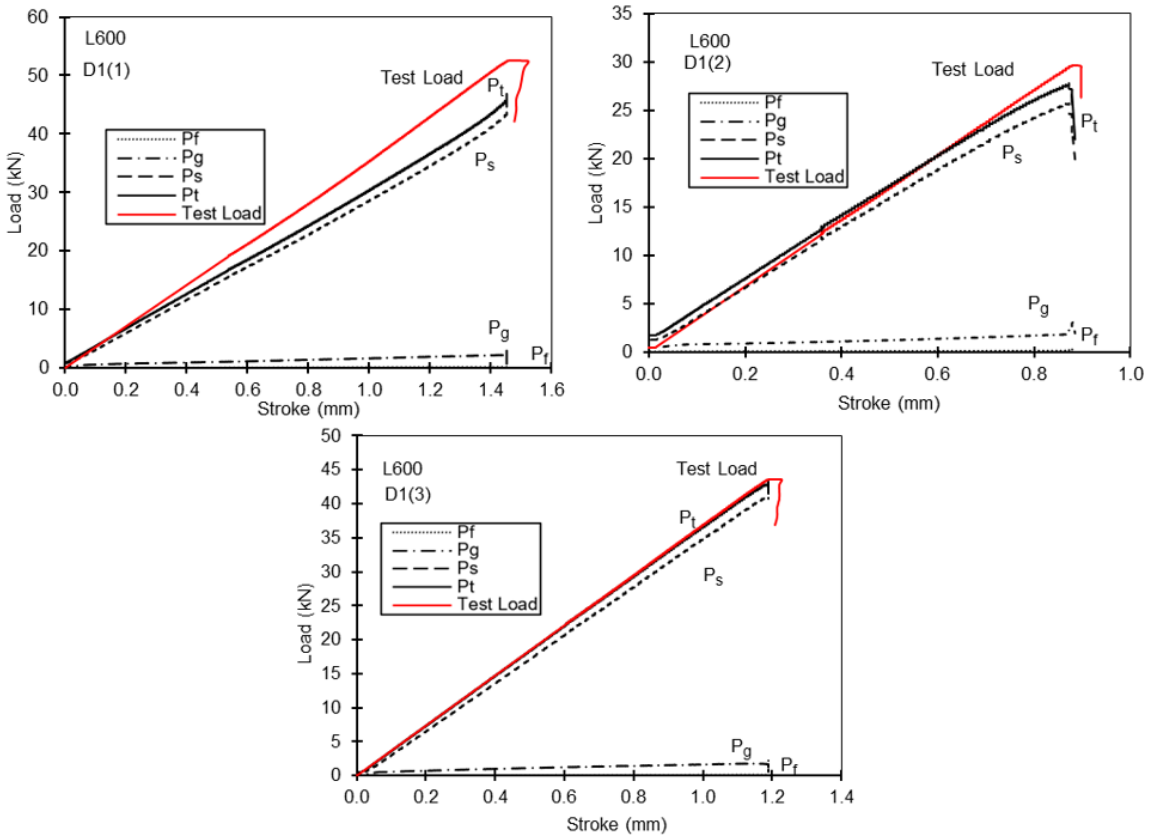

L600 D1 Contribution of materials to total load

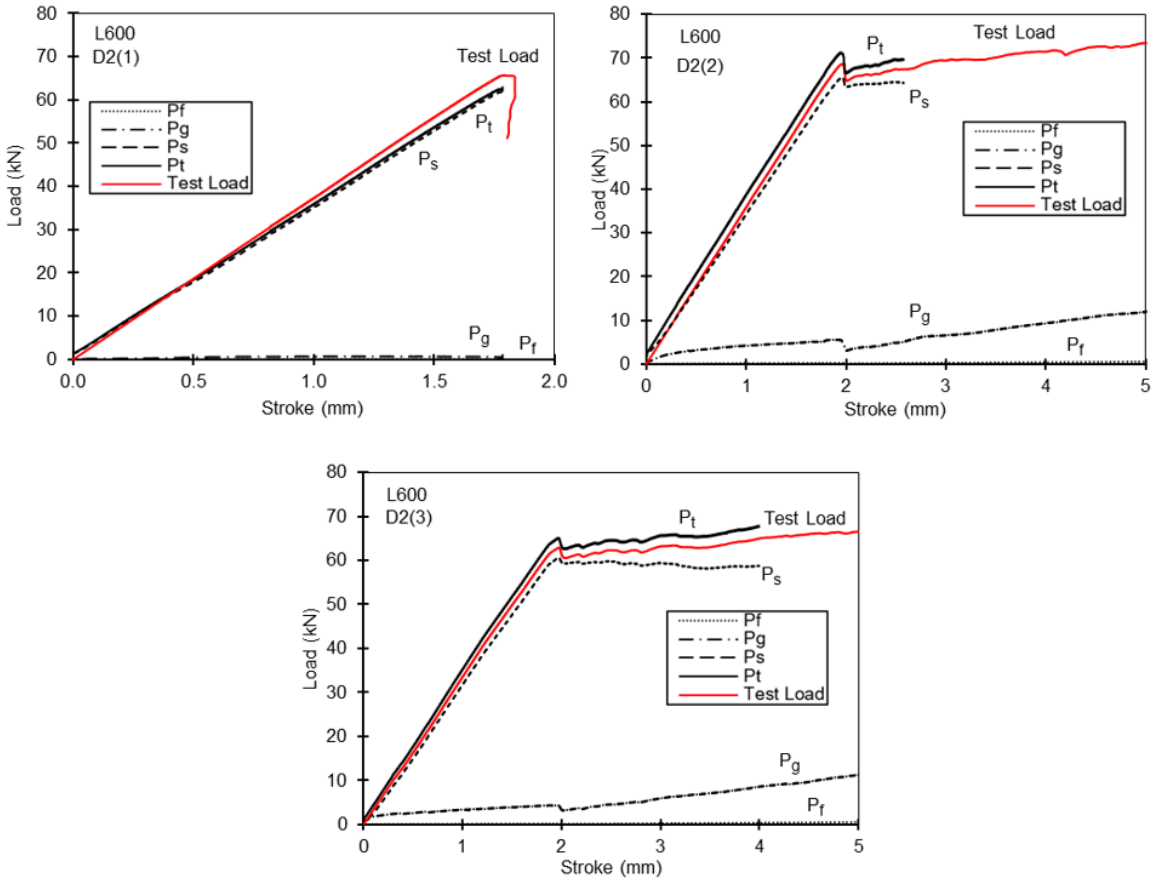

L600 D2 Contribution of materials to total load

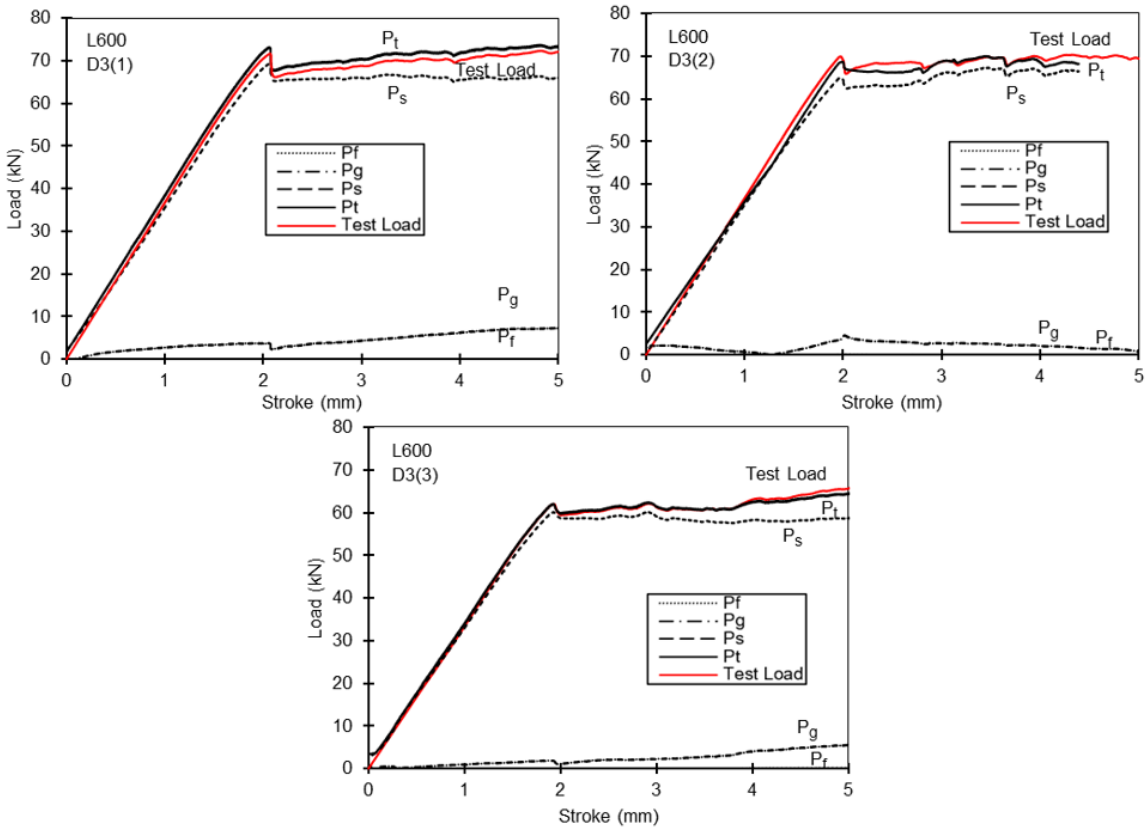

L600 D3 Contribution of materials to total load

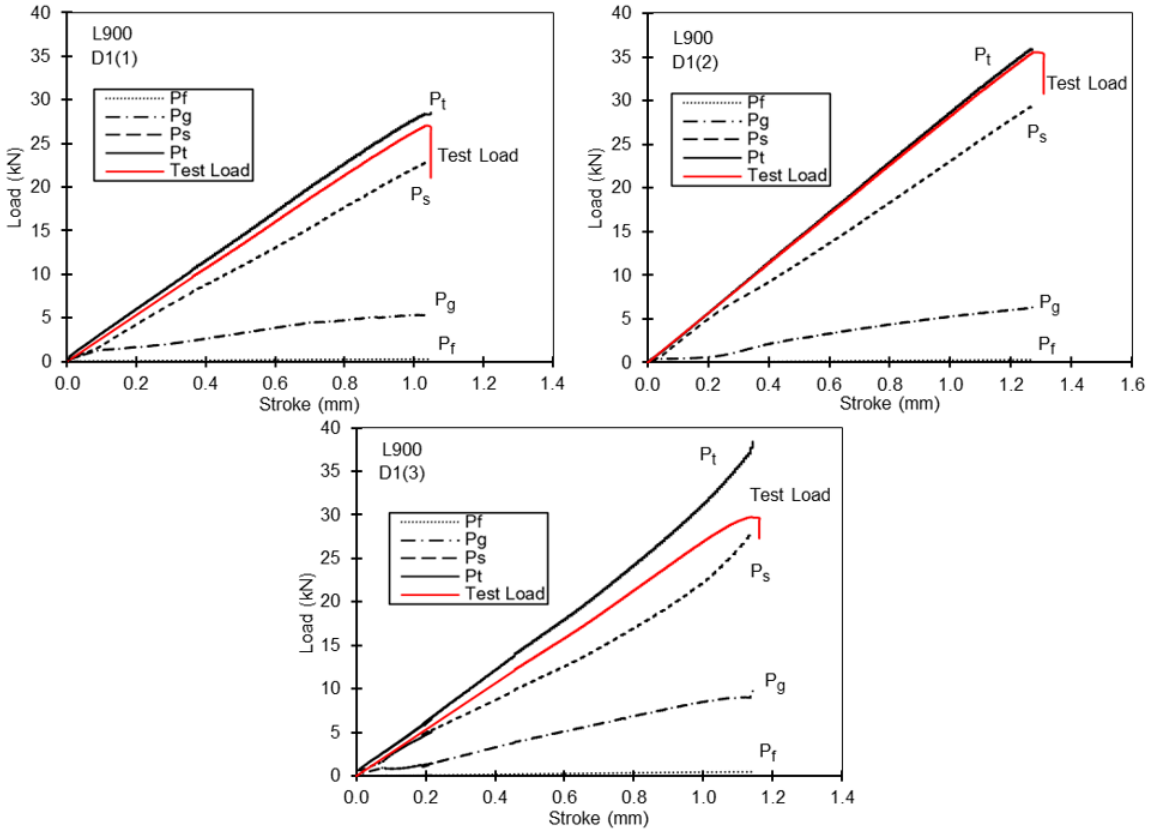

L900 D1 Contribution of materials to total load

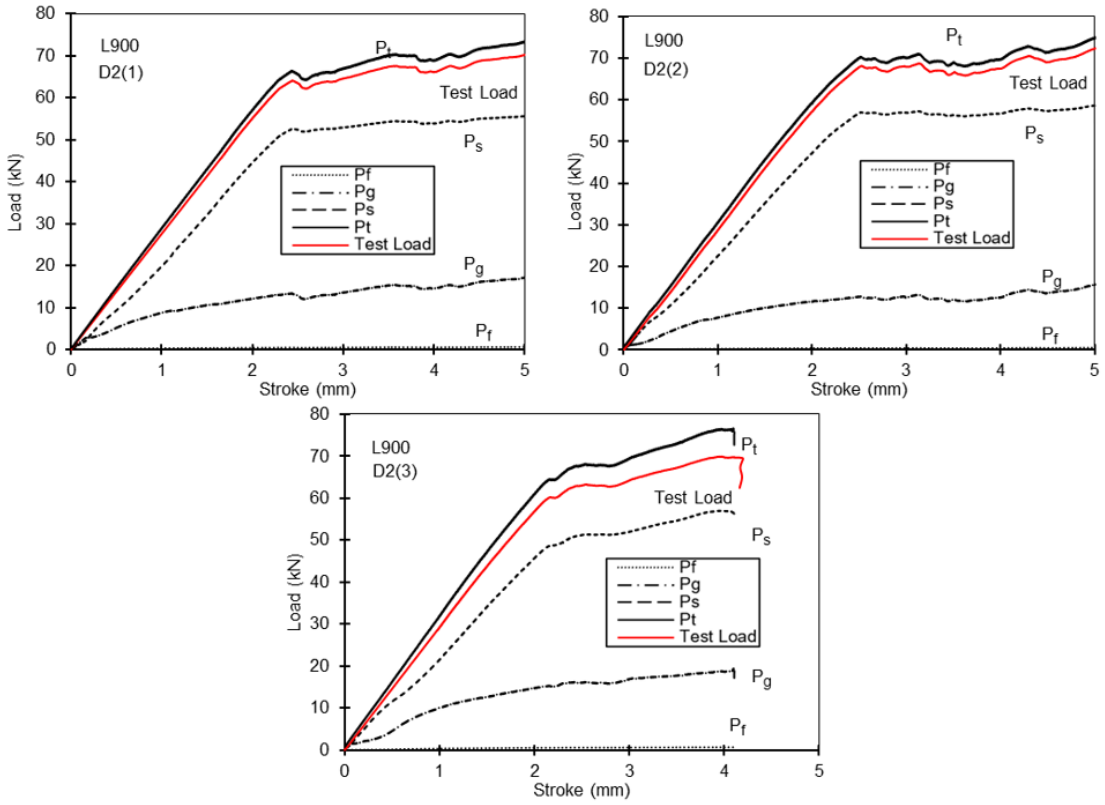

L900 D2 Contribution of materials to total load

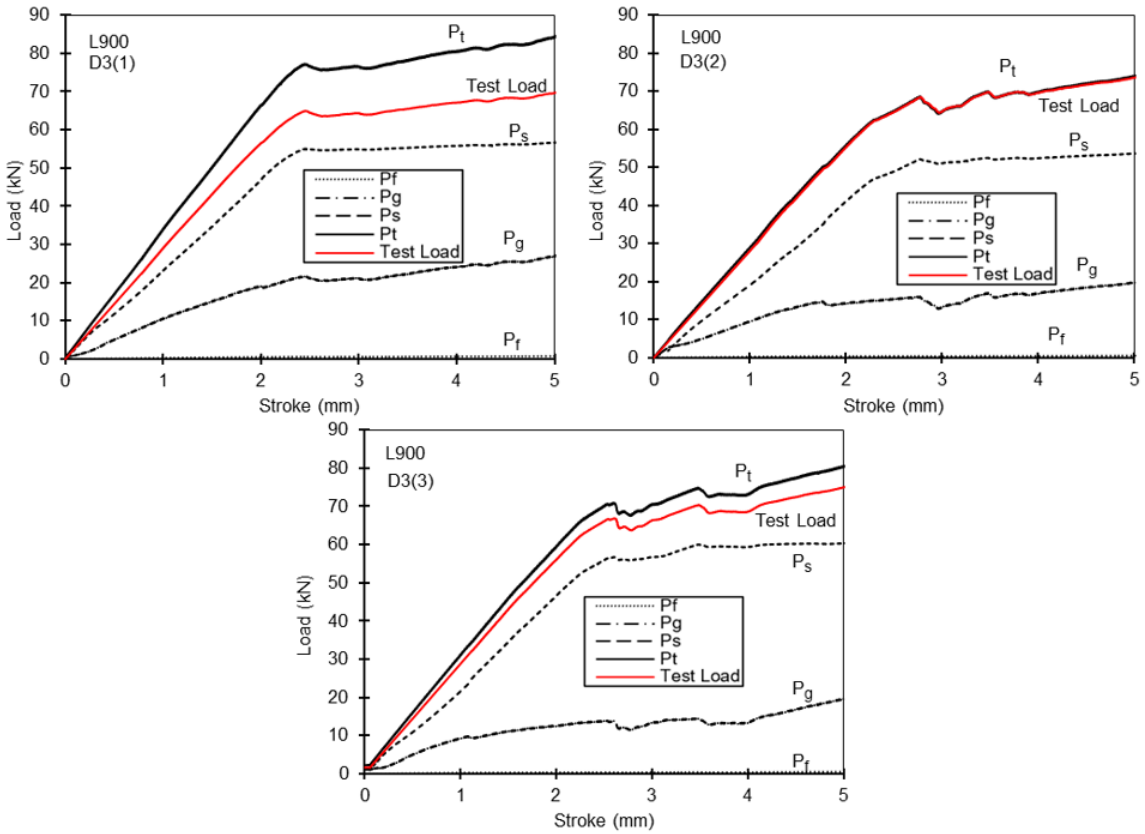

L900 D3 Contribution of materials to total load